Universidade Federal de Juiz de Fora
Programa de Pós-Graduação em Engenharia Elétrica
Doutorado em Engenharia Elétrica

Victor Fernandes

Energy Harvesting in Electric Power Systems

Juiz de Fora
2021

Victor Fernandes

Energy Harvesting in Electric Power Systems

Tese de doutorado apresentada ao Programa de Pós-Graduação em Engenharia Elétrica da Universidade Federal de Juiz de Fora, na área de concentração em sistemas eletrônicos, como requisito parcial para obtenção do título de Doutor em Engenharia Elétrica.

Orientador: Moisés Vidal Ribeiro

Juiz de Fora
2021

Ficha catalográfica elaborada através do Modelo Latex do CDC da UFJF com os dados fornecidos pelo(a) autor(a)

Fernandes, V.
Energy Harvesting in Electric Power Systems / Victor Fernandes. – 2021.
134 f. : il.

Orientador: Moisés Vidal Ribeiro
Tese de Doutorado – Universidade Federal de Juiz de Fora, Doutorado em Engenharia Elétrica. Programa de Pós-Graduação em Engenharia Elétrica, 2021.

Victor Fernandes

Energy Harvesting in Electric Power Systems

Tese de doutorado apresentada ao Programa de Pós-Graduação em Engenharia Elétrica da Universidade Federal de Juiz de Fora, na área de concentração em sistemas eletrônicos, como requisito parcial para obtenção do título de Doutor em Engenharia Elétrica.

Aprovada em: 28 de maio de 2021

BANCA EXAMINADORA

Prof. Dr. Moisés Vidal Ribeiro - Orientador
Universidade Federal de Juiz de Fora

Prof. Dr. Bartolomeu Ferreira Uchôa-Filho
Universidade Federal de Santa Catarina

Prof. Dr. Ivan Roberto Santana Casella
Universidade Federal do ABC

Prof. Dr. Luciano Manhães de Andrade Filho
Universidade Federal de Juiz de Fora

Prof. Dr. Leandro Rodrigues Manso Silva
Universidade Federal de Juiz de Fora

To my mother Maria Helena
To my father Sebastião
To my brothers Thiago and Diogo
To my girlfriend Florenza

AGRADECIMENTOS

Eu agradeço primeiramente a Deus, porque sem Ele nada seria possível. Agradeço, também, aos meus pais, Sebastião Fernandes da Silva Neto e Maria Helena dos Santos Fernandes, pelo apoio incondicional e exemplo que sempre deram em minha vida. Resumir o tamanho da importância e contribuição de vocês seria impossível, uma vez que minha existência e tudo que sou hoje veio de vocês. Além dos valores que me passaram, vocês me ensinaram como agir quando as dificuldades aparecem na vida e plantaram em mim a semente pela busca incessante pelo conhecimento e aprimoramento pessoal. Agradeço aos meus irmãos, Thiago Fernandes e Diogo Fernandes, que sempre estiveram ao meu lado, mesmo fisicamente distantes, dando-me força para seguir o meu caminho e servindo como exemplos de perseverança e resiliência para mim. A minha amada namorada, Florenza A. Noguchi, por todo amor, carinho, e companheirismo, estando ao meu lado mesmo nos momentos mais difíceis. Aos meus amigos André Luis de C. M., Douglas K. M. Gerheim e Thiago F. do A. Nogueira, cuja amizade e conselhos foram essenciais para me dar forças e passar pelas dificuldades do doutorado e da vida.

Agradeço ao professor Moisés Vidal Ribeiro pelas longas conversas, conselhos e orientações, os quais foram imprescindíveis para a realização do doutorado. Por vezes, a relação orientador-aluno é desgastada por discordâncias e expectativas de ambas as partes, porém soubemos contornar alguns conflitos com boa vontade para que fosse possível atingir um objetivo final repleto de aprendizados pelo caminho. Ao professor e mentor Weiler A. Finamore, que participou diretamente de minha formação acadêmica e me ajudou com suas orientações e a sua maneira distinta de encarar a pesquisa e a vida. Aos meus amigos e colegas de laboratório, Ândrei Camponogara, Mateus de L. Filomeno, Roberto M. de Oliveria, Guilherme R. Colen, Thiago R. Oliveira, Leonardo de M. B. A. Dib, Nathan Cravo, entre outros, cujas conversas, seja de forma direta ou indireta, ajudaram tanto no incentivo quanto na realização do meu trabalho de doutorado.

Agradeço a todos os brasileiros que, diretamente ou indiretamente, financiaram esse trabalho através do CNPq, CAPES, INERGE e FAPEMIG. O incentivo à pesquisa tem sido mostrado cada vez mais essencial nos dias atuais. Nesse contexto, a frase que coloquei na epígrafe, cuja tradução livre é: 'Se eu vi mais longe, foi por estar sobre ombros de gigantes', representa muito bem a natureza da ciência, pesquisa e desenvolvimento. A expansão da esfera de conhecimento humana só é possível através do compartilhamento de informações e, portanto, para que seja possível avançar em uma determinada área de conhecimento, é necessário se basear em documentos científicos anteriores. Sendo assim, expando e finalizo meus agradecimentos a todos cientistas e pesquisadores que contribuíram de alguma forma para que esse trabalho de doutorado fosse possível de ser realizado.

“If I have seen further than others,
it is by standing upon the shoulders of giants”
Isaac Newton.

RESUMO

Esta tese investiga a colheita de energia (do inglês, *energy harvesting*) (EH) em sistemas elétricos de potência e a sua utilidade para alimentar sistemas híbridos de comunicações de dados, baseados na combinação de sistemas de comunicações via rede de energia elétrica (do inglês, *power line communication*) (PLC) e comunicações sem fio (do inglês, *wireless communication*) (WLC). Neste contexto, são discutidos aspectos gerais do EH em sistemas elétricos de potência, destacando as vantagens e desvantagens da colheita de energia com base em classificações típicas dos sistemas elétricos de potência em termos dos níveis de tensão e das bandas de frequência do conteúdo espectral dos sinais elétricos. Primeiro, a energia colhida é avaliada quantitativamente na configuração concatenada de canais banda larga PLC e WLC, na combinação paralela de canais banda estreita PLC e WLC, e nas principais componentes harmônicas dos sinais elétricos. Em segundo lugar, o uso da energia colhida para fins de comunicação de dados é avaliado em termos de taxas de dados alcançáveis ergódicas desses canais, e o número de transceptores alimentados com essa energia é estimado para cinco padrões de comunicação de dados comumente adotados por dispositivos de comunicação de dados de baixa potência. Com base em um conjunto de dados medidos em instalações residenciais, as análises numéricas mostraram que a energia colhida dos distúrbios existentes em sinais elétricos na banda de frequência delimitada pela tecnologia PLC banda larga é uma parte considerável da quantidade de energia colhida total. Também, as comunicações de dados baseadas em EH atingiram taxas de dados alcançáveis ergódicas de dezenas de bps ou kbps a dezenas de Mbps, dependendo do uso de canais banda estreita ou banda larga. Além disso, esta tese aborda uma nova formulação matemática para quantificar com precisão o EH da potência desperdiçada em sinais elétricos e estende essa formulação para a potência colhida. Neste contexto, mostra-se que a dinâmica da energia desperdiçada das principais componentes harmônicas dos sinais elétricos em uma instalação predial pode ser considerada um processo aleatório cicloestacionário e estacionário nos dias úteis e fins de semana, respectivamente. Também, estima-se que milhões, ou mesmo bilhões, de transceptores podem ser alimentados por meio da potência colhida dos distúrbios em sinais elétricos dos sistemas elétricos de potência brasileiros e, ao mesmo tempo, são esperados impactos positivos na qualidade de energia desses sistemas. Finalmente, a energia dos distúrbios em sinais elétricos na banda de frequência de qualquer tecnologia PLC tem um enorme potencial para alimentar dispositivos de comunicação de dados de baixa potência, tais como os utilizados na Internet das Coisas, redes inteligentes e Indústria 4.0.

Palavras-chave: colheita de energia, comunicações via rede de energia elétrica, comunicações sem fio, sistema elétrico de potência, internet das coisas.

ABSTRACT

This dissertation investigates the energy harvesting (EH) in electric power systems and its usefulness to power hybrid data communication systems, based on the combination of power line communication (PLC) and wireless communication (WLC) ones. In this context, general aspects of EH in electric power systems are discussed, highlighting the advantages and drawbacks of harvesting energy based on typical classifications of the electric power systems in terms of voltage levels and on the frequency bands of the spectrum content of electric signals. First, the harvested energy is quantitatively evaluated in the concatenated configuration of broadband PLC and WLC channels, in the parallel combination of narrowband PLC and WLC channels, and in the main harmonic components of electric signals. Second, the use of the harvested energy for data communication purposes is evaluated in terms of ergodic achievable data rates of these channels, and the number of transceivers powered by this energy is estimated for five data communication standards commonly adopted by low-power data communication devices. Based on an in-home measured data set, numerical analyses showed that the energy harvested from the disturbances in electric signals on the frequency band delimited by the broadband PLC technology is a remarkable part of the amount of the total harvested energy. Also, EH-based data communications attained ergodic achievable data rates from dozens of bps or kbps to dozens of Mbps, depending on the use of narrowband or broadband channels. Moreover, this dissertation addresses a novel mathematical formulation to precisely quantify the EH from wasted power in electric signals and extends this formulation to the harvested power. In this context, it shows that the wasted energy dynamic of the main harmonic components of electric signals in a building facility can be considered cyclostationary and stationary random processes on the weekdays and weekends, respectively. As well, it estimates that millions, or even billions, of transceivers can be powered by means of the harvested power from disturbances in electric signals of the Brazilian electric power systems and, at the same time, positive impacts are expected in the power quality of these systems. Finally, the energy of disturbances in electric signals on the frequency band of any PLC technology has tremendous potential for feeding up low-power data communication devices such as the ones in the Internet of Things, smart grids, and Industry 4.0.

Key-words: energy harvesting, power line communication, wireless communication, electric power system, internet of things.

LIST OF FIGURES

Figure 1 – Electric field energy harvesting. 24
Figure 2 – Magnetic field energy harvesting. 24
Figure 3 – Electric power transmission system. 27
Figure 4 – Electric power distribution system. 28
Figure 5 – Block diagram of an EH device circuitry. 35
Figure 6 – Parallel configuration (hybrid PLC/WLC system). 37
Figure 7 – Concatenated configuration (hybrid PLC-WLC system). 38
Figure 8 – The hybrid PLC-WLC environment in in-home facilities. 42
Figure 9 – The block diagram of the measurement setup. 48
Figure 10 – The CCDFs of the harvested energy from the FoN received signal over a hybrid SP PLC-WLC channel (top) or hybrid LP PLC-WLC channel (bottom). 50
Figure 11 – The CCDFs of the harvested energy from the PLC and WLC additive noises. 51
Figure 12 – The CCDFs of the harvested energy from the total received signal in hybrid SP PLC-WLC channel (top) and hybrid LP PLC-WLC channel (bottom) considering the PLC $\rightarrow$ WLC direction. 53
Figure 13 – The CCDFs of the harvested energy from the total received signal in hybrid SP PLC-WLC channel (top) and hybrid LP PLC-WLC channel (bottom) considering the WLC $\rightarrow$ PLC direction. 53
Figure 14 – The expected values of the harvested energy from the total received signal in a hybrid SP PLC-WLC channel corrupted by the WLC (left) and PLC (right) additive noises. 54
Figure 15 – The expected values of the harvested energy from the total received signal in a hybrid LP PLC-WLC channel corrupted by the WLC (left) and PLC (right) additive noises. 55
Figure 16 – The average time interval to achieve E_x^q at the receiver side of hybrid SP PLC-WLC channels corrupted by WLC (left) or PLC (right) additive noises. 56
Figure 17 – The average time interval to achieve E_x^q at the receiver side of hybrid LP PLC-WLC channels corrupted by WLC (left) or PLC (right) additive noises. 57
Figure 18 – Three distinct scenarios: (a) Scenario #A1, (b) Scenario #A2, (c) Scenario #A3. 59
Figure 19 – The CCDFs of ergodic achievable data rates yielded by the WLC (EH) device in Scenario #A1 for $\eta^q = 1$ (continuous line) and $\eta^q = 0.5$ (dashed line). . . 61
Figure 20 – The CCDFs of ergodic achievable data rates yielded by the PLC (EH) device in Scenario #A2 for $\eta^q = 1$ (continuous line) and $\eta^q = 0.5$ (dashed line). . . 61
Figure 21 – The CCDFs of ergodic achievable data rates yielded by the WLC (EH) device in Scenario #A3 for $\eta^q = 1$ (continuous line) and $\eta^q = 0.5$ (dashed line). . . 63
Figure 22 – Two distinct scenarios: (a) Scenario #B1, (b) Scenario #B2. 64

Figure 23 – The CCDFs of ergodic achievable data rates yielded by the WLC (EH) device in Scenario #B1 for $\eta^q = 1$ (continuous line) and $\eta^q = 0.5$ (dashed line). . . 65
Figure 24 – The CCDFs of ergodic achievable data rates yielded by the PLC (EH) device in Scenario #B2 for $\eta^q = 1$ (continuous line) and $\eta^q = 0.5$ (dashed line). . . 66
Figure 25 – CCDF of the harvested energy from the FoN received signal: The five power masks, $\mathcal{P}_x^q = 20$ dBm and $\eta^q = 1$. 73
Figure 26 – CCDF of the harvested energy from the additive noises with $\eta^q = 1$. 74
Figure 27 – CCDF of the total harvested energy by the WLC device: The five power masks, $\mathcal{P}_x^{\text{PLC}\rightarrow\text{WLC}} = 20$ dBm and $\eta^{\text{PLC}\rightarrow\text{WLC}} = 1$. 75
Figure 28 – CCDF of the total harvested energy by the PLC device: The five power masks, $\mathcal{P}_x^{\text{WLC}\rightarrow\text{PLC}} = 20$ dBm and $\eta^{\text{WLC}\rightarrow\text{PLC}} = 1$. 76
Figure 29 – Scenario #A1 - CCDF of the ergodic achievable data rate for hybrid SP PLC-WLC channel (top) and hybrid LP PLC-WLC channel (bottom): Power Masks #1 and #2, $\mathcal{P}_x^q = 20$ dBm and $\eta^q = 0.5$. 78
Figure 30 – The hybrid power line/wireless dual-hop system model. 80
Figure 31 – TS strategy block diagram. 83
Figure 32 – PS strategy block diagram. 84
Figure 33 – Block diagrams of Approach A (HTS), Approach B (HTS), Approach C (TS), and Approach D (PS). 87
Figure 34 – Scenario #C1: φ_b^a versus λ, ρ for H2HS, P2HS, and W2HS. 92
Figure 35 – Scenario #C2: φ_b^a versus λ, ρ for H2HS, P2HS, and W2HS. 93
Figure 36 – Scenario #C3: φ_b^a versus λ, ρ for H2HS, P2HS, and W2HS. 94
Figure 37 – Scenario #C4: φ_b^a versus λ, ρ for H2HS, P2HS, and W2HS. 95
Figure 38 – A non-linear load model. 98
Figure 39 – Typical indoor environment. A device connected to the outlet is in contact with the AC mains signal and disturbances. 101
Figure 40 – Wasted power for distinct days of the week ($\eta = 1$). 110
Figure 41 – Harvested power for distinct values of η. 110
Figure 42 – Ergodic achievable data rate for the NB-PLC. 111
Figure 43 – Ergodic achievable data rate for the LP-RF WLC. 112
Figure 44 – Number of powered IoT devices' transceivers versus notification period (in minutes). 117
Figure 45 – Number of powered IoT devices' transceivers versus notification period (in seconds). 118
Figure 46 – A rough estimate of IoT devices' transceivers that could be powered within Brazilian electricity sectors in 2019 ($T_{\text{notif}} = 1$ min). 119

LIST OF TABLES

Table 1 – Artificial sources for EH in electric power systems. 23
Table 2 – Voltage level classification of electric power system. 26
Table 3 – The frequency bands from PLC systems. 29
Table 4 – Broadband-PLC standards. 30
Table 5 – Narrowband-PLC standards. 30
Table 6 – LLVs of the FoN received signal's harvested energy: SP channels, $\mathcal{P}_x^q$ = 20 dBm, and $\eta^q = 1$. 68
Table 7 – LLVs of the FoN received signal's harvested energy: LP channels, $\mathcal{P}_x^q$ = 20 dBm, and $\eta^q = 1$. 68
Table 8 – LLVs of the additive noises' harvested energy with $\eta^q = 1$. 68
Table 9 – Harvested energy from the FoN signal - The parameters for the fitted log-normal distribution. 70
Table 10 – Harvested energy from the additive noise - The parameters for the fitted log-normal distribution. 70
Table 11 – Zigbee states and current consumption information. 113
Table 12 – Bluetooth states and current consumption information. 114
Table 13 – LoRa states and current consumption information. 115
Table 14 – Sigfox states and current consumption information. 116
Table 15 – NB-IoT states and current consumption information. 116
Table 16 – Estimate of IoT devices' transceivers that could be powered within all Brazilian electricity sectors (in millions). 119

ACRONYMS

AC	alternating current
ACGN	additive colored Gaussian noise
AF	amplify-and-forward
AMR	automatic meter reading
ANEEL	Brazilian electricity regulatory agency (*Agência Nacional de Energia Elétrica* in Portuguese)
ARIB	Association of Radio Industries and Businesses
AWGN	additive white Gaussian noise
BB-PLC	broadband-PLC
BLE	bluetooth low energy
CENELEC	European Committee for Electrotechnical Standardization (*Comité Européen de Normalisation Électrotechnique* in French)
CCDF	complementary cumulative distribution function
CFR	channel frequency response
CGRC	circular Gaussian relay channel
CIR	channel impulse response
CSI	channel state information
CTFT	continuous-time Fourier transform
DC	direct current
DF	decode-and-forward
DR	data rate
E-field	electric field
ECP	extended complex power
eDRX	extended discontinuous reception mode
EEH	electric field energy harvesting
EH	energy harvesting
FCC	Federal Communications Commission
FD-ECP	frequency-domain extended complex power
FoN	free-of-noise
FRMPL	physical layer frame payload size
H2HS	hybrid power line/wireless dual-hop system

HEAP harvested extended active power

HECP harvested extended complex power

HS-OFDM hermitian symmetric orthogonal frequency-division multiplexing

HTS hybrid time switching

HV high-voltage

IoT Internet of Things

ISM industrial, scientific, and medical

LoRaWAN long-range wide area network

LGRC linear Gaussian relay channel

LLV log-likelihood value

LP *long-path*

LP-RF low-power radio-frequency

LPWAN low-power wide-area networks

LTE long term evolution

LV low-voltage

M-field magnetic field

MEH magnetic field energy harvesting

MIMO multiple-input multiple-output

MRC maximal ratio combining

MV medium-voltage

NB-IoT narrowband-IoT

NB-PLC narrowband-PLC

nSNR normalized signal-to-noise ratio

OA optimal power allocation

P2HS power line dual-hop system

pdf probability density function

PLC power line communication

PS power splitting

PSD power spectral density

PSM power saving mode

RF radio-frequency

RMS	root mean square
RF-EH	radio-frequency EH
SF	spreading factor
SG	smart grid
SP	*short-path*
TS	time switching
TWACS	two-way automatic communications system
UA	uniform power allocation
US	United States
UNB-PLC	ultra-narrowband-PLC
VLC	visible light communication
W2HS	wireless dual-hop system
WEH	WES EH
WES	wasted electric signal
WF	water-filling
WLC	wireless communication
WPAN	wireless personal area networks
WWAN	wireless wide area network

CONTENTS

1 INTRODUCTION 15
1.1 OBJECTIVES 17
1.2 DISSERTATION OUTLINE 18

2 ENERGY HARVESTING IN ELECTRIC POWER SYSTEMS 20
2.1 ENERGY HARVESTING 21
2.2 CLASSIFICATION OF ENERGY HARVESTING 25
2.2.1 Voltage Level 25
2.2.1.1 High-voltage level 26
2.2.1.2 Medium-voltage level 27
2.2.1.3 Low-voltage level 28
2.2.2 Frequency Band 29
2.3 HARVESTING ARCHITECTURES AND CIRCUITRY 33
2.4 HYBRID COMMUNICATION POSSIBILITIES 36
2.5 SUMMARY 39

3 DEDICATED ENERGY HARVESTING IN HYBRID PLC-WLC SYSTEMS 40
3.1 PROBLEM FORMULATION 41
3.2 HARVESTING ENERGY FROM THE HYBRID PLC-WLC CHANNELS . 42
3.2.1 FoN Received Signal's Power 43
3.2.2 Additive Noise's Power 44
3.2.3 Total Harvested Energy per Cycle 44
3.2.4 Harvesting Energy based on Power Masking 45
3.3 DATA SET 47
3.4 PERFORMANCE ANALYSES 49
3.4.1 FoN Received Signal Analyses 49
3.4.2 Additive Noise Analyses 51
3.4.3 Total Received Signal Analyses 52
3.4.4 The Expected Values Analyses 54
3.4.5 Average Time Interval Analyses 55
3.4.6 Ergodic Achievable Data Rate Analyses: Narrowband Channels 57
3.4.7 Ergodic Achievable Data Rate Analyses: Hybrid PLC-WLC Channels . 63
3.5 STATISTICAL ANALYSES 67
3.5.1 Statistical Modelings 67
3.5.2 WLC Device - Harvesting Energy 70

3.5.3 **PLC Device - Harvesting Energy** . . . 71
3.5.4 **Numerical Comparisons: Statistical Models and Measured Data Set** . . 72
3.6 SUMMARY . . . 78

4 **A HYBRID PLC/WLC DUAL-HOP SYSTEM WITH ENERGY HARVESTING RELAY** . . . **79**
4.1 PROBLEM FORMULATION . . . 80
4.2 THE PROPOSED APPROACHES IN THE H2HS MODEL . . . 82
4.2.1 **The TS and PS Strategies** . . . 83
4.2.2 **The Ergodic Achievable Data Rates** . . . 85
4.2.3 **The Proposed Approaches** . . . 88
4.3 NUMERICAL RESULTS . . . 89
4.3.1 **Scenario #C1: OA and NB-PLC Channel with ACGN** . . . 91
4.3.2 **Scenario #C2: OA and NB-PLC Channel with AWGN** . . . 93
4.3.3 **Scenario #C3: UA and NB-PLC Channel with ACGN** . . . 94
4.3.4 **Scenario #C4: UA and NB-PLC Channel with AWGN** . . . 94
4.4 SUMMARY . . . 95

5 **ENERGY HARVESTING FROM THE UNB-PLC SPECTRUM: POTENTIAL IN THE ERA OF IOT** . . . **97**
5.1 THE QUANTIFICATION OF WASTED ENERGY . . . 98
5.2 HARVESTING ENERGY IN THE UNB-PLC SPECTRUM . . . 100
5.3 NUMERICAL RESULTS . . . 107
5.3.1 **Wasted Energy Dynamics: Building Facility** . . . 109
5.3.2 **Ergodic Achievable Data Rates: Building Facility** . . . 109
5.3.3 **Number of Transceivers of IoT Devices: Building Facility** . . . 112
5.3.3.1 *Zigbee* . . . 113
5.3.3.2 *Bluetooth* . . . 113
5.3.3.3 *LoRa* . . . 114
5.3.3.4 *Sigfox* . . . 114
5.3.3.5 *NB-IoT* . . . 115
5.3.4 **Number of Transceivers of IoT Devices in the Brazilian Electricity Sector** 118
5.4 SUMMARY . . . 120

6 **CONCLUSIONS** . . . **121**

REFERENCES . . . **124**

APPENDIX A – Publications . . . **133**

1 INTRODUCTION

The increasing and astonishing demands for more energy-efficient, pervasive, and smarter data communications are motivating research efforts on how to effectively and efficiently reuse the expended energy for transmitting information through the available data communication media. In fact, this kind of energy allows a data communication device to power itself by harvesting the energy from the received signal, which is constituted by the signal transmitted by another device and the additive noise. As stated in [1], one of the dominant barriers to implement the Internet of Things (IoT) is the energy supply that is necessary to operate data networks in a self-sustainable and energy-efficient manner. Grounded on a telecommunications perspective to deal with this challenging issue, the concept of energy harvesting (EH) is being increasingly investigated. Initially, the research efforts related to EH focused on the wireless communication (WLC) field and, recently, research attention in this area has turned to power line communication (PLC) because its combination with WLC and visible light communication (VLC) will play a pivotal role in offering effective, pervasive, and flexible data networks.

It is well-established that EH has emerged in the context of green communications [2] for energy-efficient [3] and self-sustainable [4] data networks, and the reuse of the existing energy in the environment is crucial in advancing these networks because EH allows the savings of non-renewable energy and makes the data communication environmentally friendly [5]. Therefore, research efforts have focused on harvesting energy from environmental signals[1] (e.g., electromagnetic waves of the sunlight) to postpone the batteries' lifetime or even make devices self-sustainable. However, as the harvested energy from environmental signals may have an intermittent behavior over time, EH for data communication purposes is a challenging problem to be addressed because such intermittence may not guarantee the necessary energy supply [6]. In this regard, EH from non-environmental signals has been largely investigated to assist data networks to deal with the needs and demands associated with sustainability in the IoT, smart grids (SGs), and Industry 4.0 applications.

The literature states that electric power systems may be the most complex source of non-environmental signals that is suitable for EH across the globe. In these systems, EH is usually exploited in terms of the electromagnetic field generated in the vicinity of power lines. In fact, the broadcasting nature of electric power systems and the use of electromagnetically unshielded power lines make the transmission and distribution infrastructure of electric power systems an interesting source of electromagnetic radiation for EH that can be further applied to data networks. As a part of the real-world constraints, the losses related to the disturbances in electric signals[2], which are generated by the interactions between electric power systems and non-linear loads as well as by radio-frequency (RF) signals induced into electromagnetically unshielded power lines, are always present. Taking advantage, or reusing, the energy associated

[1] Environmental and non-environmental signals can be converted to electric signals by transducers.

[2] Electric signals are used to represent both voltage and current signals.

with these disturbances can improve the energy efficiency of electric power systems because disturbances are sources of power quality degradation and their energies can be used for powering devices in SGs.

Smart grids have emerged as promising trends and they have attracted the interest of many research groups of both academia and industry on how to turn electric power systems more energy-efficient, reliable, and sustainable. Due to the pervasive infrastructure of electric power systems, which is the only wireline data communication media whose deployment cost can be compared to the wireless ones [7], narrowband-PLC (NB-PLC) systems become a strong candidate for fulfilling SGs demands because NB-PLC systems operate over the infrastructure of transmission and distribution electric power systems. Electric power systems are challenger media for performing PLC because they were designed to maximize energy delivery [8]; however, some of the problems faced by PLC systems [7,9] can be seen as EH opportunities because PLC systems may take advantage of the disturbances in electric signals by reusing their energies. As a matter of fact, the propagation of PLC signals can be severely degraded due to the dynamic of loads (i.e., consumers and utilities), impedance mismatching, signal attenuation, power line breaks, electromagnetically unshielded power lines, and impulsive noise presence [9, 10].

Recently, PLC additive noises or wasted electric signals (WESs), which refer to disturbances in electric signals, are being recognized as a new frontier for recovering or harvesting energy in electric power systems. The EH applied to impulsive components of PLC additive noises was investigated in [11], in which EH was considered at the relay node in a cooperative PLC system, and the authors concluded that energy efficiency of PLC system increases if PLC nodes harvest the unwanted high-energy component (i.e., impulsive noise) from the PLC additive noise. Also, [12] considered a dual-hop amplify-and-forward (AF) PLC system with a time-switching strategy at the relay node and showed that as the PLC additive noise becomes more impulsive, higher is the harvested energy obtained from it. As well, [13] considered a dual-hop PLC system with an EH-relaying node and showed that it is possible to provide energy efficiency improvements of more than 30% in comparison to the conventional relaying scheme when energy is harvested from the impulsive component of the PLC additive noise. An interesting and missing point in these contributions is the lack of discussion based on measurements to confirm the veracity of these statements and to quantify the wasted energy[3].

Moreover, the research efforts for increasing the flexibility and coverage of data communication systems have brought attention to the benefits of the appropriate use of the hybridism concept at the physical layer level [14–21]. For instance, [22–25] discussed the challenges, drawbacks, and benefits of simultaneously using two of PLC, WLC, or VLC media for data communication purposes. However, the concatenation of these media can show interesting opportunities for assisting the introduction of energy-efficient, pervasive, and smarter data networks. That said, there are two possible single-hop configurations for the mutual use of these media, which are the parallel and the concatenated ones. In the parallel configuration, the focus of

[3] Often, the energy of disturbances in electric signals (i.e., the energy of WESs) is called wasted energy.

interest may be to ensure reliability or to increase the data rate of a data communication system, while the concatenation aims at improving the coverage of a data communication system.

When the concatenation of the broadband-PLC (BB-PLC) and WLC systems operating in the same frequency band comes to the center of the discussion, a pivotal work [26] demonstrated that PLC and WLC devices communicating to each other through a so-called hybrid data communication medium, which is composed of the electromagnetically unshielded power line and the air, can achieve up to tens of Mbps and, as a consequence, this hybrid data communication medium showed to be a potential option for introducing new generations of data networks. Concerning the parallel configuration, some works [16, 17] have shown that the use of NB-PLC and low-power radio-frequency (LP-RF) WLC[4] channels in a hybrid data communication system can enhance data rate when compared to the sole use of non-hybrid data communication systems. Note that the mutual use of PLC and WLC channels in both configurations, respectively termed *hybrid PLC-WLC channel* and *hybrid PLC/WLC channel* in the concatenated and parallel configurations, can bring improvements not only associated with the data rate, reliability or coverage of data communication systems but also related to the energy efficiency of them due to the opportunity to perform EH by exploiting the broadcasting nature of both data communication media.

Given these discussions, this dissertation addresses distinct aspects of performing EH in hybrid PLC-WLC channels, hybrid PLC/WLC channels, and WESs based on real data set to quantify, in a practical and telecommunications perspective, the usefulness of EH for supplying energy to low-power data communication devices. These investigations are of utmost importance for energy-efficient and self-sustainable data networks that operate in the vicinity of electric power systems because they can enlarge the bottleneck of energy supplying for low-power data communication devices. Considering everything discussed so far, Section 1.1 presents the objectives of this dissertation and Section 1.2 addresses how this dissertation is organized.

1.1 OBJECTIVES

The objectives of the present dissertation are listed as follows:

- To give an overview about EH in electric power systems, covering: a detailed presentation of three possible artificial sources of energy for EH; a discussion about advantages and drawbacks of realizing EH from these sources in high-voltage (HV), medium-voltage (MV), and low-voltage (LV) electric power systems; the benefits of using ambient and dedicated EH approaches in four distinct frequency bands of electric signals; a concise presentation of common architectures and circuitry for EH; the EH perspective of hybrid PLC and WLC system configurations.

[4] The LP-RF WLC channels occupy a narrow bandwidth and are adopted by low-power consumption devices that usually operate in one of the industrial, scientific, and medical (ISM) frequency bands.

- To formulate and investigate the EH from the signal received through the hybrid PLC-WLC channel in in-home facilities when the frequency band between 0 and 100 MHz is considered. Based on the amount of harvested energy, the ergodic achievable data rate evaluation of NB-PLC, LP-RF WLC, and hybrid PLC-WLC channels is presented when the energy available for data communication is that one harvested from the signal received through the hybrid PLC-WLC channel. Also, the statistical analyses and modeling of the aforementioned harvested energy are performed.

- To introduce and discuss four distinct approaches for performing EH and data communication when hybrid PLC/WLC channels in the dual-hop configuration and the frequency bands of $3 - 500$ kHz and $915 - 915.5$ MHz are considered for PLC and WLC channels, respectively. This discussion is based on the ergodic achievable data rate of the dual-hop hybrid PLC/WLC channel and includes a comparison with both the non-hybrid dual-hop PLC and WLC channels under four different scenarios.

- To formulate and investigate the EH from WESs when in-building power lines and the main harmonic components, from 2^{nd} up to 11^{th} order, are considered. By means of the harvested power from these components of WESs, the ergodic achievable data rates of NB-PLC and LP-RF WLC channels are evaluated, and the number of powered transceivers of IoT devices is estimated for five data communication standards commonly adopted by low-power data communication devices.

1.2 DISSERTATION OUTLINE

The remainder of this dissertation is organized as follows:

- Chapter 2 introduces general aspects of EH in electric power systems, highlighting the advantages and drawbacks of three distinct artificial sources of energy. Also, two classifications for harvesting energy in these systems, as well as common harvesting architectures and circuitry, are discussed. Moreover, the EH possibilities in hybrid data communication systems based on the use of PLC and WLC systems are detailed.

- Chapter 3 presents the hybrid PLC-WLC channel, its mathematical formulation, and discussion concerning the quantification of the harvested energy. Furthermore, the ergodic achievable data rate of typical scenarios is evaluated when data communication is performed in NB-PLC, LP-RF WLC, and hybrid PLC-WLC channels. In addition, the statistical analyses and modeling of the harvested energy are shown, including a comparison between the measured data set and the statistical model of this energy.

- Chapter 4 addresses the hybrid PLC/WLC channel in the dual-hop configuration with the use of four proposed approaches for performing EH and data communication. Also, a comparison among the ergodic achievable data rate attained by the dual-hop hybrid

PLC/WLC channel based on these approaches and the ones yielded by non-hybrid dual-hop channels are detailed and analyzed.

- Chapter 5 shows a novel mathematical formulation of the wasted power of WESs in electric power systems and extends this formulation to the harvested power. As well, the dynamic of the wasted energy during the weekdays and the weekends in a building facility is discussed. Then, the use of the harvested power for supplying low-power data communication devices is analyzed and discussed considering the Brazilian electric power systems.
- Chapter 6 focuses on drafting the conclusion of the previous chapters and indicates future works based on the numerical analyses and discussions of EH from hybrid PLC-WLC channels, hybrid PLC/WLC channels, and from WESs in electric power systems.

2 ENERGY HARVESTING IN ELECTRIC POWER SYSTEMS

The electric power systems were designed to deliver energy from the power plants to the loads and, therefore, such systems concentrate high energy in electric signals flowing through their transmission and distribution lines. However, the energy generated by power plants does not fully reach the loads due to technical losses along the electric power systems infrastructure. In fact, ohmic losses are the main and largest technical losses on electric power systems, which can reach up to 7.5 % of the produced electricity [27]. In addition, the interactions between non-linear loads and electric power systems generate disturbances in electric signals, which causes part of the energy transmitted through the alternating current (AC) mains signal to be shifted to other frequencies in the spectrum and, consequently, to become a kind of wasted energy. Considering that disturbances are composed of time-varying voltage and current signals that result in the creation of time-varying electric and magnetic fields, respectively, the energy in these disturbances can be harvested through capacitive or inductive circuits specifically designed to better take advantage of it. In this sense, the energy reuse, or the EH, of this wasted energy can improve the energy efficiency of electric power systems, while the correct design of the circuitry of EH devices[1] can successfully supply energy to devices in data networks. In this context, this chapter focuses on the possible sources of energy for performing EH in electric power systems and their applications for data communication purposes. Given that discussion, the main contributions of this chapter are:

- Comprehensive discussion of energy harvesting in electric power systems, bringing attention to typical sources of energy in terms of their origins and common EH approaches. Also, the inclusion of WESs as a source of energy for performing EH.
- Introduction of important aspects of electric- and magnetic-field-based EHs based on a typical classification of the electric power systems in terms of voltage levels and on the frequency bands of the spectrum content of electric signals.
- Description about some key aspects of EH devices and how they affect the efficiency of performing EH. Furthermore, a discussion about hybrid configurations of PLC and WLC systems when distinct EH approaches are adopted.

The rest of this chapter is organized as follows: Section 2.1 introduces the fundamentals about energy harvesting in electric power systems; Section 2.2 discusses the EH in terms of the voltage level and the frequency band of electric signals; Section 2.3 focuses on describing the harvesting methods and the main parts of an EH device circuitry. The EH perspective about hybrid configurations of PLC and WLC systems are then covered in Section 2.4, and, finally, Section 2.5 states the summary of this chapter.

[1] In this dissertation, EH devices can perform both energy harvesting and data communication.

2.1 ENERGY HARVESTING

Energy harvesting is defined as the procedure of extracting any form of energy from an external source, which can be *natural* or *artificial*, and converting it to electricity. The natural sources are already in the environment in which the EH device is immersed, and they generate environmental signals, such as sunlight, wind, and geothermal heat. On the other hand, the artificial sources (i.e., man-made sources) require the installation of EH devices next to them, because they are consequences of human or system activities that result in non-environmental signals, for instance, human motion, system vibration, and electromagnetic radiation from RF devices or broadcasting radio stations [28]. Regardless of their types, the main sources of energy for performing EH reported in the literature are light, heat, motion, and electromagnetic radiation [2, 6, 28, 29].

Regarding the electromagnetic radiation, it is established in the telecommunications community that radio-frequency EH (RF-EH) can be subdivided into two distinct approaches that are defined in relation to the source of energy as follows: *ambient EH*[2] or *dedicated EH* [2]. In the former, an EH device harvests its energy from a source that is already present in the environment, but is not intended to deliver energy through it, which can be accomplished through the electromagnetic waves of analog or digital RF signals generated by TV, radio stations (e.g., AM and FM), WiFi devices, Bluetooth devices, and cellular base stations, among others. On the opposite, the latter aims at energizing a particular EH device by means of directional energy transfer in a specific frequency band (e.g., one of the ISM frequency bands), and the EH device has certainty about the existence of another device that is capable of delivering continuous energy towards it. Nowadays, the opportunity of harvesting energy from WLC sources (i.e., from electromagnetic waves) based on EH has been investigated due to the possibility of creating wireless self-sustainable networks [1, 2], and it can allow 5G and 6G data networks to supply energy to a large number of IoT devices.

However, harvesting energy from electromagnetic waves over time may not result in constant power to an EH device due to propagation issues, such as reflection, scattering, and diffraction. Therefore, when there is a necessity for the continuity of energy supply to a device, the importance of electric power systems is undeniable [5]. In these systems, the energy supplying can be mainly obtained from the AC mains signal and, as is emphasized in this dissertation, EH can be applied to disturbances generated by the interactions between electric power systems and non-linear loads as well as by the RF signals induced into electromagnetically unshielded power lines. In fact, plentiful electric and magnetic fields generated from AC mains signal and disturbances are always present in the vicinity of the energized and electromagnetically unshielded power lines, being the disturbances appealing and emerging sources of energy for performing EH.

---

[2] Here, the terms ambient and natural are not related to each other, such that the former is associated with an RF-EH approach and the latter indicates the origin of the source of energy.

Energy harvesting in electric power systems has been usually investigated for powering condition monitoring sensors to ensure their observability by utilities in the occurrence of scheduled or unscheduled shutdowns. Besides the natural sources of energy, the artificial ones that can be used for EH, exclusively in electric power systems, are the electric field (E-field) and magnetic field (M-field) generated by the AC mains signal [30, 31]. These fields are promising for EH purposes due to their strengths and continuous presences in the vicinity of energized power lines. In addition, another interesting source of energy may be the combination of disturbances such as harmonics, interharmonics, supraharmonics, transients, and RF induced signals that are added to the AC mains signal, and is being so-called WES. Taking advantage, or reusing, the energy associated with WESs can bring two benefits to both the environment and the energy efficiency of electric power systems. The former is related to the reduction of global greenhouse gas emissions released during the combustion of fossil fuels while the latter is associated with the reduction of power quality problems because the disturbances in electric signals are one of the main sources of power quality degradation in electric power systems. The existing energy in WESs can be harvested by means of the electric or magnetic field generated by the components of the electric signal different from the AC mains frequency and, thus, it is also considered an artificial source of energy. In other words, EH from WES is similar to the aforementioned E-field and M-field ones; however, EH from WES distinguishes from them by exploiting the energy contained in the frequency spectrum of electric signals outside the AC mains frequency.

It is clear that the EH from artificial sources in electric power systems is performed by exploiting the E-field and M-field produced by electric signals. On the other hand, the EH from natural sources in electric power systems is realized by means of environmental signals, which are not originated from electric signals. Therefore, natural sources can be found in any other context and the focus will be on the specific ones generated by electric signals, the artificial sources. The main requirement for performing EH from artificial sources are controllability and predictability, see Table 1, in which the design of the electric power system is considered to be known and remains unchangeable over time. *Predictability* refers to the degree to which the energy availability of the source approximates of having periodic dynamic during a time interval (e.g., an hour, a day, a week, and so on), while *controllability* refers to the source's capacity of supplying energy for EH when demanded. On one hand, a controllable source is capable of providing harvested energy whenever demanded and, as a consequence, the energy availability does not need to be predicted. On the other hand, an uncontrollable source must have its energy harvested whenever energy is available, thus the energy availability of this kind of source must be predicted if it is possible. In this regard, a prediction model that forecasts energy availability can be used to assist the dynamic of the recharging cycle [32].

Electric field: The electric field energy harvesting (EEH), or capacitive energy harvesting, is the most preferable kind of EH to supply energy to condition monitoring sensors in overhead transmission lines. A time-varying E-field is produced by the AC mains voltage signal

Table 1 – Artificial sources for EH in electric power systems.

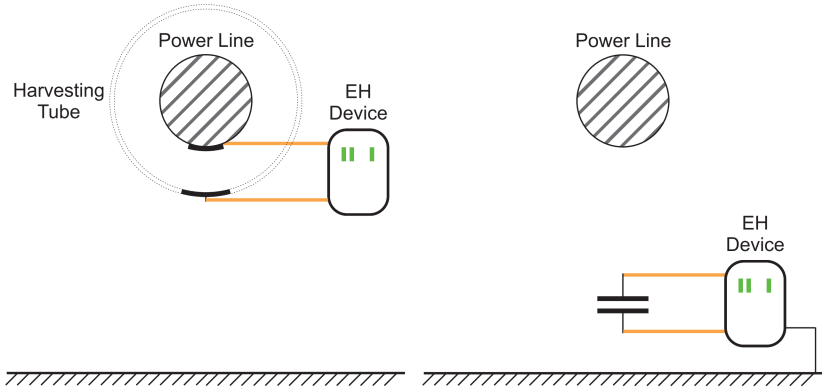
Source	Characteristics	Literature
E-Field	Controllable and predictable	[33–42]
M-Field	Controllable and predictable	[43–49]
WES	Partially controllable and partially predictable	[11–13, 50–52]

Source: Personal collection.

presence on a power line even without a current flow, and according to Maxwell's equation, a time-varying E-field produces a displacement current that can be used to charge a capacitor composed of two conducting plates, with the air being used as the dielectric. When this capacitor is connected to a load, there will be a current flowing through it due to the potential difference and, as a consequence, EEH is accomplished. Based on the fact that the intensity of the stray E-field surrounding the power line decreases with the increase of the distance from the power line, EEH can be subdivided into high- and low- potential approaches. In the former, the capacitor is near the power line while in the latter it is near the ground as illustrated in Figure 1, in which the high- and low-potential EEH can be seen, respectively, in (a) and (b). The high-potential approach assumes that the EH device is inside the harvesting tube, which is coated with an electrical conductor material and clamped to the power line. In this approach, the capacitor can be either produced by the equivalent capacitance between the power line and the harvesting tube or formed by two plates, in which one is connected to the power line and the other is in the harvesting tube. If the two plates are adopted, then two equivalent capacitances are created: i) between the two plates and ii) between the lower plate of the capacitor and the ground. In the low-potential approach, the EH device is connected to the two plates of the capacitor and grounded, resulting in two equivalent capacitances: i) between the power line and the upper plate of the capacitor and ii) between the two plates. Note that, in both approaches, the two equivalent capacitances are in series, thus they are used as voltage dividers. It is noteworthy to mention that if the voltage signal is a direct current (DC) one, then there will be a constant E-field, which does not generate a displacement current and EEH will not be produced.

Magnetic field: The magnetic field energy harvesting (MEH), or inductive energy harvesting, consists basically of a ferromagnetic core and a coil, that is wired in the core. The core is responsible for concentrating the time-varying magnetic flux from the stray M-field produced by the current flowing in the power line. According to Maxwell's equation, the time-varying magnetic flux in the core induces a voltage between the terminals of the coil. When the coil terminals are connected to a load, a current will flow through it and MEH is realized. The time-varying M-field is produced by the oscillation associated with the AC mains current signal flowing through a power line. In this case, the flowing current is a necessary condition and the variations experienced in the AC current signal implies on the variation of the M-field. For instance, the connection and disconnection of loads and other similar events (e.g., lightning

Figure 1 – Electric field energy harvesting.

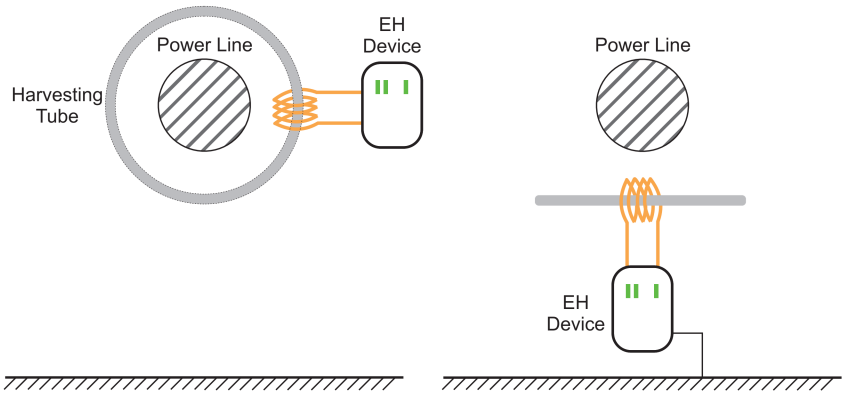


(a) High-potential EEH (b) Low-potential EEH

Source: Personal collection.

and failures) in electric power systems may result in large amplitudes for the AC current signal, therefore, the M-field around power lines can vary greatly from time to time. Due to the fact that the intensity of the M-field decays with the increasing distance from the power line, MEH can be subdivided into high- and low- potential approaches, according to the proximity between the ferromagnetic core and the power line. In the former, the ferromagnetic core usually has a ring shape and it is clamped in the section of the power line through the harvesting tube while the latter adopts the conventional cylindrical-shaped ferromagnetic core, which is placed off the power line. These approaches are shown in Figure 2, where the high- and low-potential MEH can be seen, respectively, in (a) and (b). Alternative ferromagnetic core shapes and their influence on the magnetic flux concentration were studied in [44]; however, it is important to emphasize that a DC current signal generates a constant M-field, which results in constant magnetic flux in the core that does not induce voltage between the terminals of the coil and MEH is not accomplished.

Figure 2 – Magnetic field energy harvesting.



(a) High-potential MEH (b) Low-potential MEH

Source: Personal collection.

Wasted electric signal: Both EEH and MEH were investigated in electric power systems aiming at harvesting the energy associated with AC mains voltage and current signals, respectively. However, it is possible to supply energy from the components of electric signals outside the AC mains frequency, which may own enough energy to supply low-power consumption devices (e.g., IoT devices). Disregarding the AC mains frequency and considering a telecommunications perspective, the covered frequency spectrum content that is eligible for EH purposes comprehends the so-called PLC additive noise [53], which is equivalent to the disturbances in electric signals. The well-known disturbances off the AC mains signal are harmonics, interharmonics, supraharmonics, and transients as well as RF signals induced into power lines because the majority of power lines are electromagnetically unshielded. These disturbances are seen as sources of power quality problems in the electric power systems and also considered unwanted interference in PLC systems. In this sense, the recovery of the PLC additive noise's energy, or WES EH (WEH), can be useful for improving power quality in electric power systems, supplying energy to PLC systems, and enhancing the PLC system performance. The definitions of WES and WEH to denote, respectively, the disturbances in an electric signal and their EH allow to pay attention to the fact that the energy associated with disturbances in electric signals is a kind of wasted energy, and, as a consequence, it is free of charge. Note that WESs are strongly related to the content of PLC additive noises because such noises are equal to the disturbances in electric signals. Consequently, the energy contained in the PLC additive noise can be harvested by means of WEH, which can be based on E-field or M-field. For the sake of simplicity, the term PLC additive noise will be intermittently used with WES from now on.

2.2 CLASSIFICATION OF ENERGY HARVESTING

This subsection discusses two perspectives for classifying EH in electric power systems and highlights important advantages and drawbacks of EEH, MEH, and WEH. It is expected that electric power systems present distinct characteristics and faces different problems in terms of constructions, geographical coverages, and purposes. Also, electric signals in these systems present a variety of components on their spectrum content depending on the frequency band. Therefore, EH in electric power systems is first classified according to the voltage levels of the AC mains voltage signal, and then the frequency bands of the spectrum content of electric signals are used to classify the EH.

2.2.1 Voltage Level

The classification of electric power systems based on the voltage level, see Table 2, is also applied to classify EH in these systems. In short, the EEH is widely studied in the HV [33–36] and MV [36–39] power lines while the MEH is most investigated in the HV [43–46] and LV ones [48, 49]. Regarding LV, MEH was adopted rather than EEH in the past due to size constraints [39] and EEH uses in LV power lines are recent [40]. In fact, due to the low potential

of EEH in LV, the EH device would have a dimension that could not be interesting in order to harvest a sufficient amount of energy for feeding them [30] and this was overcome by placing a conductive sheath around the power line or by using a multi-layer harvesting structure to increase the displacement current obtained from the stray E-field [40–42]. Different from EEH and MEH, WEH is mostly exploited in LV power lines [51,52] because the connection between the EH device and either one of HV or MV power lines demand a more complex and expensive coupling circuit than the one for LV power line due to the necessity to attenuate the effects of the AC mains signal, and also because it is more convenient to harvest the energy of WESs near the loads that are mainly connected to LV power lines [54]. As a major advantage, the WEH may offer a cost-effective solution because the physical connection can be easily established between the EH device and the power outlet in an LV indoor facility.

Table 2 – Voltage level classification of electric power system.

Classification	**Voltage Level**	**Geographical Range**
HV	69 – 230 kV	< 500 km
MV	1 – 69 kV	5 – 25 km
LV	< 1 kV	< 500 m

Source: Personal collection.

2.2.1.1 High-voltage level

HV electric power systems, or electric power transmission systems, as illustrated in Figure 3, operate with AC mains voltage levels typically in the order of tens and hundreds of kilovolts (69 – 230 kV), covering distances from several dozen to hundreds of kilometers (up to 500 km) because they are responsible for connecting power generation stations to distribution stations. In these levels, power lines have energy losses due to heating, leakage, and corona effects [55]. The transmission lines are usually overhead (aerial) and electromagnetically unshielded power lines.

The most investigated kinds of EH in these systems are the EEH [33–36] and MEH [43–46] due to the high potential associated, respectively, with AC mains voltage and current signals. Furthermore, the use of WEH (i.e., the EH of PLC additive noise) may not be practical in these systems due to the expensive coupling related to the use of special components necessary to withstand high differential voltages [54]. However, the impact of large-scale penetration of distributed generation in these systems may result in a power quality issue due to the harmonics and interharmonics presence, in which WEH can take advantage of it, by harvesting the energy present in them. As a consequence, this voltage level constitutes the most expensive and complex environment to deal with; however, transmission lines may be potential candidates for WEH in the future because of the presence of distributed and renewable power plants connected to the electric power transmission systems.

Figure 3 – Electric power transmission system.



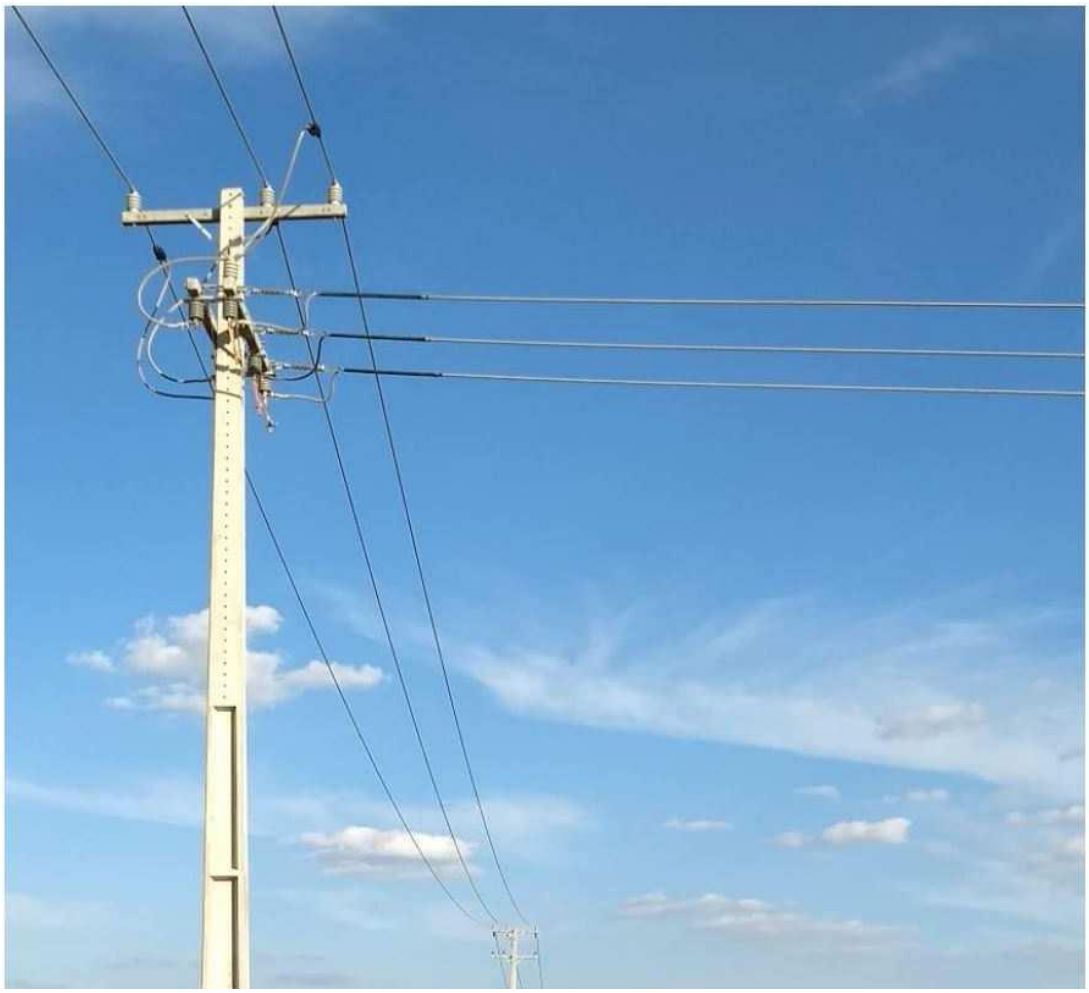
Source: [56].

2.2.1.2 Medium-voltage level

Electric power distribution systems in the MV level have AC mains voltage levels up to dozens of kilovolts ($1 - 69$ kV), spanning a few kilometers ($5 - 25$ km). They connect the distribution stations to the pole-mounted transformers and are used to supply electric energy to rural areas, cities, industries, and companies [55]. The MV power lines can be underground or overhead ones, being overhead power lines electromagnetically unshielded and widely deployed while the underground power lines are typically shielded for being resistant to corrosion and mainly used in high-density downtown areas. A picture of an overhead electric power distribution system is shown in Figure 4.

In terms of EH, MV electric power systems are mostly investigated for EEH [36–39] rather than MEH [47]. Indeed, a hybrid EH solution composed of thermal, mechanical, and M-field EHs was designed to harvest a constant amount of energy from a MV busbar over time, see [47]. Similar to the HV power lines, the AC mains voltage signal in the MV power lines can be predicted as they are designed to operate at a specific level and, disregarding natural or artificial incidents, are not subject to great variations over time. Also, MV electric power systems usually encompass the distributed generation and are cheaper to perform coupling than the HV ones [54], which can make WEH more interesting in the MV electric power systems than in HV ones. For instance, [50] investigated the WEH potential of MV power lines in the urban and rural environments and showed the usefulness of the energy contained in the PLC

Figure 4 – Electric power distribution system.



Source: [57].

additive noise for feeding low-bit-rate devices.

2.2.1.3 Low-voltage level

Electric power distribution systems in the LV level employ AC mains voltage levels below a kilovolt (< 1 kV), running over distances of a few hundred meters (up to 500 m), and connecting the pole-mounted transformers to individual households as well as appliances and electrical equipment in predial, residential, industrial, and commercial electrical circuits [55]. The LV power lines are electromagnetically unshielded and are used in indoor (e.g., residencies and buildings), outdoor (from transformers to individual households), and in-vehicle facilities (e.g., car, ship, and airplane).

Regarding EH in indoor facilities, the LV power lines are appealing for WEH due to the easy physical connection of an EH device to a power outlet [51] and low-cost coupling [54]. Moreover, the interaction of non-linear loads (e.g., appliances, motors, and others) and the LV electric power systems generate disturbances, and, consequently, a high amount of energy is

expected outside the AC mains frequency. The MEH in LV electric power systems is much more subject to time variations due to the dynamic of loads connected to them. In other words, the variety of loads, as well as their dynamics (e.g., connection/disconnection), make the AC current flowing through LV power lines less predictable in terms of voltage level. The literature shows that MEH can be applied to both indoor and outdoor facilities [48, 49] while the same can be stated for EEH [40–42]. Due to the high energy of the disturbances contained in the frequency content of the spectrum outside the DC frequency[3], electric cars [58], cruise ships [59], and other in-vehicles may be interesting for WEH as well.

2.2.2 Frequency Band

Another way to classify EH in electric power systems is in terms of the frequency band. This classification contemplates EEH, MEH, and WEH because they make use of circuitry that is responsible for performing EH, which is tuned with respect to the chosen frequency (or frequency band) of electric signals flowing through power lines. In this regard, well-established frequency bands in the PLC community are adopted to encompass the EH potential of distinct components of disturbances in power lines. The adopted frequency bands are listed in Table 3 and a brief description of them is given as follows:

Table 3 – The frequency bands from PLC systems.

Technology	Frequency Band	Data Rate	Distance Coverage
BB-PLC	1.7 MHz - 250 MHz	$<$ 1 Gbps	$<$ 500 m*
NB-PLC	3 kHz - 500 kHz	$>$ 500 kbps	$>$ 20 km
UNB-PLC	30 Hz - 3 kHz	$\leq$ 120 bps	$>$ 150 km

Source: Personal collection.
Note: *Although most of applications falls in this range, a 8 km BB-PLC link has been successfully tested in the US [60].

Broadband-PLC: The BB-PLC system is designed to operate in the frequency band from 1.7 MHz up to 250 MHz with a data rate up to 1 Gbps [61]. Although the research activities focus on the aforementioned frequencies, the BB-PLC standards and technologies usually adopt a shorter frequency bandwidth. For instance, the BB-PLC technology is upper bounded by the frequency of 30 MHz by European Committee for Electrotechnical Standardization (*Comité Européen de Normalisation Électrotechnique* in French) (CENELEC) [62], 86 MHz in accord with the ITU-T G.hn and HomePlug AV2 standards [63, 64], and 100 MHz in the IEEE 1901 standard [65]. Due to the wide frequency bandwidth, the BB-PLC system faces high attenuation with both distance and frequency, such that it can achieve data communication with a typical distance up to 500 m between transmitter and receiver. The applications covered by the main BB-PLC standards are summarized in Table 4.

[3] The common voltage signals for in-vehicle facilities are DC ones.

Table 4 – Broadband-PLC standards.

Standard	Main Applications
HomePlug 1.0 [66]	Home area networks
HomePlug AV [67]	Multimedia
HomePlug AV2 [64]	Multimedia
HomePlug GP [68]	Smart things*, in-vehicular, multimedia
IEEE 1901 [65]	Smart things, in-vehicular, multimedia
HD-PLC [69]	Smart home
ITU-T G.hn [63]	Smart things, in-vehicular
ITU-T G.hn-MIMO [70]	Home networks

Source: [71].
Note: **Smart things* encompass smart grids, smart cities, and so on.

Narrowband-PLC: The NB-PLC system comprises the technologies that operate in the frequency band from 3 kHz up to 500 kHz. NB-PLC systems can be categorized as low-data-rate or high data-rate ones. The former is related to a single-carrier scheme that achieves data rates of few kilobits per second, while the latter is associated with multi-carrier systems capable of achieving data rates over 500 kbps [61]. Furthermore, distinct frequency bands are used around the world, for instance, Europe standardized the use of NB-PLC in the CENELEC band (3 – 148.5 kHz) [62], the United States (US) standardized the Federal Communications Commission (FCC) band (10 – 490 kHz) [72], Japan adopted the Association of Radio Industries and Businesses (ARIB) band (10 – 450 kHz), while China adopted the Chinese band (3 – 500 kHz). Due to the short frequency bandwidth covered by NB-PLC systems in relation to the BB-PLC one, NB-PLC systems are less subject to attenuations and, thus, they can establish data communication in link with more than 20 km of distance between transmitter and receiver. The applications related to the main NB-PLC standards are shown in Table 5.

Table 5 – Narrowband-PLC standards.

Standard	Main Applications
IEEE 1901.2 [73]	Smart things, in-vehicular
G3-PLC [74]	Smart things, in-vehicular
ITU-T G.hnem [75]	Smart things, in-vehicular
PRIME [76]	Smart things

Source: [71].

Ultra-narrowband-PLC: The ultra-narrowband-PLC (UNB-PLC) system operates in

the upper part of the super-low frequency (30-300 Hz) band or in the ultra-low frequency (0.3-3 kHz) band and offers data rates up to 120 bps [7]. The main advantage of it is the long-distance coverage (150 km or more). Most of UNB-PLC systems transmit the data during zero crossings of the AC mains voltage signal because it avoids being affected by the high amplitude of AC mains signal. Some examples are the automatic meter reading (AMR) Turtle System, which is capable of transmitting data at extremely low speed ($\sim$ 0.001 bps), and the two-way automatic communications system (TWACS), which can transmit data at a maximum data rate of two bits per cycle of the AC mains signal, i.e. 100 bps in Europe and 120 bps in North America or Brazil [7]. It is important to mention that no standards were developed for UNB-PLC technology and their commercial solutions are proprietary.

At this point, it is important to emphasize that the definition of ambient and dedicated EH approaches from RF-EH can be extended to more general applications and environments from a telecommunication perspective. In other words, the ambient EH approach will be used to refer to the EH applied to the additive noise of data communication media, while the dedicated EH approach will stand for the EH performed in both the additive noise and the free-of-noise (FoN) received signal from a data communication media. For instance, the dedicated EH approach applied to a wireless medium can take advantage of both WLC additive noise and FoN received signal. In the manner it was defined, the ambient EH approach applied to WES corresponds to the harvesting of the PLC additive noise by an EH device, which is exactly the same as what was previously defined as WEH. However, the use of a dedicated EH approach in power lines results in the harvesting of both PLC additive noise and FoN received signal and the harvested energy is expected to be greater than in the wireless medium because the high power nature of the PLC additive noise.

Note that the higher is the occupied frequency bandwidth by a PLC system, the higher is the lower bound frequency of its frequency band, and, as a consequence, few high-amplitude components of disturbances, which are mainly related to the AC mains signal and loads' dynamics, are present in this frequency band. Also, a wide frequency bandwidth implies that a numerous variety of RF induced signals are encompassed and, therefore, the harvested energy from the disturbances in electric signals may be large in a wide frequency bandwidth. Grounded on these discussions, the use of distinct frequency bands for EH in power lines may present different advantages and drawbacks, thus four frequency bands can be proposed to easily highlight these features. These suggested frequency bands are described as follows:

- *AC mains frequency*: The AC mains frequency is 50 or 60 Hz depending on the country and its purpose is to deliver energy to loads. As a matter of fact, the energy associated with it is the highest one in comparison to any other spectral components. Therefore, both E-field and M-field associated with the AC mains signal are strong in the vicinity of a power line. Naturally, the EEH and MEH were designed to harvest the energy generated by, respectively, the E-field and M-field of the AC mains signal.

- *UNB-PLC spectrum*: Assuming the AC mains frequency equal to 50 or 60 Hz, this frequency band covers the spectrum content from the 2^{nd} up to the 60^{th} or 50^{th} harmonic component of the voltage signal, interharmonics, and the lower part of the supraharmonics[4]. Note that this frequency band presents the lower frequency bandwidth in comparison to the ones used by any other PLC system. Also, this frequency band is appealing for WEH because the frequency proximity between harmonic components and AC mains frequency may result in a high amount of harvested energy to the EH device. Regarding the use of WEH, some low-frequency PLC additive noise components can be harvested in this frequency band, such as the low-frequency colored background, periodic and non-periodic impulsive ones [55, 77–79]. As previously mentioned, most of the UNB-PLC systems perform data communication around zero crossings of the AC mains voltage signal and, therefore, the presence of UNB-PLC signals and disturbances due to the loads' dynamics is periodic and does not occur simultaneously over time. The data communication results in energy at the EH device that comes from the UNB-PLC signal that traveled through power lines while the disturbances in electric signals generate the energy contained in the UNB-PLC additive noise. If a dedicated EH approach is adopted, then the EH device could take advantage of this non-simultaneously occurrence between the data communication and disturbances in electric signals to harvest a constant amount of energy over time.

- *NB-PLC spectrum*: The majority of the supraharmonics components are concentrated in the lower frequencies related to the NB-PLC systems. With the exception of the narrowband and high-frequency colored background noises, the WEH in the NB-PLC frequency band can harvest energy from any components of the PLC additive noise. In fact, the spectral content of the disturbances in electric signals in the frequency band related to NB-PLC systems has an interesting EH potential, especially due to the colored background noise that presents a high power below 500 kHz. Furthermore, WEH can be designed to encompass the frequencies from 500 kHz to 1.7 MHz, which is the frequency band gap between BB-PLC and NB-PLC technologies, because it allows to harvest the energy from AM signals (narrowband noise) induced into power lines. If a dedicated EH approach is used, then an EH device could also take advantage of the frequency selectivity of the NB-PLC channel to optimize power transmission. In other words, a NB-PLC transmitter device could allocate the power to the subchannels that present the lowest attenuations and, thus, the received signal by the EH device would have a large amount of energy.

- *BB-PLC spectrum*: This frequency band covers some high-frequency PLC additive noise components, specifically a broadband spectral content of electric signals related to the BB-PLC systems is due to RF signals induced in power lines (narrowband noise) from

[4] Supraharmonics are the disturbances in electric signals with frequencies between 2 kHz and 150 kHz.

the radio broadcasting stations, amateur citizen radios, broadcasting TV stations, and so on. Due to the wide frequency bandwidth of this frequency band, it can be expected that a numerous variety of narrowband disturbances are present in it and, thus, the energy obtained from this spectrum is expected to be high. Similar to NB-PLC systems, BB-PLC ones could be designed to perform WEH to harvest energy from AM signals in the lower part of this frequency range ($0.5 - 1.7$ MHz in America) as well as from the FM signals in the higher part of this frequency band ($88 - 108$ MHz in America). If the dedicated EH approach is considered, then the received BB-PLC signal, which traveled through the BB-PLC channel, by an EH device can be seen as a source of energy as well. In this regard and similar to NB-PLC systems, optimum power allocation techniques could be used to improve the energy harvesting process by an EH device because of the frequency selectivity of BB-PLC channels. Also, if a BB-PLC system allocates the power in the lower frequencies of the spectrum, which impose the lower attenuations in a BB-PLC signal, then more energy would be harvested by the EH device.

2.3 HARVESTING ARCHITECTURES AND CIRCUITRY

Unlike the usual loads that are connected to the electric power systems for energy supplying through the AC mains signal, the EH-based supplying devices count with the energy obtained from an artificial or natural source, in which the former can be harvested at any time while the latter may be intermittent over time. In order to carry out the energy harvesting process, an EH device can make use of three typical harvesting methods: *harvest-use*, *harvest-store-use*, and *harvest-use-store*, which are briefly outlined as follows [6, 80]:

- *Harvest-use*: The harvested energy is immediately used to supply the EH device. In other words, there is no buffer to store the harvested energy for future use, and the normal operation of the EH device over time requires that the harvested energy constantly exceed the minimum demand. Otherwise, this device will not be able to operate and it will stay in sleep mode or turned off.

- *Harvest-store-use*: The harvested energy is initially stored in the buffer (energy storage element) and then it supplies a given device. If the harvested energy surpasses the EH device's energy consumption at any time, then the energy excess is stored in the buffer for future use. A drawback is that the self-discharging feature of the energy storage element can negatively affect the stored energy.

- *Harvest-use-store*: This method counts with two energy storage elements. The harvested energy is temporarily stored in one energy storage element and can be used immediately on demand by the EH device, while the remaining energy is transferred to another energy storage element for later use. Note that this method is the most complex one due to energy management and can result in high relative energy losses.

In the era of the IoT, many low-power consumption devices that intermittently exchange data are connected to data networks, and consequently, they can perform scheduled or unscheduled data communication over time. Note that the unscheduled data communication can occur over user demand or anytime that an EH device has achieved energy that exceeds the minimum energy demand in order to perform data communication. If scheduled data communication is used, then the preferable harvesting methods would be the harvest-store-use and harvest-use-store ones because they guarantee the necessary energy whenever data communication needs to be performed. However, an EH device that uses unscheduled data communication would adopt any of the harvesting methods. It is important to emphasize that this discussion also depends on the predictability of the chosen source of energy for performing EH. For instance, if WEH is used, then the dynamics of harvested energies associated with wasted powers during the weekdays present a cyclostationary behavior as is emphasized in Chapter 5 of this dissertation, and, as a consequence, the energy harvested by the EH device can be predicted, such that the harvest-use method could be used at any time the harvested energy is greater than an energy threshold, which is used to start the data communication by an EH device.

Based on the fact that the main application of EH is to feed low-power consumption devices that are capable of intermittently transmitting data in low-bit-rate sensor networks, which can be based on wireless or wireline media (e.g., air and power lines), the combined use of EH and data communication is a powerful approach to come up with effective and efficient low-bit-rate sensor networks. When data communication and EH occur in the same frequency band, it is called *in-band* strategy, while the data communication and EH occurrence in distinct frequency bands is named *out-of-band* strategy. The former benefits from less complex circuitry, which is used for both EH and data communication, while the latter is more complex because the circuitry for EH and data communication are independent of each other. Despite the energy availability of a specific source of energy, the full potential of EH can only be achieved if the circuitry responsible for harvesting the energy offers high efficiency. In other words, this circuitry needs to optimally take advantage of the AC input power in the EH device, by using low-power losses components in the circuitry. In this regard, Figure 5 shows the block diagram of a typical EH device circuitry, where its main parts are represented by blocks that offer individuals efficiency factors, which are detailed in [80, 81].

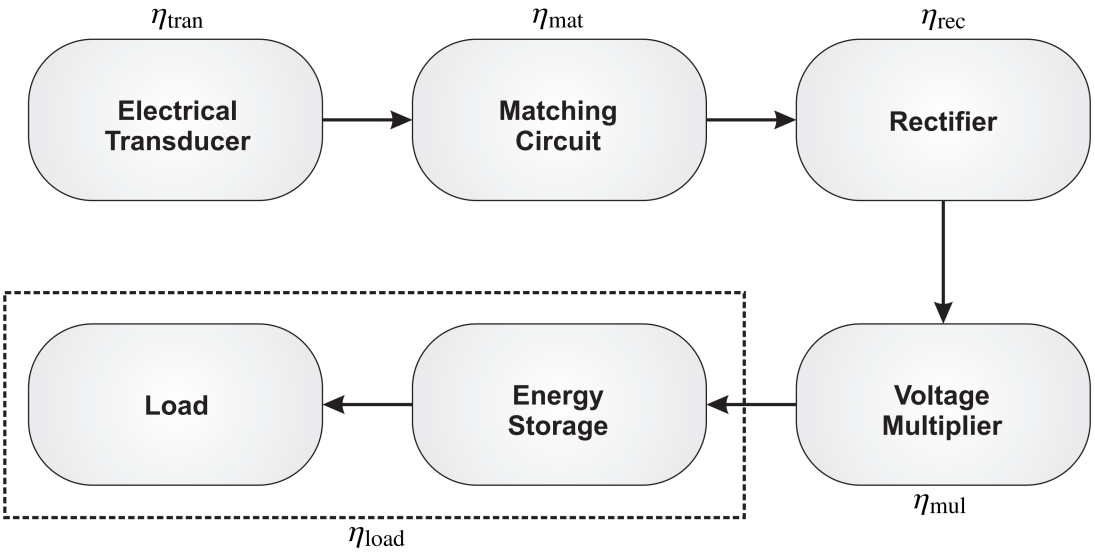
The overall efficiency factor[5], $\eta \in \mathbb{R}_+$, $1 \geq \eta > 0$, of the EH device circuitry is given by [81]

$$\eta = \frac{\text{DC output power}}{\text{AC input power}}, \tag{2.1}$$

in which the DC output power is the power delivered to the load and the AC input power is the received power at the input of the EH device. The circuitry that turns the AC input power into the DC output power counts with the electrical transducer, matching circuit, rectifier, voltage multiplier, and energy storage. Note that the load can represent a data communication module,

[5] Usually, it is called RF-to-DC efficiency (or conversion) factor in wireless EH [80].

Figure 5 – Block diagram of an EH device circuitry.



Source: Personal collection.

among others.

Electrical transducer (η_{tran}): The electrical transducer is the part of the EH circuitry that converts an AC input power associated with the time-varying E-field or M-field, radiated from the power line, into an AC voltage signal. Note that EEH and MEH are accomplished by using a capacitor and an inductor, respectively, while WEH is implemented by using the usual PLC coupling circuit, which can be inductive or capacitive [54].

Matching circuit (η_{mat}): The matching circuit is responsible for realizing the impedance matching, and, as a consequence, maximizing the power transfer between the electrical transducer and the rectifier. It is a resonator circuit usually composed of reactive components as capacitors and inductors operating at the desired frequency band, in which the efficiency of the impedance matching is designed to be high at the used frequency band. It is noteworthy to mention that this part of the EH circuitry is complex since the dynamics of access impedances in electric power systems is a challenging problem to deal with [82].

Rectifier (η_{rec}): The general purpose of a rectifier is to make the conversion of AC voltage signals into DC voltage ones. It is usually composed of diodes and capacitors. The most common circuits in the literature are half-wave, full-wave, and bridge rectification. Also, the Schottky diodes are preferred in the rectifier circuits due to their low forward-voltage drop, low-power consumption, low parasitic effects, and high switching speed [81].

Voltage multiplier (η_{mul}): The voltage multiplier is used to increase the output DC voltage level of the rectifier, which may be not sufficient to drive a device or to store in a battery. As it is composed of capacitors and diodes, high-efficiency factors can be achieved in the voltage multiplier by using diodes with a low forward-voltage drop (i.e., Schottky diodes). The capacitor ensures the smooth delivery of power to the load or energy storage element and it can also serve as a short-duration energy reserve when energy is unavailable at the input of the EH device.

Energy storage or load (η_{load}): The last part of the EH circuitry is responsible for storing or consuming the DC output power. If the *harvest-use* method is used, then the load will be directly connected to the voltage multiplier, and, as a consequence, the efficiency factor depends upon the impedance matching between load and voltage multiplier circuit. However, if either *harvest-store-use* or *harvest-use-store* methods is applied, then the energy storage takes place before its consumption. In this case, the efficiency factor is also affected by the self-discharging feature of the energy storage element. The energy can be stored by batteries, supercapacitors, or a combination of them [81].

In the way it was described, the overall efficiency factor can be modeled by

$$\eta = \eta_{\text{tran}}\ \eta_{\text{mat}}\ \eta_{\text{rec}}\ \eta_{\text{mul}}\ \eta_{\text{load}}. \tag{2.2}$$

As a numerical example, the overall efficiency factor for wireless EH devices can vary from 0.15 up to 0.83 [81]. It is noteworthy that it depends on many parameters such as the AC input power, the operational center frequency, the frequency bandwidth, the load impedance, and so on. Generally, the higher the AC input power, the higher is the overall efficiency. For low AC input power levels, the overall efficiency factor can even drop to zero because the diodes' forward-voltage drop of both rectifier and voltage multiplier circuits can be high in comparison to the AC voltage signal at the output of the electrical transducer.

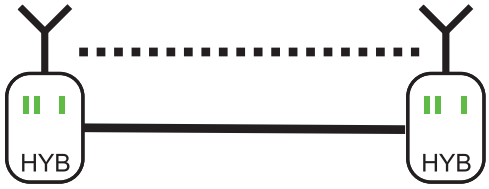
2.4 HYBRID COMMUNICATION POSSIBILITIES

Nowadays, the necessity of advances in data communication pushes forward the development of hybrid data communication systems [21, 22, 83]. Although an improvement in data communication through the individual use of power line or wireless medium can be attained with cooperative protocols [84–87], the exploitation of the existing diversity between both media [15] can offer remarkable benefits to the low-bit-rate applications (e.g., flexibility and reliability). As a signal carrying information can be seen as a source of energy as well, many possibilities of using EH emerge when hybrid data communication systems are used. In the following, it is described the two possible configurations for hybrid systems based on the combination of PLC and WLC ones.

- *Parallel configuration*: In this case, both data communication media are used simultaneously in order to increase the reliability or the data rate in comparison to non-hybrid data communications. The former occurs when the same information is transmitted through both media and the latter when distinct information is transmitted through each medium. In this configuration, the arrival of signal carrying information at the receiver device is more certainly as one of the media can be drastically affected by temporary interferences while the other keeps in a good condition and vice-versa. As shown in Figure 6, the parallel configuration of PLC and WLC systems, results in the so-called hybrid PLC/WLC system. Here, the hybrid PLC/WLC device uses distinct frequency bands in PLC and

WLC and relay devices are usually associated with this configuration. This configuration was extensively investigated in [16–18, 20–22, 88–91].

Figure 6 – Parallel configuration (hybrid PLC/WLC system).

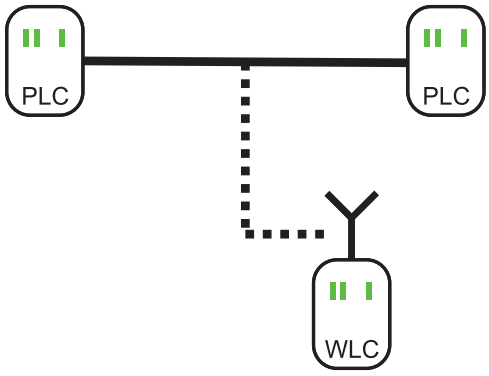


Source: Personal collection.
Note: The continuous and dashed lines represent, respectively, the power line and wireless media.

As the hybrid PLC/WLC device is capable of communicating through two different media, it can harvest energy from four distinct sources in a dedicated EH approach: i) PLC FoN received signal; ii) PLC additive noise; iii) WLC FoN received signal and; iv) WLC additive noise. On the other hand, an ambient EH approach includes only additive noises from power line and wireless media. In this sense, this configuration may guarantee an effective energy transference between data communication devices. It is important to highlight that, in this case, a hybrid PLC/WLC device can simultaneously perform data communication in one medium while making EH in another one, resulting in a continuous activity of this device.

- *Concatenated (cascade) configuration*: This is a recent configuration of a hybrid data communication system. Here, the signal transmitted by a device in one data communication medium is radiated and sensed by another one that is designed to operate in other data communication medium, but in the same frequency band. This results in a novel data communication medium, which is the so-called concatenated hybrid PLC-WLC medium because it combines the power line and wireless media. According to [26], an illustration of this configuration is shown Figure 7. Here, the signal carrying information (transmitted signal) can travel in two possible and opposite directions because the same frequency band is used for data communication by both PLC and WLC devices, which is supposed to be in the baseband. In the first direction, which is named PLC-to-WLC (PLC $\rightarrow$ WLC), the transmitted signal is injected into the power line by a PLC device through a PLC coupler and, posteriorly, its distorted version is captured by a nearby WLC device using an antenna that is capable of sensing the energy radiated by electromagnetically unshielded power lines. On the other hand, the signal injected into the air by a WLC device with the use of an antenna is induced into the power line and the induced signal is later extracted from the power line by the PLC device, defining the so-called WLC-to-PLC (WLC $\rightarrow$ PLC) direction. The literature on this configuration can be seen in [26, 52, 61, 92–94].

Figure 7 – Concatenated configuration (hybrid PLC-WLC system).



Source: Personal collection.
Note: The continuous and dashed lines represent, respectively, the power line and wireless media.

Assuming a dedicated EH approach and the PLC→WLC direction, the EH can occur, at the receiver device, in both WLC FoN received signal and additive noise. On the other hand, the receiver device of the WLC→PLC direction can take advantage of both the PLC FoN received signal and additive noise. Interestingly, the data communication device that was not intended to be directly participating in the data communication can also take advantage of it. For instance, the left PLC device in Figure 7 is communicating with the WLC device. However, the right PLC device is capable of energizing itself by means of both PLC FoN received signal and additive noise due to the broadcasting nature of power lines.

If a relaying EH device is considered, either one of the *in-band* or *out-of-band* strategy can be used in tandem with any of the aforementioned configurations. As a matter of fact, the use of a relay is necessary for the adoption of any strategy because both strategies depend on the device performing both EH and data communication in a single medium, which is not the case of any EH device in the previously presented configurations. For instance, the concatenated configuration could consist of a WLC (EH) receiver device that harvests its energy from the electromagnetic wave radiated from the electromagnetically unshielded power line (baseband) and, then, it could realize data communication to another WLC (EH) device in one of the ISM frequency bands. On one hand, the *in-band* strategy consists of a single circuitry for both EH and data communication, thus the commutation between these two purposes is necessary. In this case, the EH device depends upon the use of an energy storage element and the data communication only reaches a reduced data rate. On the other hand, if the *out-of-band* strategy is adopted, then independent circuits for EH and data communication are used, and the use of an energy storage element is not required. Therefore, the data communication could be continuous and a higher data rate is expected in comparison to the previous strategy.

Based on the presented discussion, Chapter 3 addresses the dedicated EH in the hybrid PLC-WLC system, based on a data set obtained from LV electric power systems in the BB-PLC spectrum, when *in-band* and *out-of-band* strategies are adopted. Moreover, Chapter 4 investigates the dedicated EH in the hybrid PLC/WLC system, by means of a LV power line channel model in the frequency band of the NB-PLC spectrum, with the use of *in-band* strategy. Then Chapter 5 estimates the energy potential of WEH, based on a data set measured from the LV power lines in the UNB-PLC spectrum, for feeding up low-power data communication devices when *out-of-band* strategy is adopted. All of the aforementioned studies implement the *harvest-store-use* method in the EH device.

2.5 SUMMARY

This chapter presented a comprehensive discussion about energy harvesting in electric power systems. In this context, it introduced energy harvesting classifications according to the voltage levels of the AC mains voltage signal and frequency bands of the spectrum occupied by the electric signals. Furthermore, it detailed energy harvesting architectures and the efficiency associated with the main parts of an EH device circuitry as well as the possible hybrid PLC and WLC system configurations for performing EH.

3 DEDICATED ENERGY HARVESTING IN HYBRID PLC-WLC SYSTEMS

The advance of energy-efficient and self-sustainable data networks is a trend that is highly related to SG, the IoT, and Industry 4.0. As part of this trend, telecommunications technologies are being investigated, specified, and designed to be flexible and adaptable. In this sense, the use of cognitive, full-duplex, massive multiple-input multiple-output (MIMO), cooperative communication concepts that are capable of optimizing channel resource usages is being deeply investigated. However, the evolution of these technologies collides with limitations on the available sources of energy at untethered terminals. In order to explore the full potential of EH in indoor facilities, this chapter addresses the dedicated energy harvesting in hybrid PLC-WLC[1] systems. Aiming to provide a comprehensive investigation of energy harvesting in these hybrid PLC-WLC systems, this chapter focuses on the additive noise's energy as well as the energy coming from the signal that traveled through hybrid PLC-WLC channels, which is so-called free-of-noise (FoN) received signal. In this regard, some power masks are considered for evaluating the effectiveness of harvesting energy in these systems when the dedicated EH approach applies. Concisely, the main contributions of this chapter are as follows:

- Formulation of FoN received signals and additive noises of the hybrid PLC-WLC channel in terms of the harvested energy, the expected harvested energy, and the average time interval to achieve a specified amount of energy at the receiver side by considering the PLC $\rightarrow$ WLC and WLC $\rightarrow$ PLC directions. Also, the introduction of five transmission power masks to harvest energy from the FoN received signals that traveled through hybrid PLC-WLC channels.

- Based on a measured data set of in-home hybrid PLC-WLC channels, which are associated with two relevant sets of distances between the WLC device and the power line, a comparative discussion about the energy contributions of the FoN received signal and the additive noise in the PLC $\rightarrow$ WLC and WLC $\rightarrow$ PLC directions is presented. Moreover, the use of these energies to perform data communication through NB-PLC and LP-RF WLC channels is evaluated by means of ergodic achievable data rates. As well, similar ergodic achievable data rate analysis is performed when the hybrid PLC-WLC channel is used as both the source of energy and the data communication medium.

- Introduction of statistical models of the harvested energy from the FoN received signal, the additive noises, and the total received signal, based on the maximization of the log-likelihood value (LLV) statistic criterion. Also, comparisons among the complementary cumulative distribution functions (CCDFs) related to the harvested energy obtained from the proposed statistical model and the measured data set in the PLC $\rightarrow$ WLC and WLC $\rightarrow$ PLC directions, when distinct power masks and two typical distance ranges of the WLC device from the power line are considered.

[1] The use of a hyphen between PLC and WLC means that the concatenation takes place.

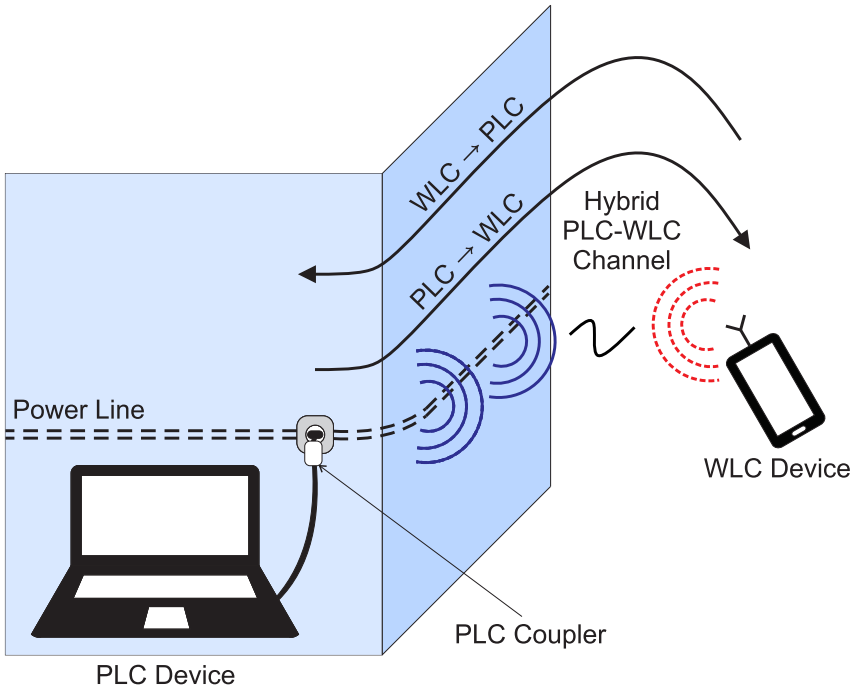
The rest of this chapter is organized as follows: Section 3.1 formulates the investigated problem. Section 3.2 details the energy harvesting in hybrid PLC-WLC channels while Section 3.3 describes how the data set was obtained based on the measurement setup and campaign. In the sequel, Section 3.4 discusses numerical results of performance analyses. Then Section 3.5 presents the statistical analyses and comparison between the statistical model and measured data set. Finally, Section 3.6 states concluding remarks.

3.1 PROBLEM FORMULATION

At the beginning of the XX Century, electromagnetically unshielded power lines were exploited for data communication purposes [95]; however, the limitation of data communication technologies at that time did not allow its further development. Currently, the lack of electromagnetic shield of power lines has only been treated as a relevant problem for telecommunication systems operating in the same frequency band as PLC devices (e.g., interference with amateur radio, police radio, etc) [96–98]; however, [26] presented an interesting investigation about the concatenated hybrid PLC-WLC medium by means of a measured data set, which was obtained from a measurement campaign carried out to characterize these channels in in-home facilities. Essentially, it was shown that electromagnetically unshielded power lines can potentially benefit indoor data communications. Indeed, this work concluded that PLC and WLC devices can communicate with each other if both of them operate in the same frequency band and, most importantly, data rates as high as hundreds of Mbps may be achieved if the chosen frequency band is 1.7 – 100 MHz. Furthermore, this pivotal analysis showed that the PLC $\rightarrow$ WLC and WLC $\rightarrow$ PLC channel impulse responses (CIRs) are symmetric and, therefore, their channel frequency responses (CFRs) are the same in both directions if the access impedance of the PLC and WLC devices are equal (i.e., 50 Ω). On the other hand, the PLC and WLC additive noises are different. Note that the PLC additive noise in the chosen frequency band corresponds to the BB-PLC additive noise.

A typical illustration of the hybrid PLC-WLC medium is shown in Figure 8. This data communication medium is constituted by electromagnetically unshielded power lines belonging to the electric power systems and the air. In addition to establish a data communication system constituted by PLC and WLC devices operating in the same frequency band, the main idea is to use the electromagnetic characteristic of electromagnetically unshielded power lines for EH purposes. In fact, the quantification of the harvested energy in this kind of environment is appealing because signals carrying information, which are transmitted through PLC and other signals (i.e., WLC operating in the same frequency band and man-made noise), are sources of energy that can potentially be used for charging batteries. As a matter of fact, this quantification is a *sine qua non* condition for properly verifying the feasibility of the concatenated hybrid PLC-WLC medium for EH purposes, and, as a consequence, for powering a device with self-sustainable energy capacity. Also, it is relevant to point out that radiated signals from power lines can be sensed by WLC devices as well as induced signals into power lines can be sensed by

Figure 8 – The hybrid PLC-WLC environment in in-home facilities.



Source: Personal collection.

PLC devices. In other words, the use of electromagnetically unshielded power lines in in-home facilities always produces waste of energy in both power line and wireless media, such that a WLC or PLC device can be used for harvesting, or recovering this energy.

In this regard, it is interesting to answer the following research questions: i) *Could a significant amount of energy be harvested from the transmitted signal propagating through a concatenated hybrid PLC-WLC medium in the PLC → WLC or WLC → PLC direction*?; ii) *In terms of harvested energy, the additive noise at the input of PLC and WLC devices may be useful*?; iii) *Quantitatively speaking, what is the channel ergodic achievable data rate that can be obtained by means of the dedicated energy harvesting from the hybrid PLC-WLC channels*?; iv) *Can one derive simple statistical modeling of the harvested energy from hybrid PLC-WLC channels when the dedicated energy harvesting approach applies*? Answers to these research questions are provided in the following sections.

3.2 HARVESTING ENERGY FROM THE HYBRID PLC-WLC CHANNELS

For carrying out mathematical analyses, the term hybrid PLC-WLC channels will designate both PLC → WLC and WLC → PLC concatenated channels, in which the symmetry property of CIRs associated with both links applies, and $q \in \{\text{PLC} \rightarrow \text{WLC}, \text{WLC} \rightarrow \text{PLC}\}$ will denote the data communication link associated with the two directions. Assuming that a hybrid PLC-WLC channel is modeled as a linear and time-varying stochastic process, then the output of the time-varying and stochastic channel (i.e., the total received signal) is a random

process that is represented by

$$\begin{aligned} Y^q(t) &= \tilde{Y}^q(t) + V^q(t), \\ &= \int_{-\infty}^{\infty} X^q(\tau) h^q(t,\tau) d\tau + V^q(t), \end{aligned} \tag{3.1}$$

in which $X^q(t)$ is a sample function of the transmitted signal; $h^q(t,\tau)$ is a sample function of the CIR of the hybrid PLC-WLC channel at the instant t when an impulse is applied at the instant τ at the channel's input; and $V^q(t)$ is the sample function of the additive noise at the receiver's input, which is modeled as a random process. It is important to highlight that $V^{\text{PLC}\rightarrow\text{WLC}}(t)$ refers to the WLC additive noise while $V^{\text{WLC}\rightarrow\text{PLC}}(t)$ represents the PLC additive noise. Furthermore, $\tilde{Y}^q(t)$ is a sample function of the FoN received signal. Also, note that $X^q(t)$ and $V^q(t)$ are independent stochastic processes.

3.2.1 FoN Received Signal's Power

Assume that $X^q(t)$ has a power spectral density (PSD) equal to $S^q_X(f) = \varrho^q(f) S^q_{\tilde{X}}(f)$ and the signal generated (i.e., the stochastic process) by the transmitter is expressed as $\tilde{X}^q(t)$ with a PSD of $S^q_{\tilde{X}}(f) = 1, B_w \geq f \geq 0$, in which B_w is the frequency bandwidth and $\tilde{X}^q(t)$ is an uncorrelated and wide-sense stationary process. It is important to emphasize that $X^q(t)$ is the resulting signal after the submission of the generated signal to a bit and power allocation technique. The rationale for multiplying $S^q_{\tilde{X}}(f)$ by $\varrho^q(f)$ is that its usage facilitates the application of a power mask, which is defined as $\varrho^q(f)$, for powering the transmitted signal. In other words, $\varrho^q(f)$ denotes the result of the allocation of the transmission power, which is given by $\mathcal{P}^q_x = \int_{-\infty}^{\infty} \varrho^q(f) df$, to transmit information through the hybrid PLC-WLC channel.

Let $H^q(t,f) = \mathcal{F}\{h^q(t,\tau)\}$ be the CFR of the sample function of the CIR of the hybrid PLC-WLC channel in the instant t, in which $\mathcal{F}\{\cdot\}$ is the Fourier transform operator. Furthermore, one may state that the CFRs of hybrid PLC-WLC channels are time-invariant during the coherence time, $T_c \in \mathbb{R}_+$, of such channels and, thus, $H^q(t,f) = H^q_i(f)|_{t\in[iT_c,(i+1)T_c]}, \forall i \in \mathbb{Z}_+$. Given these definitions, the power of the FoN received signal at the output of a hybrid PLC-WLC channel within the time interval T_c is given by

$$\mathcal{P}^q_{\tilde{Y},i} = \int_{B_w} \varrho^q_i(f) |H^q_i(f)|^2 df, \tag{3.2}$$

where $|H^q_i(f)|^2$ and $\varrho^q_i(f)$ denote the squared magnitude of $H^q_i(f)$ and the power mask of the i^{th} channel realization, respectively.

Let $T_{AC} \in \mathbb{R}_+$ denote the cycle of the AC mains voltage signal, then the FoN received signal's expected power per cycle of the AC mains voltage signal can be expressed as

$$\mathcal{P}^q_{\tilde{Y},c} = \sum_{i=1}^{N_P} \mathcal{P}^q_{\tilde{Y},i} p_i \tag{3.3}$$

in which p_i is the probability of the occurrence of $\mathcal{P}^q_{\tilde{Y},i}$ (or $H^q_i(f)$) and $\{N_P \in \mathbb{Z} | N_P = \lfloor T_{AC}/T_c \rfloor\}$, where $\lfloor x \rfloor = \max\{m \in \mathbb{Z} | m \leq x\}$.

3.2.2 Additive Noise's Power

When the additive noise comes to the center of the discussion, distinct approaches to deal with PLC and WLC additive noises are applied. The PLC additive noise is modeled as a cyclostationary random process [99], and, as a consequence, the PLC additive noise has both periodic mean value and autocorrelation function with respect to the cycle of the AC mains voltage signal. On the other hand, the WLC additive noise is modeled as a colored Gaussian random process. For both of them, an estimate of the additive noise's average power per cycle of the AC mains voltage signal is evaluated as

$$\mathcal{P}_{V,c}^{q} = \frac{1}{T_{AC}} \int_{T_{AC}} |V^{q}(t)|^{2} dt. \tag{3.4}$$

3.2.3 Total Harvested Energy per Cycle

Now, by assuming that the electronic circuit responsible for harvesting and storing the energy from the hybrid PLC-WLC channel has an overall efficiency factor [100], $\eta^{q} \in \mathbb{R}_{+}, 1 \geq \eta^{q} > 0$, the total harvested energy during a time interval equal to T_{AC} can be expressed as

$$\begin{aligned} \mathcal{E}_{Y}^{q} &= \eta^{q}\, \mathcal{P}_{Y,c}^{q} T_{AC}, \\ &= \eta^{q}\, \mathcal{P}_{\tilde{Y},c}^{q} T_{AC} + \eta^{q}\, \mathcal{P}_{V,c}^{q} T_{AC}, \\ &= \mathcal{E}_{\tilde{Y}}^{q} + \mathcal{E}_{V}^{q}, \end{aligned} \tag{3.5}$$

where $\mathcal{E}_{\tilde{Y}}^{q}$ is a random variable that models the harvested energy from the FoN received signal of the hybrid PLC-WLC channel, while $\mathcal{E}_{V}^{q}$ is a random variable that models the harvested energy from the additive noise. Further, $\mathcal{E}_{Y}^{q}$ is the random variable that models the total harvested energy from the total received signal (FoN received signal + additive noise) as well as the total received signal's expected power per cycle of the AC mains voltage signal is given by $\mathcal{P}_{Y,c}^{q}$. Note that each cycle of the AC mains voltage signal yields a value of $\mathcal{E}_{\tilde{Y}}^{q}$, $\mathcal{E}_{V}^{q}$, and $\mathcal{E}_{Y}^{q}$. Moreover, expected values of $\mathcal{E}_{\tilde{Y}}^{q}$, $\mathcal{E}_{V}^{q}$, and $\mathcal{E}_{Y}^{q}$ are expressed as $\mu_{\mathcal{E}_{\tilde{Y}}^{q}} = \mathbb{E}\{\mathcal{E}_{\tilde{Y}}^{q}\}$, $\mu_{\mathcal{E}_{V}^{q}} = \mathbb{E}\{\mathcal{E}_{V}^{q}\}$, and $\mu_{\mathcal{E}_{Y}^{q}} = \mathbb{E}\{\mathcal{E}_{Y}^{q}\} = \mu_{\mathcal{E}_{\tilde{Y}}^{q}} + \mu_{\mathcal{E}_{V}^{q}}$, respectively, in which $\mathbb{E}\{\cdot\}$ denotes the expectation operator.

Furthermore, it is possible to associate the expected values of harvested energy at the receiver, which was obtained from each one of the FoN received signal, the additive noise, or the total received signal, with a specific time interval. In this context, the time interval to achieve an energy threshold at the receiver side can be calculated. More specifically, if this threshold is made equal to the energy of a single signal transmission, i.e. $E_{x}^{q} = \mathcal{P}_{x}^{q} T_{TX}$, then the receiver harvests this amount of energy in an average time interval given by

$$\Delta T_{y}^{q} = T_{AC} \frac{E_{x}^{q}}{\mu_{\mathcal{E}_{y}^{q}}}, \tag{3.6}$$

in which $y \in \{\tilde{Y}, V, Y\}$ is straightforwardly related to the FoN received signal, additive noise, or total received signal, respectively. These average time intervals are very important for designing real-time energy harvesting solutions or assessing the time period for charging the communication node's battery.

3.2.4 Harvesting Energy based on Power Masking

Based on the fact that both PLC and WLC devices perform dedicated energy transfer through the hybrid PLC-WLC channels, it is important to investigate some typical situations in which the energy at the output of the hybrid PLC-WLC channel is available for being harvested. In this sense, it is possible to come up with five different transmission power masks, $\varrho^q(f)$, that can be applied to the generated signal. These masks vary from the most practical (uniform power allocation) to the most theoretical (the availability of complete channel state information (CSI) for power allocation) assumptions by the transmitter and they are described as follows:

- Power Mask #1 (Uniform): in this case, the PLC or WLC device performs a uniform power allocation. In other words, the transmission power $\mathcal{P}_x^q$ is equally distributed all over the whole frequency bandwidth. Mathematically, $\varrho^q(f) = \mathcal{P}_x^q/B_w, \forall f \in \mathcal{S}_{B_w}$, in which $\mathcal{S}_{B_w}$ denotes the range of frequencies which are contained in the frequency bandwidth.

- Power Mask #2 (IEEE 1901): the PLC or WLC device applies the power mask adopted by the IEEE 1901 Standard [65], in which $\varrho^q(f) = (\mathcal{K} - 55)$ dBm/Hz is used in the frequency band covered by $1.7 - 30$ MHz and $\varrho^q(f) = (\mathcal{K} - 85)$ dBm/Hz applies in the frequency band delimited by $30 - 100$ MHz. The proportionality factor $\mathcal{K} \approx \mathcal{P}_x^q - 20$ is used to correctly distribute the transmission power respecting the aforementioned power densities and it is given in dB, whereas $\mathcal{P}_x^q$ and 20 are dBm values.

- Power Mask #3 (Uniform B_u): based on the knowledge of the statistical expectation of the squared magnitude of CFRs, which constitute the data set, $\overline{|H^q(f)|^2} = \mathbb{E}\left\{|H_i^q(f)|^2\right\}$, an uniform power mask is applied to a shorten frequency bandwidth $B_u < B_w$ by means of the median operator. For applying the median operator, $\overline{|H^q(f)|^2}$ is discretized. To do so, it is assumed that the discrete-time representation of the statistical expectation of the squared magnitude of CFRs is given by

$$\overline{|H^q[k]|^2} = \overline{|H^q(f)|^2}|_{f=kB_s}, k = 0, 1, \ldots, N-1, \tag{3.7}$$

  where N is the discretized CFR's length of the hybrid PLC-WLC channel and $B_s = B_w/N$ is the subchannel bandwidth. This shortened frequency bandwidth, B_u, covers a range of frequencies that is centered at the frequency $f_c = N_C f_s$, in which $\overline{|H^q[N_C]|^2} = \max_k\{\overline{|H^q[k]|^2}\}$ and, upper and lower, bounded by the frequencies $f_c \pm f_u$. Such bounds are given by maximizing B_u subjected to $10\log_{10}(\overline{|H^q[N_C]|^2} - \textbf{median}\{\overline{|H^q[\ell]|^2}\}) \leq A$ dB, where $\ell \in \{N_C - N_u, N_C - (N_u - 1), \ldots, N_C, \ldots, N_C + (N_u - 1), N_C + N_u\}$, $N_u = \lceil f_u/f_s \rceil$, and $\lceil x \rceil = \min\{n \in \mathbb{Z} | n \geq x\}$. Also, the median is chosen as the metric for this power mask because it neither has a high sensitivity to the $\overline{|H^q[k]|^2}$ variations over distinct frequencies, which is different behavior of mean and variance, nor a low sensitivity to it, which characterizes the mode. In the way it was designed, it is ensured that $\overline{|H^q[\ell]|^2}$ has an odd length equal to $2N_u + 1$ and its median is given by the N_u-*th* term. That said,

$\varrho^q(f) = \mathcal{P}_x^q/B_u, \forall f \in \mathcal{S}_{B_u}$, in which $\mathcal{S}_{B_u}$ denotes the range of frequencies which follow this restriction.

- Power Mask #4 (Optimal B_o): in this situation, the power mask optimally allocates $\mathcal{P}_x^q$ to the set of frequency tones associated with the highest squared magnitudes of CFR. This kind of power allocation is performed in the frequency bandwidth equal to $B_o = \gamma B_w$, $1 \geq \gamma > 0$, and $\varrho^q(f) = \mathcal{P}_x^q/B_o, \forall f \in \mathcal{S}_{B_o}$, in which $\mathcal{S}_{B_o}$ denotes the set of frequencies (consecutive or not) of the highest squared magnitudes of the CFR.

- Power Mask #5 (Single Tone): it is similar to the Power Mask #4, except that $\mathcal{P}_x^q$ is totally allocated to the single frequency tone associated with the unique highest squared magnitude of the CFR. The bandwidth of this sole tone is equal to the bandwidth occupied by one subchannel, B_s, i.e., $\varrho^q(f) = \mathcal{P}_x^q/B_s, \forall f \in \mathcal{S}_{B_s}$, in which $\mathcal{S}_{B_s}$ denotes the range of frequencies occupied by the Single Tone with the highest squared magnitude value of the CFR.

It is important to emphasize that the data transmission occurs in the frequency band from 1.7 up to 100 MHz [65]. However, the EH is realized in the frequencies from 0 up to 100 MHz. In this context, it is worthwhile to mention that the additive noise in the frequency band below 1.7 MHz is attenuated by the capacitive coupling circuit, which was designed with a cutoff frequency equal to 1.7 MHz. Although the frequency band from 0.5 MHz up to 1.7 MHz is not interesting for data communication purposes due to interference with AM broadcasting stations, its use can be advantageous in terms of energy harvesting because of the high level of power associated with AM signals.

It is important to point out that Power Masks #1, #2, and #3 apply the uniform power allocation, in which Power Masks #1 and #2 does not require the knowledge of CSI while Power Mask #3 depends on the statistical average of CFRs. Regarding Power Masks #4 and #5, the power allocation of the transmission power is no longer uniform. In fact, Power Mask #4 equally allocates the transmission power to a part of the frequency band associated with the highest magnitudes of CFR, which may not be consecutive, while Power Mask #5 allocates the transmission power to a single frequency tone. Therefore, Power Masks #4 and #5 rely on the knowledge of the complete CSI at each time period that corresponds to the coherence time of the hybrid PLC-WLC channel.

Note that Power Masks #1 and #2 are simple to implement due to their uniform shape and independence of CSI. Furthermore, Power Mask #3 requires the knowledge of the statistical average of the squared magnitude of the CFR; however, it is still based on the uniform power allocation. As a result, Power Mask #3 offers the best trade-off between practical and theoretical assumptions. Lastly, Power Masks #4 and #5 require complete CSI during a time interval corresponding to the coherence time of the hybrid PLC-WLC channel, which make them the most theoretical power masks. In possession of this set of distinct power masks, it is possible to

analyze a variety of possibilities ranging from the less complex/practical case (Power Mask #1) to the most complex/theoretical case (Power Mask #5) for performing dedicated EH.

3.3 DATA SET

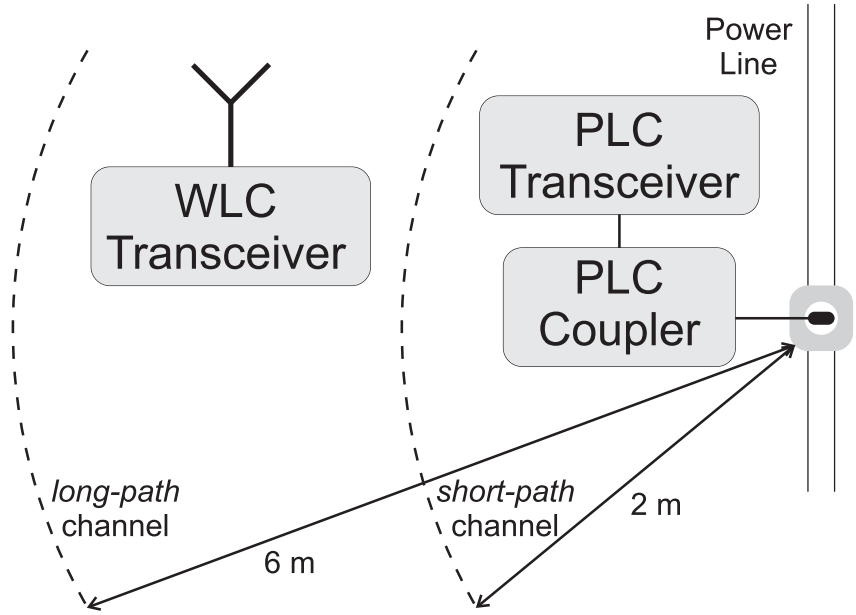
The measured data set consists of several CFRs of hybrid PLC-WLC channels provided by [26], in which a measurement campaign was carried out in indoor facilities located at Juiz de Fora, a Brazilian city belonging to Minas Gerais State (see more details about the measurement places, methodology, equipment, and the PLC coupler, respectively, in [54, 101–103]). During this measurement campaign, seven middle-class residences were taken into account. The measurement setup is based on the use of the methodology presented in [102] and equipment discussed in [103]. The block diagram of the adopted measurement setup is shown in Figure 9. Basically, it was designed for measuring the hybrid PLC-WLC channel and is composed of the following components [26]:

- PLC transceiver: it refers to the PLC device, which is connected to the power outlet by means of the PLC coupler, for injecting and extracting sounding signals into and from the power line medium, respectively.
- PLC coupler: it is a passband analog filter that promotes the interface between the PLC transceiver and the power line. Also, it blocks the AC mains signal to prevent damage to the PLC transceiver and limits the frequency band of injected and extracted signals (more details about its design can be found in [54]).
- WLC transceiver: it refers to the WLC device, which is connected to the air by means of the antenna, for injecting and extracting sounding signals into and from the wireless medium, respectively.
- Antenna: it is a transducer designed to convert electric signals into electromagnetic waves and vice-versa.

The following two kinds of hybrid PLC-WLC channels, which define two ranges of distances from the power lines, were considered during the measurement campaign [26]:

- *short-path* (SP) channel: it defines a kind of a channel in which the WLC transceiver is randomly positioned within a 2 meter radius circle centered at the outlet in which the PLC transceiver is connected. This kind of channel will be called hybrid SP PLC-WLC channel.
- *long-path* (LP) channel: it refers to the channel in which the WLC transceiver is randomly placed into an area defined as a swept circle, having an outer and inner radius of 6 meters and 2 meters, respectively, centered in the outlet in which the PLC transceiver is connected. The channel associated with LP channels will be called hybrid LP PLC-WLC channel.

Figure 9 – The block diagram of the measurement setup.



Source: Personal collection.

During the measurement campaign, the WLC transceiver was positioned near to (SP channel) and far from (LP channel) the outlet in 200 and 93 measurements, respectively. As a result, 293 distinct position combinations for both PLC and WLC transceivers were measured. Also, approximately 600 estimates of the CIR and, as a consequence, of their CFRs were obtained for each combination. Consequently, a total of 175, 428 estimates of the hybrid PLC-WLC CFRs were obtained during the measurement campaign. In addition, samples of the PLC and WLC additive noises at the inputs of both PLC and WLC transceivers, respectively, were acquired. It is important to emphasize that one CFR estimate is obtained during a time interval corresponding to one hermitian symmetric orthogonal frequency-division multiplexing (HS-OFDM) [104] symbol period duration (T_{sym}), consequently, it assumes that the time interval duration of the HS-OFDM symbol must be shorter than the coherence time of the hybrid PLC-WLC channel. Based on the set of parameters of the channel estimation technique, a channel estimate is obtained every $T_{\text{sym}} = (2N + L_{cp})T_s = 23.04$ μs, where $N = 2048$ is the number of BPSK modulated subcarriers of the HS-OFDM symbol, $L_{cp} = 512$ samples is the length of the cyclic prefix, $f_s = 200$ MHz is the sampling rate, and $T_s = 1/f_s = 5$ ns is the sampling period. According to [26], $T_c = 156$ μs is the minimum time period within which the hybrid SP PLC-WLC channel can be considered time-invariant, while for the hybrid LP PLC-WLC channel, the minimum time period of time invariance is $T_c = 39.5$ μs. Regardless of the channel distances, the time interval duration necessary to yield one CFR estimate (T_{sym}) is shorter than the coherence time. Moreover, the assumed value of N and the chosen frequency bandwidth results in CFR estimates with a corresponding frequency resolution of $\Delta f = 48.83$ kHz, which is shorter than the coherence bandwidth of Brazilian in-home hybrid PLC-WLC channels [26]. Also, Δf being shorter than the coherence bandwidth means that each sample of the magnitude of a CFR

estimates is representative of the whole subband, and it can be used for carrying out performance and statistical analyses.

3.4 PERFORMANCE ANALYSES

This section focuses on numerical analyses of the harvested energy from the hybrid PLC-WLC channels when the data set of measured CFRs and additive noises described in Section 3.3 is taken into account. Also, it offers a discussion about the ergodic achievable data rates of narrowband and indoor PLC and WLC channels as well as the ones obtained through the use of hybrid PLC-WLC channel, when the harvested energy from the hybrid PLC-WLC channels is considered the only available source of energy. Based on the provided data set of measured hybrid PLC-WLC channels [26], the numerical simulations assume that $B_w = 100$ MHz, $B_u \approx 7$ MHz (with $A = 6$ dB and the frequencies ranging from approximately 20 MHz to 27 MHz, taken from the statistical average of the CFR squared magnitudes), $B_o = 10$ MHz ($\gamma = 0.1$ is heuristically chosen), and $B_s \approx 48.83$ kHz for the PLC $\rightarrow$ WLC and WLC $\rightarrow$ PLC directions; $\mathcal{P}_x^q \approx 20$ dBm is adopted based on the power mask of the IEEE 1901 Standard [65]; and $\eta^q = 1$ is chosen to illustrate the case of an ideal overall efficiency factor. Also, it is assumed that $T_{TX} = T_{\text{sym}}$ because it allows us to easily and quantitatively relate the harvested energy to a time interval necessary to reach a given energy threshold in terms of the time interval of an HS-OFDM symbol. Further, the Brazilian AC mains frequency is $f_{AC} = 60$ Hz, then $T_{AC} = 1/f_{AC} \approx 16.67$ ms and the realizations of each CFR are assumed to be equally likely ($p_i = 1/N_P, \forall i$).

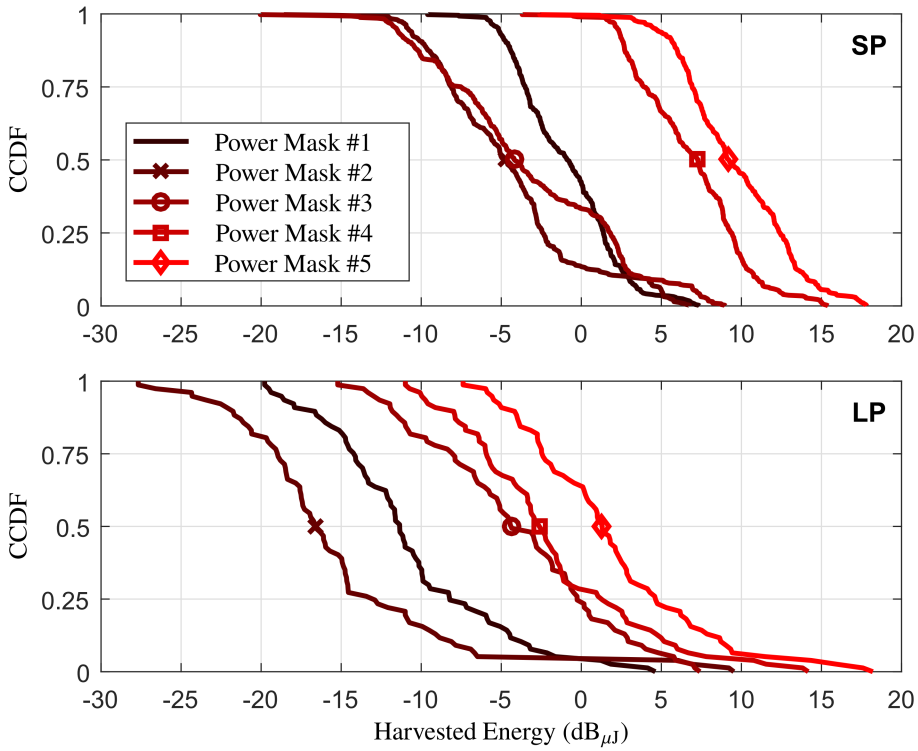
Subsection **3.4.1** drives attention to the numerical results and discussions concerning the harvested energy only from the FoN received signal; Subsection **3.4.2** from the receiver's additive noise; Subsection **3.4.3** from the total received signal. In the sequel, the expected harvested energy is discussed in Subsection **3.4.4**, while the necessary average time interval to achieve an energy threshold at the receiver side is analyzed in Subsection **3.4.5**. Finally, Subsections **3.4.6** and **3.4.7** focus on the numerical analyses of the ergodic achievable data rate when the total harvested energy from the hybrid PLC-WLC channel is used for performing data communication through narrowband PLC or WLC channels and through hybrid PLC-WLC channels, respectively.

3.4.1 FoN Received Signal Analyses

The discussion carried out in this subsection is useful to bring attention to the importance of choosing a power mask. In fact, this choice can either make an energy threshold to have a high or low probability of occurrence. Also, it can make a given probability of harvesting an energy value decreases to a lower one and vice-versa. It is important to highlight that the term FoN received signal is used to denote the transmitted signal that traveled through the hybrid PLC-WLC channel and is without the additive noise corruption.

The CCDF of the harvested energy taken from the FoN received signal in both directions are shown in Figure 10 for the hybrid SP PLC-WLC channel (top) and hybrid LP PLC-WLC channel (bottom), when the five suggested power masks are taken into account. Here, it is defined $\text{dB}_{\mu\text{J}} \triangleq 60 + 10\log_{10}(\text{Energy [J]})$. By means of this figure and for probabilities above 0.75, it can be seen that the best power mask is the Power Mask #5 for both SP and LP channels while the worst is the Power Masks #3 for hybrid SP PLC-WLC and the Power Masks #2 for hybrid LP PLC-WLC channels. It is important to point out that the Power Mask #1 yields better results than the Power Mask #2 because the highest values of CFR squared magnitudes occur around $26 - 50$ MHz frequency range (refer to Figure 5 in [26]), in counterpart the Power Mask #2 imposes the allocation of most of the power below the 30 MHz frequency.

Figure 10 – The CCDFs of the harvested energy from the FoN received signal over a hybrid SP PLC-WLC channel (top) or hybrid LP PLC-WLC channel (bottom).



Source: Personal collection.

For the Power Mask #4 and a given probability, the chosen $\gamma = 0.1$ makes this mask the second better option in terms of harvested energy for both SP and LP channels. Moreover, it may yield results ranging from the best to the worst (uniform) power masks due to its high flexibility. For instance, if $\gamma \to 0$, then this power mask mimics the Power Mask #5. On the other hand, if $\gamma \to 1$, then it will yield similar results to the Power Mask #1. As expected, due to the short distance to the power line and, as a consequence, less channel attenuation, hybrid SP PLC-WLC channels present higher values of harvested energy than hybrid LP PLC-WLC ones for a given probability.

Moreover, the use of the Power Mask #3 shows interesting behavior. It yields similar

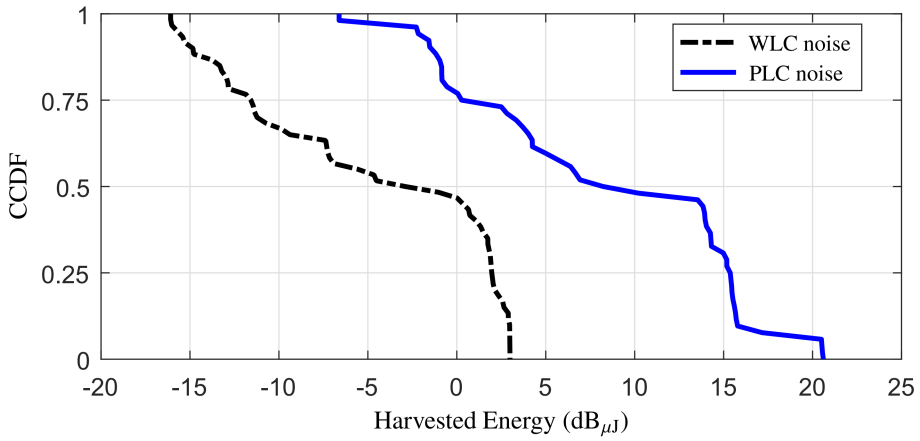
values of harvested energy from hybrid LP PLC-WLC channels compared to hybrid SP PLC-WLC channels, which is a different behavior to the other power masks. In other words, the CCDF of Power Mask #3 is located between the ones of Power Mask #1 and #2 for hybrid SP PLC-WLC channels and between Power Masks #2 and #4 for hybrid LP PLC-WLC channels. In this context, this shows that the criteria adopted for this power mask may not be good in order to better take advantage of the FoN received signal's energy in both SP and LP channels. Also, it is important to mention that this power mask is the one offering the best trade-off between theoretical (CSI availability) and practical (low complexity) assumptions.

That said, the focus of the numerical analyses is mostly on Power Masks #1 and #2 because they are associated with the most practical assumptions due to their uniform shape and no CSI need. Regarding the hybrid SP PLC-WLC channels, it is noticed that 0 $dB_{\mu J}$ of energy can be obtained with a probability of 0.42 and 0.13 by using the Power Mask #1 and the Power Mask #2, respectively. Furthermore, the probability of 0.04 is achieved for the same 0 $dB_{\mu J}$ of harvested energy when hybrid LP PLC-WLC channels are considered for both Power Masks #1 and #2.

3.4.2 Additive Noise Analyses

The aim of this subsection is to figure out the usefulness of additive noises at the input of either PLC or WLC device for EH purposes. In this sense, Figure 11 shows the CCDF of the harvested energy from the PLC and WLC additive noises. Note that PLC and WLC additive noises refer to the noises at the inputs of the PLC and WLC devices, respectively.

Figure 11 – The CCDFs of the harvested energy from the PLC and WLC additive noises.



Source: Personal collection.

Based on Figure 11, it can be seen that the PLC additive noise offers higher values of harvested energy than the WLC one, for a given probability. Furthermore, if the target is to harvest at least 0 $dB_{\mu J}$ of energy from the noise, then the PLC additive noise has a probability of 0.77 and the WLC one has only 0.47 of probability to yield it. In other words, the PLC additive noise, which is commonly considered as an unwanted signal, can bring a lot of benefits

for performing EH. For instance, if an energy of 5 $dB_{\mu J}$ is wanted, the WLC additive noise is not useful; however, the PLC additive noise has a probability of 0.60 of yielding this amount of energy. Also, it is important to note that most of the PLC additive noise's energy comes from the frequency band between $0 - 1.7$ MHz, which is due to the AM broadcasting stations and other man-made noise close to the low frequencies.

An important and necessary comparison involves the values of the harvested energy from the FoN received signal and additive noise. If the target is 5 $dB_{\mu J}$, then the Power Mask #1 achieves probabilities up to 0.03 and 0.0 for hybrid SP PLC-WLC and hybrid LP PLC-WLC channels, respectively. A comparison among these probabilities with the ones offered by PLC (0.60) and WLC (0.0) additive noises shows that, sometimes, PLC additive noise can bring much more benefits in terms of EH than the FoN received signal. However, if the WLC additive noise is taken into account, then the FoN received signal may offer a higher contribution than this kind of noise. It is important to point out that this analysis heavily depends upon the chosen power mask.

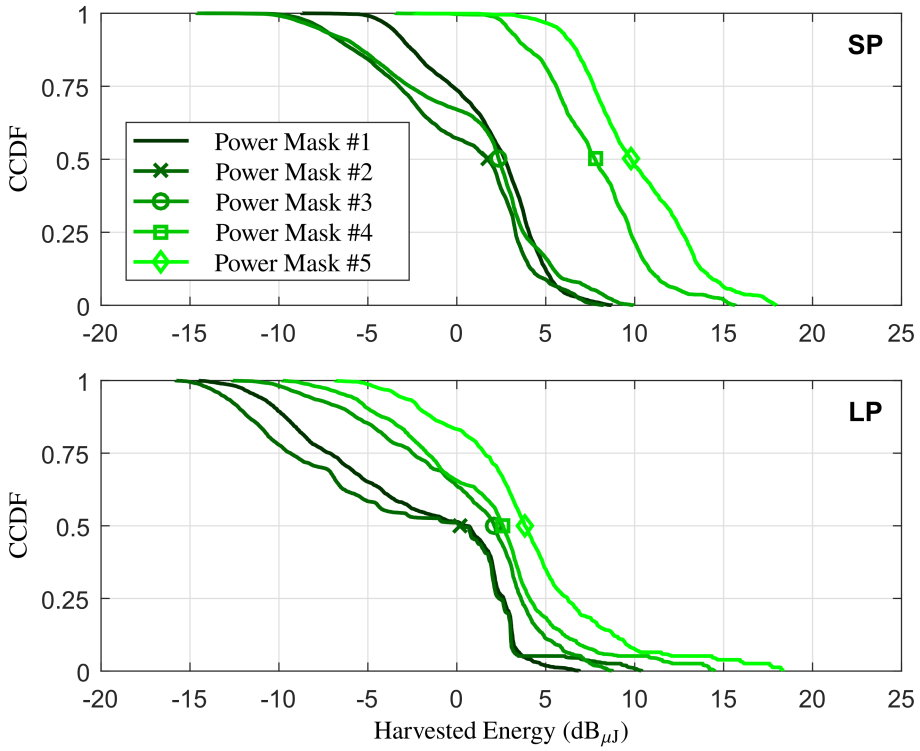
3.4.3 Total Received Signal Analyses

In real and practical scenarios, the total received signal cannot be physically split into FoN received signal and additive noise. Therefore, this subsection contemplates the case in which the energy is harvested from the total received signal, composed of FoN received signal and additive noise. In this context, Figure 12 shows the CCDF of the harvested energy from the total received signal at the output of hybrid SP PLC-WLC and hybrid LP PLC-WLC channels, respectively, when the receiver is the WLC device. Also, Figure 13 shows the same kind of information when the receiver is the PLC device.

By performing a comparative analysis between Figures 12 and 10, it is noticed similar trends in their plots (i.e., the order of the best to the worst power mask does not change, as expected). As a consequence, the results in Figure 12 are similar to the ones discussed in Subsection **3.4.1** with a shift to the right, which corresponds to the WLC additive noise contribution to the total harvested energy. When the discussion is about Figure 13, a visible increase in the values of the total harvested energy is observed due to the high power of the PLC additive noise. For hybrid SP PLC-WLC channels, a probability of 0.70 for harvesting, at least, 5 $dB_{\mu J}$ of energy is observed with the Power Mask #1. On the other hand, regarding hybrid LP PLC-WLC channels and the same power mask and energy threshold, the value of probability decays to 0.67, which still is a good result.

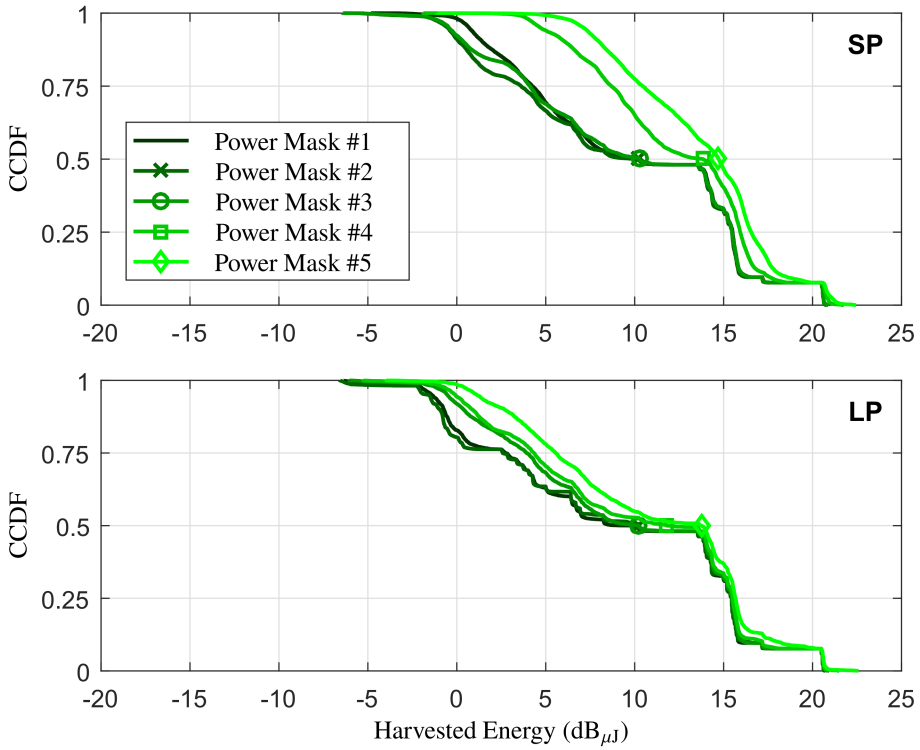
The key rationale behind the higher distances among the CCDFs of Power Masks #4 and #5 in Figure 13 associated with hybrid SP PLC-WLC channels than hybrid LP PLC-WLC channels is the fact that in the former the contribution of the FoN received signal may be relevant, while in the latter the PLC additive noise has a greater contribution to the total harvested energy. Therefore, the power mask may not exert the main role when the energy is harvested from the total received signal corrupted by the PLC additive noise.

Figure 12 – The CCDFs of the harvested energy from the total received signal in hybrid SP PLC-WLC channel (top) and hybrid LP PLC-WLC channel (bottom) considering the PLC → WLC direction.



Source: Personal collection.

Figure 13 – The CCDFs of the harvested energy from the total received signal in hybrid SP PLC-WLC channel (top) and hybrid LP PLC-WLC channel (bottom) considering the WLC → PLC direction.

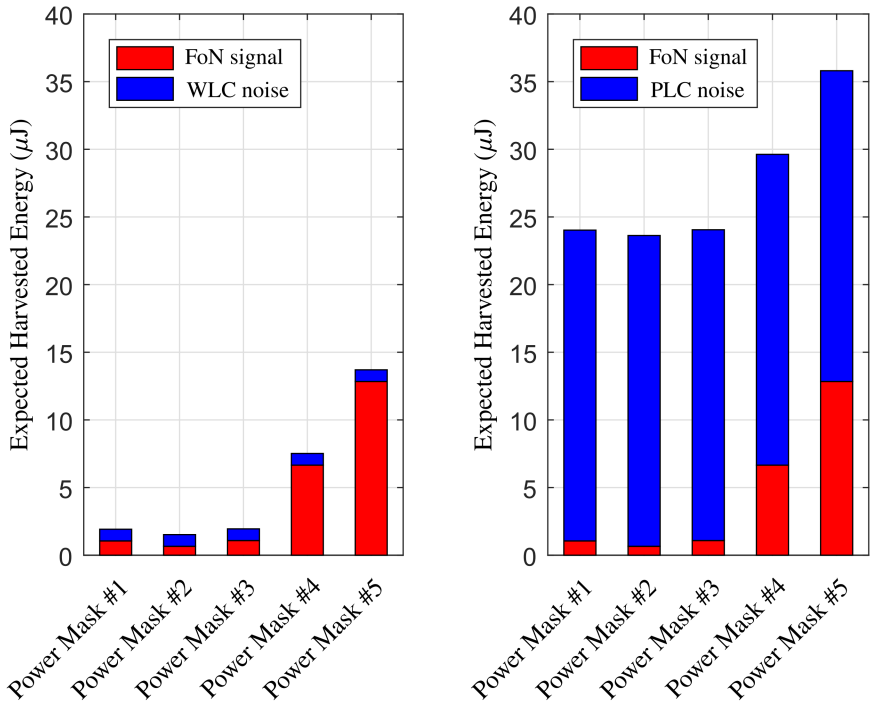


Source: Personal collection.

3.4.4 The Expected Values Analyses

Figures 14 and 15 show the expected values of the harvested energy from the FoN received signal ($\mu_{\mathcal{E}_{\tilde{Y}}^q}$) and the additive noise ($\mu_{\mathcal{E}_V^q}$) at the output of hybrid SP PLC-WLC and hybrid LP PLC-WLC channels, respectively. These plots are interesting for revealing the individual contribution of each component of the total received signal for EH purposes. Looking at Figure 14 (hybrid SP PLC-WLC channels) and the Power Masks #1, #2, and #3, it is shown that the FoN received signal has low contributions to the total harvested energy when a PLC device is used. Note that the expected harvested energy of the WLC additive noise is low, while the PLC additive noise shows the highest contribution to the total harvested energy for all power masks.

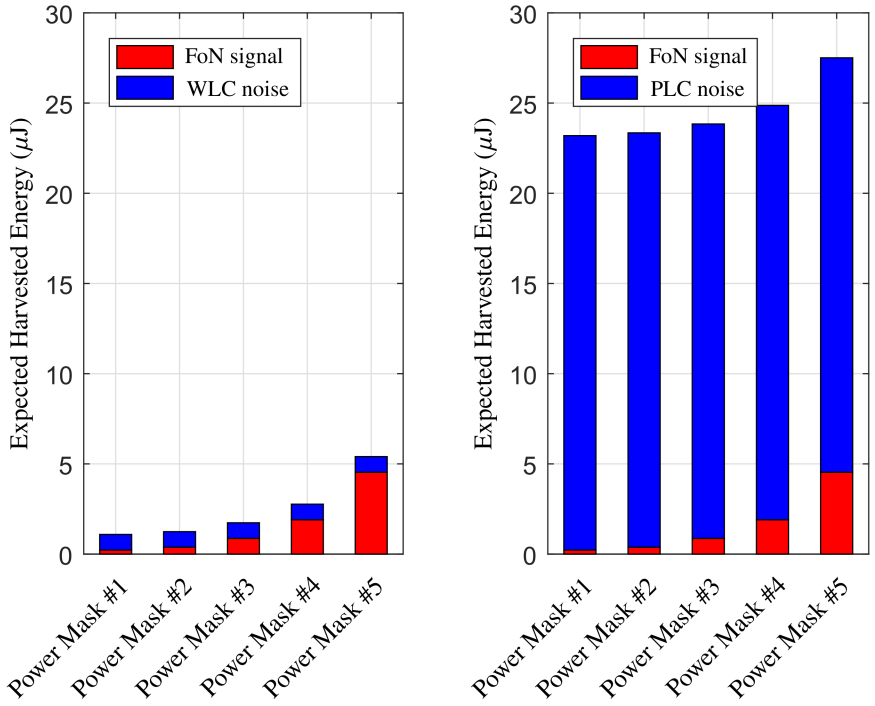
Figure 14 – The expected values of the harvested energy from the total received signal in a hybrid SP PLC-WLC channel corrupted by the WLC (left) and PLC (right) additive noises.



Source: Personal collection.

Figure 15 (hybrid LP PLC-WLC channels) shows a clear difference between the expected harvested energy from the FoN received signal in terms of the power mask usage. Again, the amount of $\mu_{\mathcal{E}_V^q}$ from the PLC additive noise in Figure 15 is greater than the one yielded by $\mu_{\mathcal{E}_{\tilde{Y}}^q}$ for all power masks. Nevertheless, the greatest contribution in the PLC $\rightarrow$ WLC direction comes from the FoN received signal in the Power Masks #4 and #5. In contrast, for all power masks, the highest contribution in the WLC $\rightarrow$ PLC direction is related to the additive noise because the PLC additive noise has a high power feature due to the nature of loads connected to electric power systems.

Figure 15 – The expected values of the harvested energy from the total received signal in a hybrid LP PLC-WLC channel corrupted by the WLC (left) and PLC (right) additive noises.



Source: Personal collection.

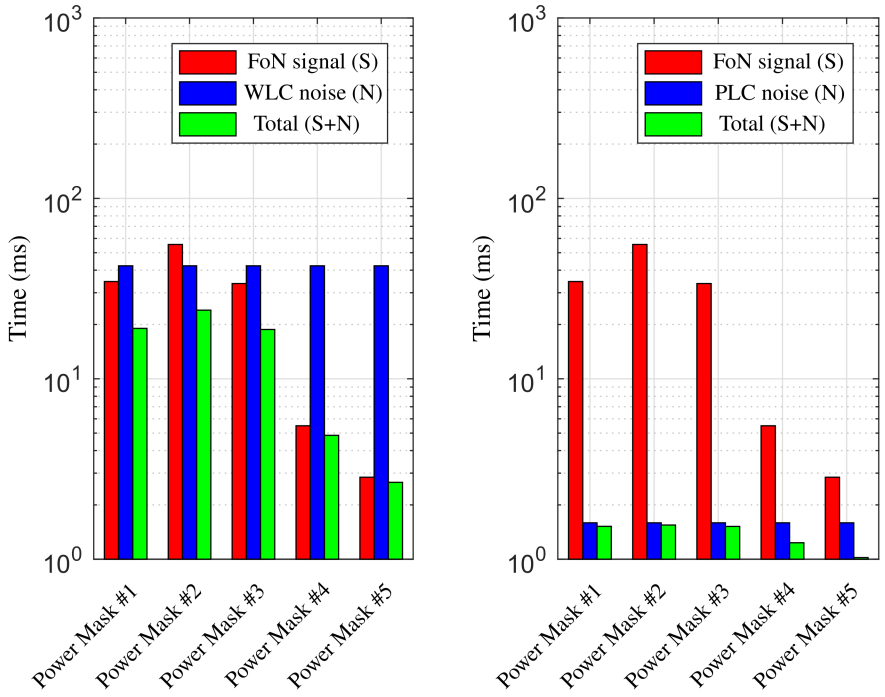
Looking at the hybrid SP PLC-WLC channels (Figure 14) and considering the Power Mask #1, the yielded expected values of total harvested energy is 1.9 and 24.0 μJ, by considering WLC or PLC additive noise, respectively. For the same power mask and hybrid LP PLC-WLC channels (Figure 15), these values are 1.1 and 23.0 μJ, showing a predicted, but low, decrease in the expected value of the total harvested energy. Overall, one points out that the WLC additive noise has a low contribution to the amount of total harvested energy in comparison to the PLC additive noise. On the other hand, the PLC additive noise constitutes the greatest portion of total harvested energy in all of the cases associated with hybrid SP PLC-WLC and hybrid LP PLC-WLC channels.

3.4.5 Average Time Interval Analyses

Figures 16 and 17 show the average time intervals needed to yield the energy of a single signal transmission, which is chosen to be equal to $E_x^q = \mathcal{P}_x^q T_{TX} \approx 2.3$ μJ, at the receiver side when the energy is harvested only from the FoN received signal ($\Delta T_{\tilde{Y}}^q$), from the additive noise (ΔT_V^q), and from the total received signal (ΔT_Y^q). This analysis is important for evaluating the average time interval that a receiver, with the same specifications of the transmitter, would demand to obtain the same amount of energy that was used in one HS-OFDM symbol transmission by the transmitter. This comparison, which is in terms of the chosen power masks, addresses the hybrid SP PLC-WLC and hybrid LP PLC-WLC channels.

Concerning Figure 16, it is important to mention that the WLC additive noise has a relevant energy harvesting contribution to the total harvested energy when associated with Power Masks #1, #2, and #3 because it takes around 42.3 ms to achieve E_x^q, which is close to the average time intervals needed by these power masks – 34.6 ms, 56.0 ms, and 33.0 ms, respectively – to achieve the same energy threshold. On the other hand, the PLC additive noise is a very good option for EH as it needs only 1.6 ms for yielding the same amount of energy.

Figure 16 – The average time interval to achieve E_x^q at the receiver side of hybrid SP PLC-WLC channels corrupted by WLC (left) or PLC (right) additive noises.

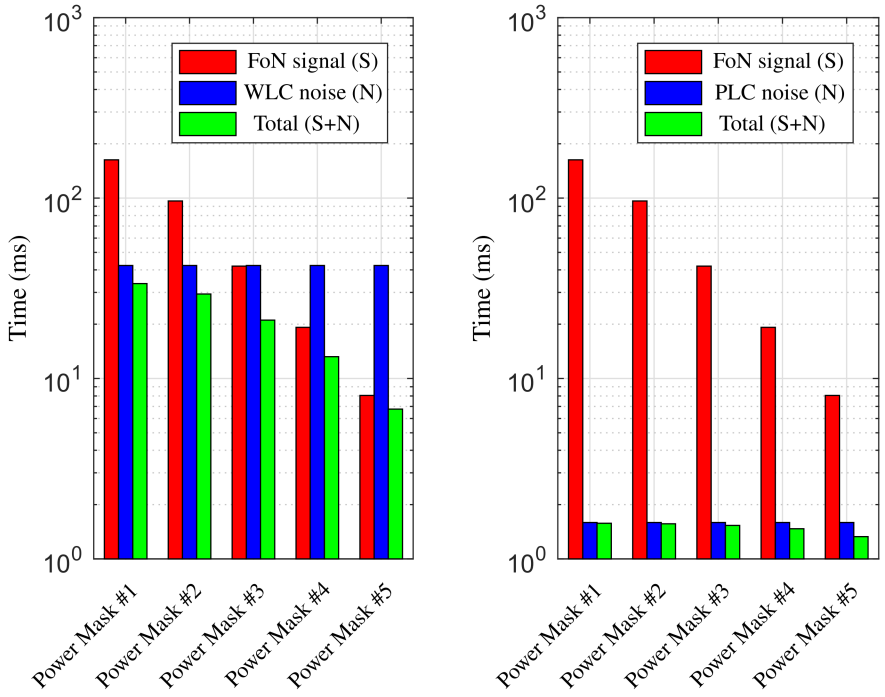


Source: Personal collection.

When the discussion refers to the FoN received signal, the comparison between Figure 16 (hybrid SP PLC-WLC channels) and Figure 17 (hybrid LP PLC-WLC channels) is of utmost importance. The Power Mask #1 would take 34.6 ms or almost 162.9 ms to achieve E_x^q by only harvesting energy from the FoN received signal that travels through the hybrid SP PLC-WLC and hybrid LP PLC-WLC channels, respectively. If the WLC additive noise is taken into account, these average time intervals decrease to 19.0 and 33.6 ms, respectively. On the other hand, when the PLC additive noise is considered, these values reduce to 1.5 ms and 1.6 ms, respectively.

Overall, Figures 16 and 17 confirm the fact that the PLC additive noise has a high contribution to the total harvested energy. For instance, when the PLC additive noise and the Power Mask #1 are considered, the average time interval necessary to achieve an energy threshold at the receiver side decreases $34.6/1.5 \approx 23.06$ and $162.9/1.6 \approx 101.81$ times in comparison to the sole use of the FoN received signal for harvesting energy from the hybrid SP PLC-WLC and hybrid LP PLC-WLC channels, respectively. Furthermore, the energy associated with the

Figure 17 – The average time interval to achieve E_x^q at the receiver side of hybrid LP PLC-WLC channels corrupted by WLC (left) or PLC (right) additive noises.



Source: Personal collection.

WLC additive noise makes a relevant, but lower impact in the average time interval to achieve E_x^q when it is added to the energy related to the FoN received signal.

3.4.6 Ergodic Achievable Data Rate Analyses: Narrowband Channels

This subsection aims at evaluating the performance of the narrowband PLC and WLC channels in terms of ergodic achievable data rate when the available transmission power is that one harvested from the total received signal that traveled through the hybrid PLC-WLC channels and *out-of-band* strategy is adopted. This is an important investigation because a large number of devices in SGs, the IoT, and Industry 4.0 demands low-data-rate communication interfaces.

In possession of the total harvested energy through the total received signal's expected power per cycle of the AC mains voltage signal, the ergodic achievable data rates of the NB-PLC and LP-RF WLC channels are calculated by using

$$C = \mathbb{E}_{H_j^\ell(f)}\left\{\max_{\upsilon_j^\ell(f)} \int_{B'_w} \log_2\left(1 + \frac{\upsilon_j^\ell(f) S_{\tilde{X}}^\ell(f) |H_j^\ell(f)|^2}{S_V^\ell(f)}\right) df\right\}, \tag{3.8}$$

subject to $\int_{-\infty}^{\infty} \upsilon_j^\ell(f) df \leq \mathcal{P}_{Y,c}^q$, in which $\mathbb{E}_{H_j^\ell(f)}\{.\}$ is the expectation operation related to NB-PLC and LP-RF WLC channel realizations, $|H_j^\ell(f)|^2$ is the CFR squared magnitude of the sample function of the CIR associated with the ℓ^{th} data communication medium, where $\ell \in \{\text{P,W}\}$ represents the power line and wireless media, respectively, and $j \in \mathbb{Z}$ is the index of

the channel realization. Further, the PSD of the signal generated by the transmitter is expressed as $S^{\ell}_{\tilde{X}}(f)$, in which $\int_{B'_w} S^{\ell}_{\tilde{X}}(f)df = 1$ with $B'_w \approx 500$ kHz being the frequency bandwidth for data communication. Also, $S^{\ell}_{V}(f)$ refers to the PSD of the ℓ^{th} data communication medium receiver's additive noise, which is supposed to be modeled as a stochastic process.

In order to carry out numerical simulations regarding the NB-PLC and LP-RF WLC channels, the data communication is assumed to occur in the ISM frequency band centered at 5.8 GHz for WLC and in the narrow-regulated frequency band (3 – 500 kHz) for PLC [73]. The occupied frequency bandwidth is approximately 500 kHz in both media to ensure fairness. Brief descriptions of the adopted NB-PLC and LP-RF WLC channel models are as follows:

NB-PLC channel model: the well-known Zimmermann and Dostert [10] channel model is used, by assuming the parameters taken from the IEEE 1901.2 standard [73, Annex D]. The additive noise in this NB-PLC channel is modeled as a zero-mean and colored Gaussian random process. Adopted from [105], its PSD is expressed by $S^{P}_{V}(f) = \varsigma/2 \exp(-\nu|f|)$ dBm/Hz, where $\nu, \varsigma \in \mathbb{R}_{+}$ are constants equal to 1.2×10^{-5} and 1.0×10^{-15}, respectively, and f is the frequency in Hertz.

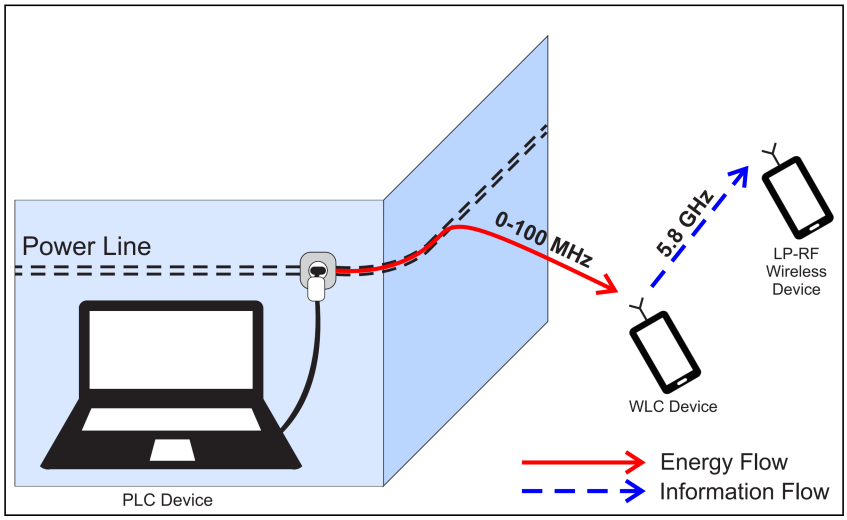
LP-RF WLC channel model: this channel model is obtained from a wideband wireless one by adopting the procedure suggested in the 802.15.4a IEEE wireless channel model report [106]. Essentially, it is accomplished by filtering the wideband wireless channel model. The zero-mean circularly symmetric and complex Gaussian assumption is made for the LP-RF WLC additive noise. From [21], the PSD of the additive noise in the LP-RF WLC channel is considered to be $S^{W}_{V}(f) = -173.8 + NF$ dBm/Hz, where the receiver noise figure NF is equal to 7 dB.

Furthermore, for the channel ergodic achievable data rate evaluation, it is relevant to assume that $\int_{B'_w} |H^{P}_{j}(f)|^2 df = \int_{B'_w} |H^{W}_{j}(f)|^2 df$ and $\int_{B'_w} S^{P}_{V}(f)df = \int_{B'_w} S^{W}_{V}(f)df$ due to the need for ensuring fairness. Also, it is considered that the full CSI is available and the optimal power allocation is applied in $\upsilon^{\ell}_{j}(f)$ by means of the water-filling (WF) technique [107]. Moreover, the PLC device, which realizes the data communication through NB-PLC channels, harvests its energy from the total received signal at the output of the hybrid PLC-WLC channels in the WLC → PLC direction. On the other hand, the WLC device that performs data communication through the LP-RF WLC channels, harvests its energy from the total received signal at the output of the hybrid PLC-WLC channels in the PLC → WLC direction. As well, the total harvested energy in both cases is associated with a time interval equal to $T_{AC} \approx 16.67$ ms.

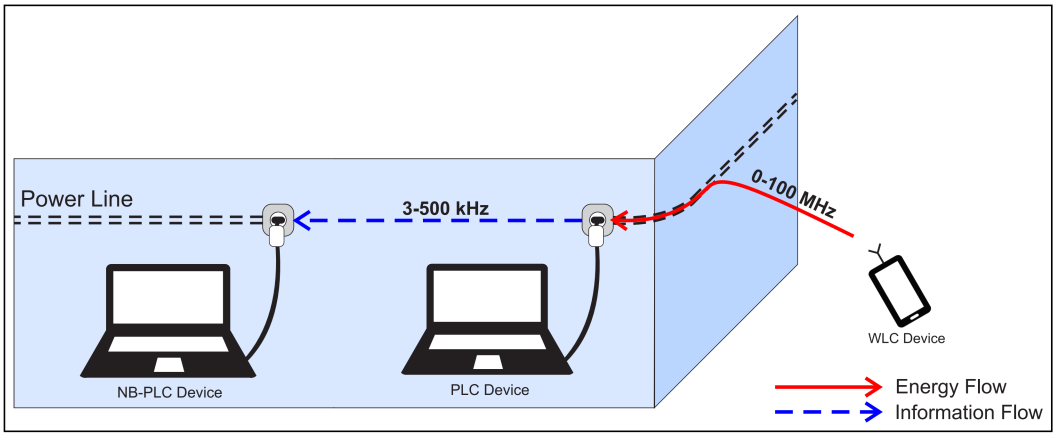
At this point, three distinct scenarios are highlighted as follows:

- Scenario #A1 (Figure 18(a)): the harvested energy by the WLC (EH) device is from the hybrid PLC-WLC channel in the PLC → WLC direction, assuming the use of the frequency band from 0 to 100 MHz. Therefore, the resulting energy is the sum of FoN received signal and WLC additive noise energies in this frequency range. After that, this amount of energy is used for data communication from this WLC device, which is supposed to be a LP-RF wireless device, to another LP-RF wireless device. In this case,

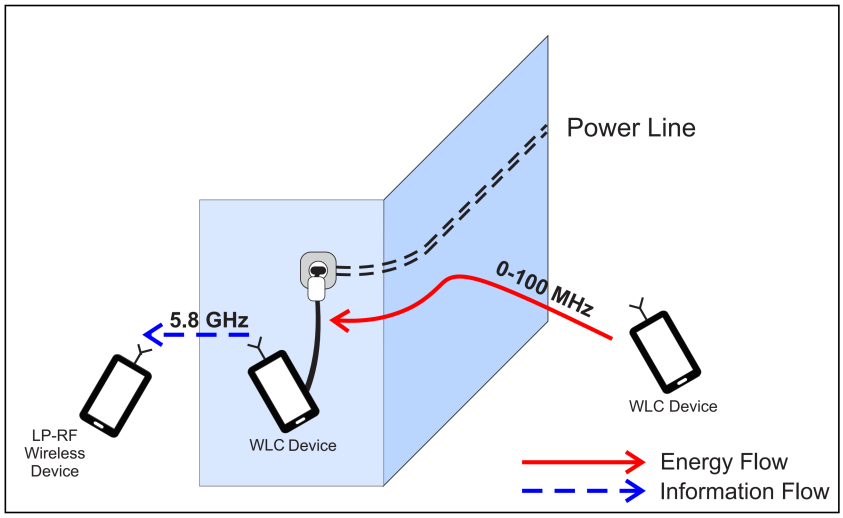
Figure 18 – Three distinct scenarios: (a) Scenario #A1, (b) Scenario #A2, (c) Scenario #A3.



(a) WLC (EH) device with LP-RF WLC.



(b) PLC (EH) device with NB-PLC.



(c) WLC (EH) device connected to the power outlet with LP-RF WLC.

Source: Personal collection.

the data communication is realized at one of the unlicensed ISM frequency bands, which is centered at 5.8 GHz, with a frequency bandwidth of 500 kHz.

- Scenario #A2 (Figure 18(b)): a PLC (EH) device harvests the energy from a WLC device by means of the hybrid PLC-WLC channel in the WLC → PLC direction by considering the frequency band delimited by 0 and 100 MHz. Thus, the harvested energy by the PLC device is used for data communication from this device, which is supposed to be a NB-PLC, to another NB-PLC device at the frequency band from 3 kHz up to 500 kHz. In this case, the total harvested energy is the sum of the FoN received signal and the PLC additive noise energies.

- Scenario #A3 (Figure 18(c)): a WLC (EH) device is connected to the power line outlet and it harvests the energy from the electric power system by means of the hybrid PLC-WLC channel in the frequency band delimited by 0 and 100 MHz. Thus, the harvested energy by the WLC device is used for data communication from this device, which is a LP-RF wireless device, to another LP-RF wireless device with a frequency bandwidth of 500 kHz and centered at 5.8 GHz. Therefore, the total harvested energy is the sum of the FoN received signal and the PLC additive noise energies.

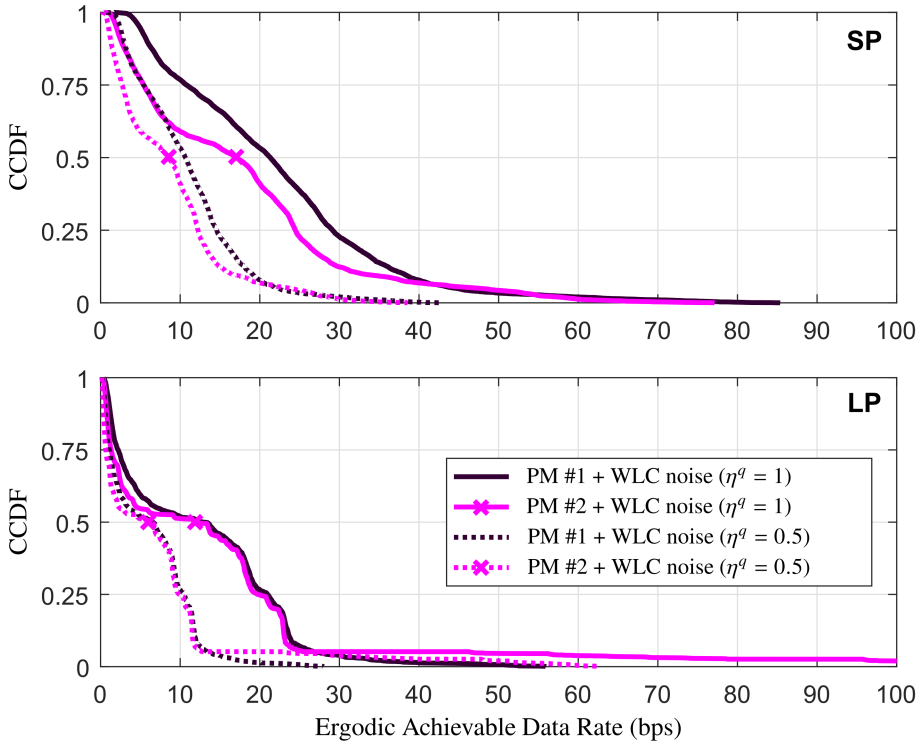
Also, assume that the communication through the hybrid PLC-WLC channel occurs during κT_{AC} seconds per cycle of the AC mains voltage signal, in which $0 < \kappa < 1 \in \mathbb{R}_+$. In other words, in the first scenario, the PLC device is using its power to transfer energy to the WLC (EH) device during κT_{AC} seconds and the remaining $(1-\kappa)T_{AC}$ seconds is available for data communication between this WLC device and its destination node, the LP-RF wireless device. In the second scenario, the WLC device uses its power to transfer energy to the PLC (EH) device during κT_{AC} seconds, while the remaining $(1-\kappa)T_{AC}$ seconds is available for data communication between the PLC device and the NB-PLC device (destination node).

Concerning the third scenario, the untethered WLC device is using its power to transfer energy to the WLC (EH) device that is connected to the electric power system during κT_{AC} seconds, while $(1-\kappa)T_{AC}$ seconds is used for data communication between the WLC device, that is connected to the electric power system, and the LP-RF wireless device. In the three cases, it is assumed $\kappa = 0.5$ and the use of the Power Masks #1 and #2 as they represent the most practical and implementable features. In fact, these power masks do not demand complete CSI as they have always the same power distribution pattern over the whole frequency band.

Figure 19 shows the CCDFs of the ergodic achievable data rates for the Power Masks #1 (labeled as PM #1) and #2 (PM #2) in the Scenario #A1 when EH is, respectively, carried out by means of a hybrid SP PLC-WLC channel (top) or hybrid LP PLC-WLC channel (bottom) with two distinct values of η^q, in which $\eta^q = 0.5$ is represented by dashed line and $\eta^q = 1$ is drawn in continuous line. The same information is depicted for the Scenario #A2 in Figure 20.

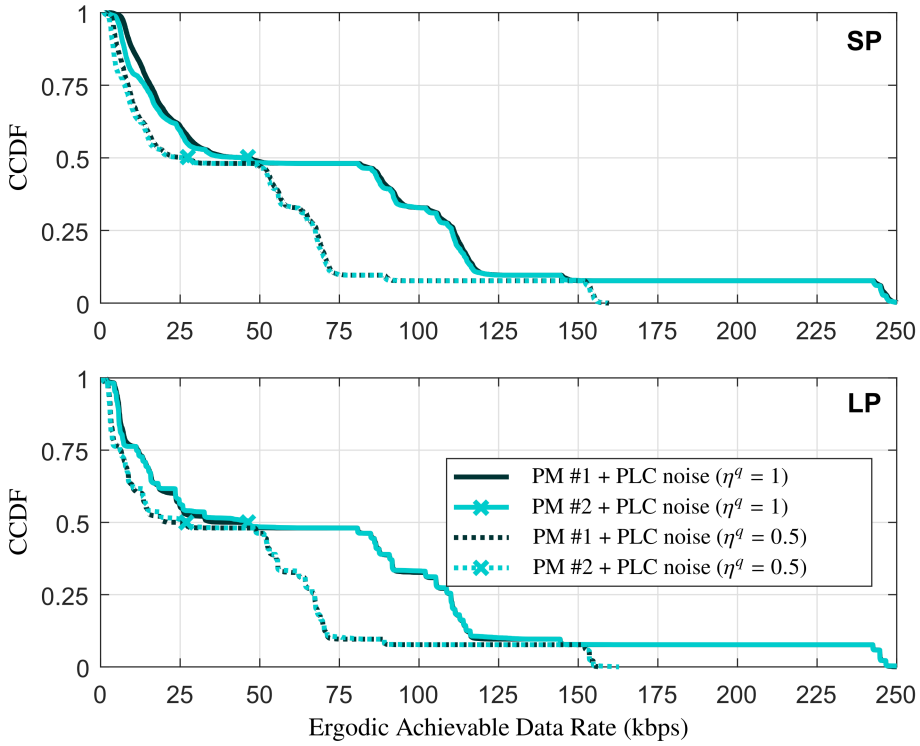
Looking at Figure 19 (Scenario #A1) and focusing on the Power Mask #1 with $\eta^q = 1$, the data communications through the LP-RF WLC channels yield, with a probability of 0.75,

Figure 19 – The CCDFs of ergodic achievable data rates yielded by the WLC (EH) device in Scenario #A1 for $\eta^q = 1$ (continuous line) and $\eta^q = 0.5$ (dashed line).



Source: Personal collection.

Figure 20 – The CCDFs of ergodic achievable data rates yielded by the PLC (EH) device in Scenario #A2 for $\eta^q = 1$ (continuous line) and $\eta^q = 0.5$ (dashed line).



Source: Personal collection.

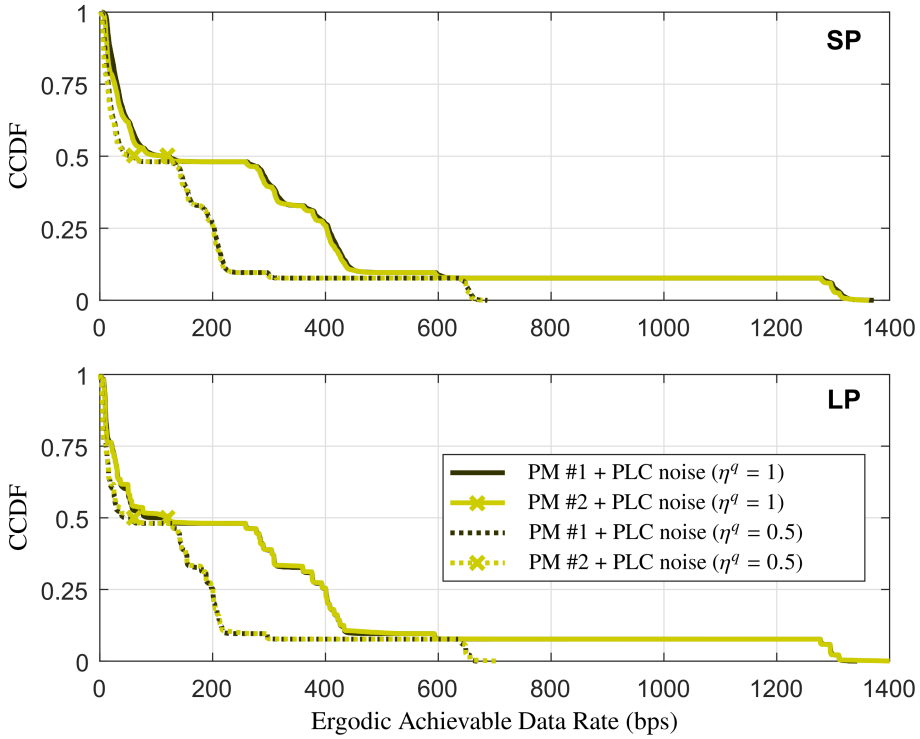
ergodic achievable data rates of, at least, 10 bps and 3 bps with the harvested energy from the hybrid SP PLC-WLC and hybrid LP PLC-WLC channels, respectively. On the other hand, by inspecting Figure 20 (Scenario #A2), for the same power mask, $\eta^q = 1$, and probability value, the data communications through the NB-PLC channels offer more than 17 kbps and 15 kbps for the harvested energy from the hybrid SP PLC-WLC and hybrid LP PLC-WLC channels, respectively. It is important to point out that the data communication through the NB-PLC channels achieves higher data rates due to the high power associated with the PLC additive noise, which was carefully discussed in the previous subsections.

When $\eta^q = 0.5$ (dashed lines), both the yielded ergodic achievable data rate and the probability of a given ergodic achievable data rate threshold reduces in comparison to $\eta^q = 1$, as it is expected. These plots ($\eta^q = 0.5$) represent a more realistic scenario, in which the receiver is capable of harvesting only 50% of the energy associated with the total received signal due to the overall efficiency factor (see Table III in [80] for more details). Furthermore, assuming a probability of 0.75 and the Power Mask #1, the LP-RF WLC channels yield an ergodic achievable data rate of, at least, 6 bps and 1 bps by using the harvested energy from the hybrid SP PLC-WLC and hybrid LP PLC-WLC channels, respectively. Also, for the same probability threshold and chosen power mask ($\eta^q = 0.5$), the NB-PLC channels yield more than 9 kbps or 7 kbps with the harvested energy from either one of the hybrid SP PLC-WLC or hybrid LP PLC-WLC channel, respectively. This analysis illustrates the decrease of the ergodic achievable data rates when η^q reduces.

Although the values of ergodic achievable data rates have decreased with the use of $\eta^q = 0.5$, see the values for 0.75 of probability for example, these values − 6 bps (hybrid SP PLC-WLC channels) and 1 bps (hybrid LP PLC-WLC channels) for the LP-RF WLC channels and 9 kbps (hybrid SP PLC-WLC channels) and 7 kbps (hybrid LP PLC-WLC channels) for the NB-PLC channels − may be significant for fulfilling several low-data-rate demands associated with SG, the IoT, and Industry 4.0 applications. Finally, but not least, it is important to highlight that the total harvested energy could be used in other applications or even for charging the battery of devices belonging to sensors networks.

Regarding the third scenario, Figure 21 shows the CCDFs of the ergodic achievable data rates for the Power Masks #1 and #2 in the Scenario #A3 when EH is done by means of hybrid SP PLC-WLC channels (top) or hybrid LP PLC-WLC channels (bottom) with two distinct values of η^q. In this scenario, the values of the ergodic achievable data rate are up to 1400 bps in both cases. However, when considering the probability of 0.75 and $\eta^q = 1$, these values are 30 bps for the hybrid SP PLC-WLC channels and 22 bps for the hybrid LP PLC-WLC channels with both considered power masks. This scenario shows the usefulness of the EH together with hybrid channels for WLC applications. Also, it is important to emphasize that the PLC additive noise is being recycled and this process will improve the quality of energy delivery by electric utilities.

Figure 21 – The CCDFs of ergodic achievable data rates yielded by the WLC (EH) device in Scenario #A3 for $\eta^q = 1$ (continuous line) and $\eta^q = 0.5$ (dashed line).



Source: Personal collection.

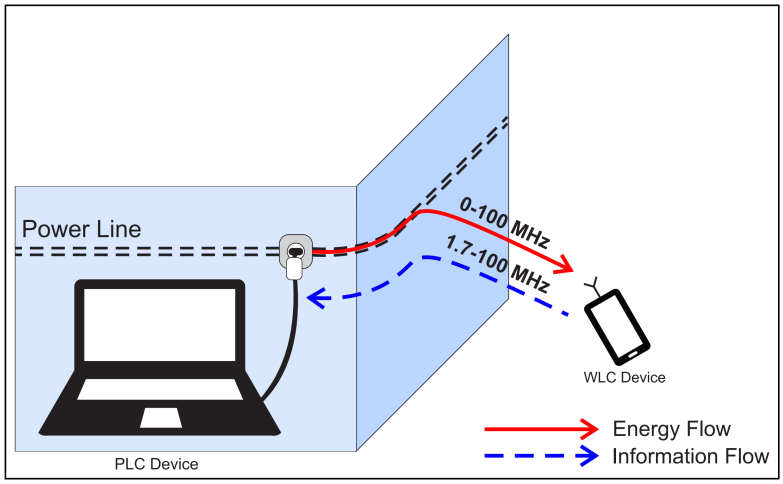
3.4.7 Ergodic Achievable Data Rate Analyses: Hybrid PLC-WLC Channels

In order to bring attention to the usefulness of the data communication through the hybrid PLC-WLC channel and *in-band* strategy, another two scenarios are introduced as follows:

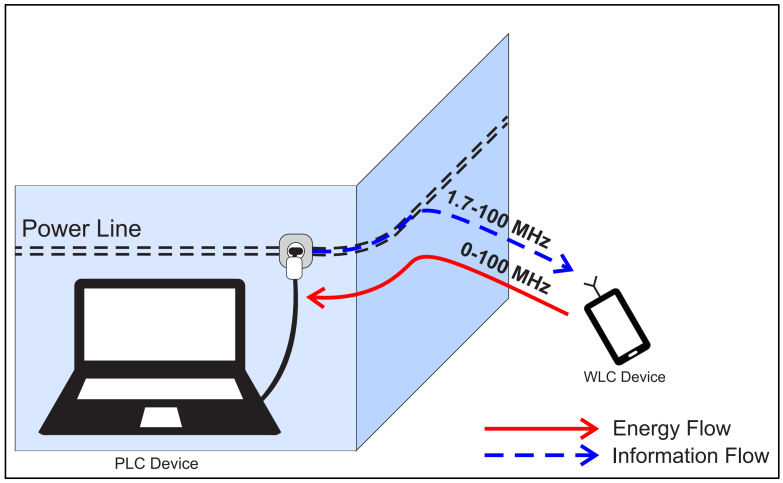
- Scenario #B1 (Figure 22(a)): the WLC (EH) device harvests energy from the hybrid PLC-WLC channel (PLC → WLC direction), assuming the use of the frequency band from 0 to 100 MHz. That is, the total harvested energy is the sum of FoN received signal and WLC additive noise energies. After that, this amount of energy is used for data communication from this WLC device to a PLC device through the hybrid PLC-WLC channel (WLC → PLC direction), in the frequency range from 1.7 to 100 MHz. Thus, the hybrid channel acts as a source of energy in the PLC → WLC direction and then it works as a data communication medium in the WLC → PLC direction.

- Scenario #B2 (Figure 22(b)): the PLC (EH) device harvests the energy from the hybrid PLC-WLC channel in the WLC → PLC direction by considering the frequency band delimited by 0 and 100 MHz. In other words, the total harvested energy is the sum of FoN received signal and PLC additive noise energies. In the sequence, the total harvested energy is used for data communication from the aforementioned PLC device to a WLC device (PLC → WLC direction) in the frequency band from 1.7 up to 100 MHz. Note

Figure 22 – Two distinct scenarios: (a) Scenario #B1, (b) Scenario #B2.



(a) WLC (EH) device with WLC → PLC direction.



(b) PLC (EH) device with PLC → WLC direction.

Source: Personal collection.

that the frequencies under 1.7 MHz are not used for data communication due to the high interference with AM signals.

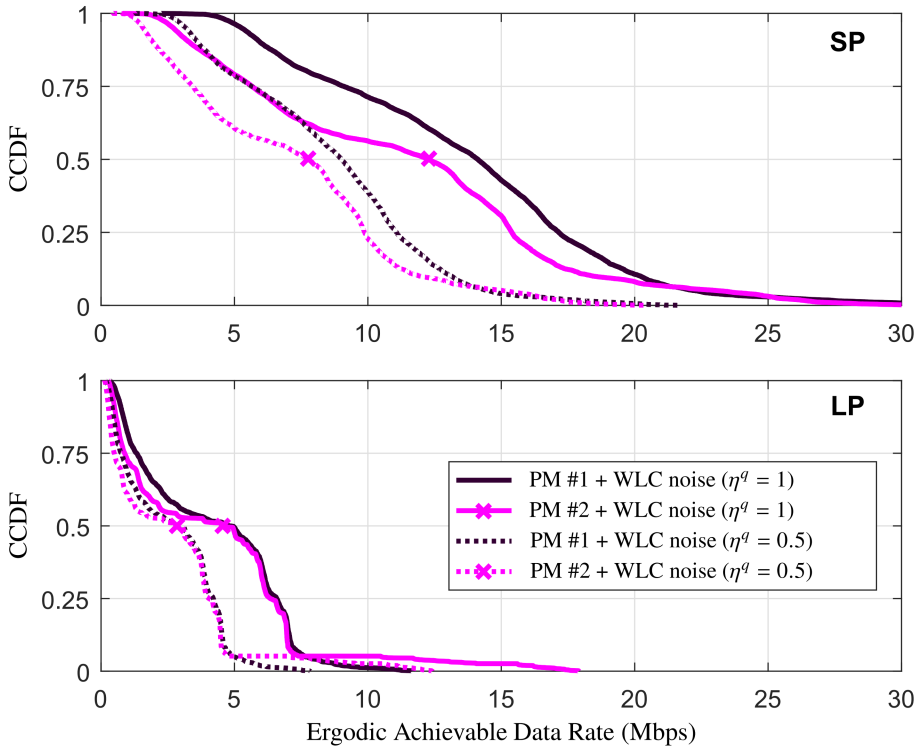
The mathematical formulation of Subsection **3.4.6** is used to evaluated the ergodic achievable data rates of the hybrid PLC-WLC channels. For the sake of simplicity, it is defined $\overline{q} \triangleq$ PLC $\rightarrow$ WLC, if $q =$ WLC $\rightarrow$ PLC and $\overline{q} \triangleq$ WLC $\rightarrow$ PLC, otherwise. With this definition, it can be easily indicated that the data communication occurs in the $\overline{q}$ direction while the energy flows in the opposite direction (i.e., the q one). Mathematically, one may calculate the ergodic achievable data rate by means of (3.8) substituting ℓ with $\overline{q}$, therefore (3.8) is subject to $\int_{-\infty}^{\infty} \upsilon_j^{\overline{q}}(f)df \leq \mathcal{P}_{Y,c}^{q}$. Here, both the CFRs and additive noise' PSDs are the ones obtained from the measured data set (see Section 3.3) and both are associated with $\overline{q}$. Furthermore, the PSD of the signal generated by the transmitter is $S_{\tilde{X}}^{\overline{q}}(f)$ with $\int_{B'_w} S_{\tilde{X}}^{\overline{q}}(f)df = 1$ and $B'_w \approx 98.3$ MHz being the data communication's frequency bandwidth. Also, $S_V^{\overline{q}}(f)$ refers to the PSD of the $\overline{q}^{th}$

communication direction receiver's additive noise. Moreover, it is considered that the full CSI is available only for the data communication through the hybrid PLC-WLC channel, thus the optimal power allocation is applied in $\upsilon_j^{\overline{q}}(f)$ with the use of WF technique.

In general, similar assumptions as the ones in the previous scenarios are made, i.e., the energy harvester has κT_{AC} seconds per cycle of the AC mains voltage signal to perform EH while the remaining $(1-\kappa)T_{AC}$ seconds are used for data communication through the hybrid PLC-WLC channel in the opposite direction. As well, κ is made equal to 0.5 and the Power Masks #1 and #2 are applied.

In this sense, Figure 23 shows the CCDFs of the ergodic achievable data rates for the use of the Power Masks #1 and #2 in the Scenario #B1 when both EH and data communication are carried out by means of hybrid SP PLC-WLC channels (top) or hybrid LP PLC-WLC channels (bottom), with $\eta^q = 0.5$ represented by dashed line and $\eta^q = 1$ in continuous line. The same information is shown in Figure 24, for the Scenario #B2.

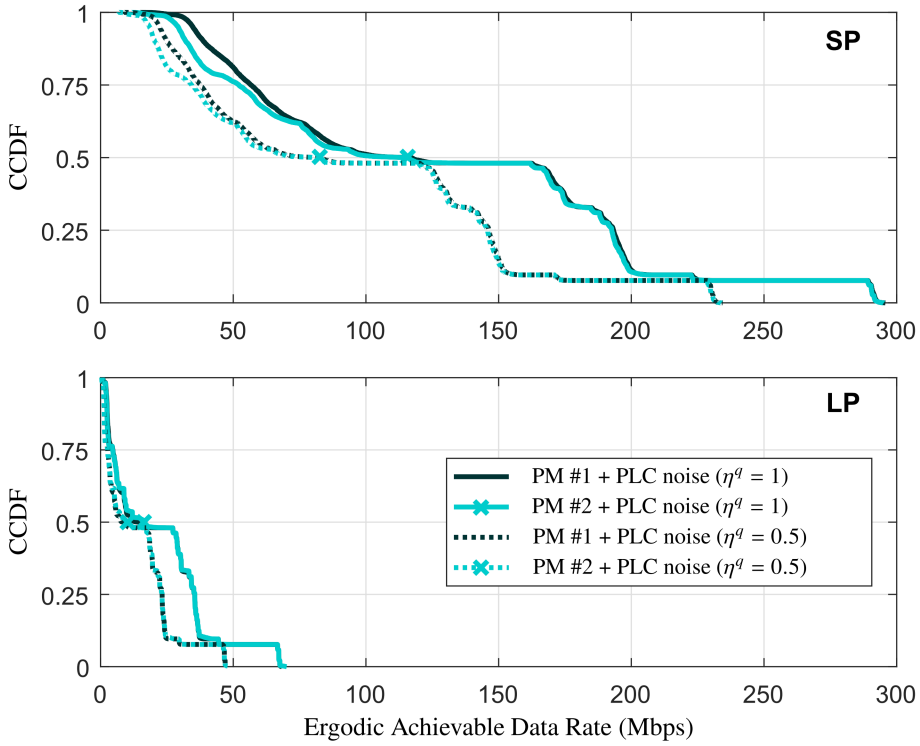
Figure 23 – The CCDFs of ergodic achievable data rates yielded by the WLC (EH) device in Scenario #B1 for $\eta^q = 1$ (continuous line) and $\eta^q = 0.5$ (dashed line).



Source: Personal collection.

Looking at Figure 23 (Scenario #B1), it can be seen that for Power Mask #1, $\eta^q = 1$, and a high probability (0.75), an ergodic achievable data rate of 9 and 1.5 Mbps can be yielded in hybrid SP PLC-WLC and hybrid LP PLC-WLC channels, respectively. In comparison, when assuming Scenario #B2 (Figure 24), the same power mask ($\eta^q = 1$) and a probability of 0.75, these values increase to 57 and 4 Mbps for hybrid SP PLC-WLC and hybrid LP PLC-WLC channels, respectively.

Figure 24 – The CCDFs of ergodic achievable data rates yielded by the PLC (EH) device in Scenario #B2 for $\eta^q = 1$ (continuous line) and $\eta^q = 0.5$ (dashed line).



Source: Personal collection.

Now, by assuming $\eta^q = 0.5$ with Power Mask #1 and a probability of 0.75, the Scenario #B1 results in an ergodic achievable data rate of 6 and 1 Mbps, respectively, for hybrid SP PLC-WLC and hybrid LP PLC-WLC channels. When considering Scenario #B2 with the previous assumptions as well, these values are 38 Mbps for the hybrid SP PLC-WLC and 2 Mbps for the hybrid LP PLC-WLC.

As expected, the decrease in the value of η^q, resulted in a reduction of the ergodic achievable data rate values for the same conditions. As well, it can be seen that the Power Mask #1 always outperforms the Power Mask #2 for high probability. Lastly, but not least, the ergodic achievable data rate values related to Scenarios #A1 and #A2 are lower than the ones obtained in Scenarios #B1 and #B2 mainly due to the use of a narrowband channel (NB-PLC or LP-RF WLC), in the former scenarios, instead of a broadband one (hybrid PLC-WLC channel) in the latter scenarios. This occurs because, the broader is the frequency bandwidth of a frequency-varying channel, the higher is the probability of occurrence of a high SNR value in a single subchannel, resulting in a better choice for optimal power allocation technique. Therefore, the values of ergodic achievable data rate changed from dozens of bits or kbps to dozens of Mbps.

Based on the performance analyses of the measured data set of hybrid PLC-WLC channels and additive noises, this section has shown that the BB-PLC additive noise significantly contributes to increase the total harvested energy and to decrease the average time interval to achieve an energy threshold due to the high power nature of this noise. Also, these analyses

have shown how the total harvested energy is impacted by the type of harvesting signal and the choice of the power mask, whereas the obtained values of ergodic achievable data rates may be significant for fulfilling several low-data-rate demands associated with SG, the IoT, and Industry 4.0 applications.

3.5 STATISTICAL ANALYSES

This section discusses statical analyses of the harvested energy from the hybrid PLC-WLC channels when the data sets of measured CFRs and additive noises described in Section 3.3 are considered. In this context, the statistical modeling of the harvested energies from the FoN received signal, the additive noises, and the total received signal is carried out. Moreover, two cases of application of proposed statistical models are detailed, one for WLC devices and another for PLC device. Also, it offers a discussion about the comparison between CCDFs of total harvested energies obtained from the measured data set and statistical model.

In this regard, Subsection **3.5.1** details the statistical modeling of the harvested energy, while Subsections **3.5.2** and **3.5.3** bring application examples of the statistical modeling of the harvested energy from the total received signal for WLC and PLC devices, respectively. Finally, Subsection **3.5.4** presents the numerical comparison between the harvested energy generated by the statistical model and calculated from the measured data set.

3.5.1 Statistical Modelings

The statistical modelings consist of fitting the harvested energy from the data set (CFRs and additive noises), assuming the five power masks and distinct values of both transmission power and overall efficiency factor, with a given statistical distribution such that its probability density function (pdf) approximates the harvested energy's histogram shape based on a certain statistic criterion. In other words, the parameters of each statistical distribution (i.e., $\mathcal{S}_{rv}$ = {Log-normal, Beta, Exponential, Rayleigh}) are varied and the one with the maximum log-likelihood value (LLV) in relation to the histogram generated with the samples of the harvested energy is selected. The elements of the set of statistical distributions, $\mathcal{S}_{rv}$, were chosen in order to represent the statistical distributions that model random variables belonging to $\mathbb{R}_+$ and that are commonly used in the telecommunications field. Concerning the choice of fitting criterion, the maximization of LLV, often known as maximum likelihood estimation in its non-logarithmic form, is widely adopted in the literature [93, 108, 109] because it is typically used as the strongest indication in comparison to other criteria such as the Akaike information criterion, Bayesian information criterion, and Efficient determination criterion.

In this regard, Tables 6, 7, and 8 list LLVs when $\mathcal{P}_x^q = 20$ dBm and $\eta^q = 1, \forall q$ for the harvested energy from the FoN received signal of hybrid SP PLC-WLC channels, hybrid LP PLC-WLC channels, and from the additive noises, respectively. With the exception of the WLC additive noise, the log-normal distribution yields the highest LLVs among the ones belonging to

Table 6 – LLVs of the FoN received signal's harvested energy: SP channels, $\mathcal{P}_x^q = 20$ dBm, and $\eta^q = 1$.

Power Mask \ Distribution	Log-normal	Beta	Exponential	Rayleigh
#1	$\mathbf{5.2969 \times 10^3}$	5.2694×10^3	5.2191×10^3	5.1745×10^3
#2	$\mathbf{5.4786 \times 10^3}$	5.4134×10^3	5.4127×10^3	4.9863×10^3
#3	$\mathbf{5.2638 \times 10^3}$	5.2240×10^3	5.2086×10^3	4.7017×10^3
#4	$\mathbf{4.5257 \times 10^3}$	4.5022×10^3	4.4663×10^3	4.3884×10^3
#5	$\mathbf{4.2499 \times 10^3}$	4.2277×10^3	4.1976×10^3	4.1120×10^3

Source: Personal collection.

Table 7 – LLVs of the FoN received signal's harvested energy: LP channels, $\mathcal{P}_x^q = 20$ dBm, and $\eta^q = 1$.

Power Mask \ Distribution	Log-normal	Beta	Exponential	Rayleigh
#1	$\mathbf{1.1273 \times 10^3}$	1.1078×10^3	1.1019×10^3	0.9490×10^3
#2	$\mathbf{1.1857 \times 10^3}$	1.1388×10^3	1.0614×10^3	0.7022×10^3
#3	$\mathbf{1.0050 \times 10^3}$	0.9992×10^3	0.9974×10^3	0.9106×10^3
#4	$\mathbf{0.9678 \times 10^3}$	0.9466×10^3	0.9373×10^3	0.7661×10^3
#5	$\mathbf{0.9021 \times 10^3}$	0.8795×10^3	0.8703×10^3	0.6946×10^3

Source: Personal collection.

Table 8 – LLVs of the additive noises' harvested energy with $\eta^q = 1$.

Additive Noise \ Distribution	Log-normal	Beta	Exponential	Rayleigh
WLC	0.7771×10^3	$\mathbf{0.7810 \times 10^3}$	0.7777×10^3	0.7300×10^3
PLC	$\mathbf{0.5113 \times 10^3}$	0.5112×10^3	0.5034×10^3	0.4287×10^3

Source: Personal collection.

the $\mathcal{S}_{rv}$ set. Concerning the WLC additive noise, it can be seen in Table 8 that the LLV difference between beta and log-normal distributions is almost negligible. Mathematically, the difference between these values does not exceed 0.5 %, which makes them very close approximations to each other. Although the beta distribution is the best fitting distribution for the WLC additive noise, the log-normal distribution is easier to handle mathematically than the beta one, and, as a consequence, the log-normal distribution will be used to the statistical modeling of the WLC additive noise.

By means of the LLVs in Tables 6, 7, and 8, one can conclude that the log-normal distribution yields the best representation of the harvested energy from FoN received signals and additive noises in hybrid PLC-WLC channels. In addition, the harvested energy from the total received signal (FoN received signal + additive noise) is straightforwardly made the summation of these two distinct parts, and consequently it is modeled as the summation of these

two log-normally distributed random variables. Mathematically, the total harvested energy from hybrid PLC-WLC channels during T_{AC} is a random variable expressed as

$$\mathcal{E}_Y^q = \mathcal{E}_{\tilde{Y}}^q + \mathcal{E}_V^q, \tag{3.9}$$

in which $\mathcal{E}_{\tilde{Y}}^q \sim \exp(Z_{\mathcal{E}_{\tilde{Y}}}^q)$ and $\mathcal{E}_V^q \sim \exp(Z_{\mathcal{E}_V}^q)$ are random variables with log-normal distribution that model the harvested energy of the FoN received signal and additive noises during T_{AC}, respectively. Furthermore, $Z_{\mathcal{E}_{\tilde{Y}}}^q \sim \mathcal{N}(\mu_{\tilde{Y}^q}, \sigma_{\tilde{Y}^q}^2)$ is normally distributed with mean $\mu_{\tilde{Y}^q}$ and variance $\sigma_{\tilde{Y}^q}^2$, while $Z_{\mathcal{E}_V}^q \sim \mathcal{N}(\mu_{v^q}, \sigma_{v^q}^2)$ is normally distributed with mean μ_{v^q} and variance $\sigma_{v^q}^2$. Note that (3.9) allows to easily obtain the total harvested energy of a WLC or PLC device, which is immersed in a environment characterized by hybrid PLC-WLC channels. This can be accomplished by substituting q by PLC $\rightarrow$ WLC or WLC $\rightarrow$ PLC.

In this regard, the log-normal distribution is described by two parameters (μ and σ) and these parameters are directly related to its mean and variance [110]. As expected, changing $\mathcal{P}_x^q$ and η^q only affects the amplitude of harvested energies. Therefore, for a given power mask, σ does not change for distinct values of $\mathcal{P}_x^q$ and η^q. However, it is observed that there is a logarithmic relation between μ and η^q as well as between μ and $\mathcal{P}_x^q$. Mathematically, for the harvested energy from the FoN received signal, this relation can be expressed as

$$\mu_{\tilde{Y}^q}(\eta^q, \mathcal{P}_x^q) = \mu_0 + \ln(\eta^q \mathcal{P}_x^q), \tag{3.10}$$

where $\mathcal{P}_x^q$ is the value of transmission power in mW and μ_0 represents the parameter μ of a log-normal distribution when $\mathcal{P}_x^q = 1$ mW and $\eta^q = 1$. The parameters $(\mu_0, \sigma_{\tilde{Y}^q})$ are obtained by the statistical modeling procedure, described at the beginning of this section, and are given in Table 9 for the five distinct power masks and distinct channel distance ranges.

Also, PLC and WLC additive noises can be similarly modeled. Nevertheless, it is important to emphasize that $\mathcal{P}_x^q$ does not affect the modeling of the harvested energy from additive noises because it only influences the FoN received signal. Therefore, the relation between μ and η^q for the harvested energy from additive noises is given by

$$\mu_v^q(\eta^q) = \mu_0 + \ln(\eta^q), \tag{3.11}$$

in which μ_0 denotes the μ parameter of the log-normal distribution for $\eta^q = 1$. The parameters (μ_0, σ_{v^q}) are also obtained by the statistical modeling procedure, and are given in Table 10 by considering q = PLC $\rightarrow$ WLC and q = WLC $\rightarrow$ PLC, respectively.

In the following, Subsections **3.5.2** and **3.5.3** detail two cases for the application of the presented statistical modeling. The first case assumes that a WLC device harvests energy from the total received signal that was transmitted by a PLC device, through the hybrid SP PLC-WLC channel, with Power Mask #2 and $\mathcal{P}_x^{\text{PLC}\rightarrow\text{WLC}} = 23$ dBm because the given power mask and the amount of transmission power are usually adopted by BB-PLC devices. Also, a practical value of overall efficiency factor for WLC device's EH circuitry is used, $\eta^{\text{PLC}\rightarrow\text{WLC}} = 0.5$. The second case provides an evaluation of the harvested energy by a PLC device from the

Table 9 – Harvested energy from the FoN signal - The parameters for the fitted log-normal distribution.

Power Mask \ Channel	SP $(\mu_0, \sigma_{\tilde{Y}q})$	LP $(\mu_0, \sigma_{\tilde{Y}q})$
#1	(-18.5801, 0.7088)	(-20.8168, 1.2314)
#2	(-19.3577, 1.0494)	(-21.7950, 1.6284)
#3	(-19.1162, 1.3136)	(-19.2780, 1.2938)
#4	(-16.7773, 0.7699)	(-18.7911, 1.2889)
#5	(-16.1395, 0.7985)	(-17.9191, 1.2645)

Source: Personal collection.

Table 10 – Harvested energy from the additive noise - The parameters for the fitted log-normal distribution.

Additive Noise	(μ_0, σ_{vq})
WLC	(-14.8483, 1.6263)
PLC	(-11.8117, 1.7687)

Source: Personal collection.

total received signal that was transmitted by a WLC device, through the hybrid LP PLC-WLC channel, using Power Mask #1 and $\mathcal{P}_x^{\text{WLC}\to\text{PLC}} = 20$ dBm because the chosen power mask and the value of transmission power are commonly adopted by WLC devices. Furthermore, the overall efficiency factor of the PLC device's EH circuitry is expected to be low due to time-varying access impedance of electric power systems, as pointed out in Chapter 2, thus $\eta^{\text{WLC}\to\text{PLC}} = 0.2$ is adopted.

3.5.2 WLC Device - Harvesting Energy

Let assume that the WLC device has $\eta^{\text{PLC}\to\text{WLC}} = 0.5$ and harvests its energy from a hybrid SP PLC-WLC channel during a cycle of the AC mains voltage signal, $T_{AC} \approx 16,667$ ms, while the PLC device uses Power Mask #2 and $\mathcal{P}_x^{\text{PLC}\to\text{WLC}} = 23$ dBm. The total harvested energy during T_{AC} is modeled as a random variable equal to $\mathcal{E}_Y^{\text{PLC}\to\text{WLC}} = \mathcal{E}_{\tilde{Y}}^{\text{PLC}\to\text{WLC}} + \mathcal{E}_V^{\text{PLC}\to\text{WLC}}$, where

$$\mathcal{E}_{\tilde{Y}}^{\text{PLC}\to\text{WLC}} \sim \exp\left(\mathcal{N}(\mu_{\tilde{Y}^{\text{PLC}\to\text{WLC}}}, \sigma^2_{\tilde{Y}^{\text{PLC}\to\text{WLC}}})\right)$$

and

$$\mathcal{E}_V^{\text{PLC}\to\text{WLC}} \sim \exp\left(\mathcal{N}(\mu_{v^{\text{PLC}\to\text{WLC}}}, \sigma^2_{v^{\text{PLC}\to\text{WLC}}})\right).$$

The two log-normals' μ parameters can be calculated using (3.10) and (3.11) with the values presented in Tables 9 and 10, while σ parameters are taken directly from these tables. As a result, $\mu_{\tilde{Y}^{\text{PLC}\to\text{WLC}}} = -14.7550$ and $\mu_{v^{\text{PLC}\to\text{WLC}}} = -15.5414$ as well as $\sigma_{\tilde{Y}^{\text{PLC}\to\text{WLC}}} = 1.0494$ and $\sigma_{v^{\text{PLC}\to\text{WLC}}} = 1.6263$. These values are obtained as follows:

$$\begin{aligned}\mu_{\tilde{Y}^{\text{PLC}\to\text{WLC}}} &= -19.3577 + \ln(0.5 \cdot 199.5) \\ &= -14.7550\end{aligned}$$

and

$$\begin{aligned}\mu_{v}^{\text{PLC}\rightarrow\text{WLC}} &= -14.8483 + \ln(0.5)\\ &= -15.5414.\end{aligned}$$

Quantitatively, the harvested energy from the FoN received signal that was transmitted by the PLC device, through the hybrid SP PLC-WLC channel, and received by the WLC device during T_{AC} follows a log-normal distribution with mean and standard deviation values approximately equal to 0.68 μJ and 0.96 μJ, respectively. Also, the WLC additive noise resulted in an energy amount described by a log-normal distribution with mean and standard deviation equal to 0.67 μJ and 2.42 μJ, respectively, at the WLC device's energy storage element. By assuming their mean values, the summation of the harvested energies would result in 1.35 μJ of average energy during T_{AC}. Note that, in this case, both FoN received signal and WLC additive noise contributes similarly to the total harvested energy.

3.5.3 PLC Device - Harvesting Energy

In this case, the PLC device has $\eta^{\text{WLC}\rightarrow\text{PLC}} = 0.2$ and harvests the energy from a hybrid SP PLC-WLC channel, while the WLC device uses Power Mask #1 and $\mathcal{P}_{x}^{\text{WLC}\rightarrow\text{PLC}} = 20$ dBm. Thus, the total harvested energy during T_{AC} is a random variable given by $\mathcal{E}_{Y}^{\text{WLC}\rightarrow\text{PLC}} = \mathcal{E}_{\tilde{Y}}^{\text{WLC}\rightarrow\text{PLC}} + \mathcal{E}_{V}^{\text{WLC}\rightarrow\text{PLC}}$, in which

$$\mathcal{E}_{\tilde{Y}}^{\text{WLC}\rightarrow\text{PLC}} \sim \exp\left(\mathcal{N}(\mu_{\tilde{Y}^{\text{WLC}\rightarrow\text{PLC}}}, \sigma^{2}_{\tilde{Y}^{\text{WLC}\rightarrow\text{PLC}}})\right)$$

and

$$\mathcal{E}_{V}^{\text{WLC}\rightarrow\text{PLC}} \sim \exp\left(\mathcal{N}(\mu_{v^{\text{WLC}\rightarrow\text{PLC}}}, \sigma^{2}_{v^{\text{WLC}\rightarrow\text{PLC}}})\right).$$

Again, the μ parameters of $\mathcal{E}_{\tilde{Y}}^{\text{WLC}\rightarrow\text{PLC}}$ and $\mathcal{E}_{V}^{\text{WLC}\rightarrow\text{PLC}}$ can be calculated using (3.10) and (3.11), supported by the values presented in Tables 9 and 10, while σ parameters are taken directly from these tables. Consequently, $\mu_{\tilde{Y}^{\text{WLC}\rightarrow\text{PLC}}} = -15.5844$ and $\mu_{v^{\text{WLC}\rightarrow\text{PLC}}} = -13.4211$. Also, $\sigma_{\tilde{Y}^{\text{WLC}\rightarrow\text{PLC}}} = 0.7088$ and $\sigma_{v^{\text{WLC}\rightarrow\text{PLC}}} = 1.7687$. These values are obtained as follows:

$$\begin{aligned}\mu_{\tilde{Y}^{\text{WLC}\rightarrow\text{PLC}}} &= -18.5801 + \ln(0.2 \cdot 100)\\ &= -15.5844\end{aligned}$$

and

$$\begin{aligned}\mu_{v}^{\text{WLC}\rightarrow\text{PLC}} &= -11.8117 + \ln(0.2)\\ &= -13.4211.\end{aligned}$$

The FoN received signal originated in the WLC device, transmitted through the hybrid SP PLC-WLC channel, and received by the PLC device resulted in a harvested energy that follows a log-normal distribution with mean and standard deviation that are approximately equal to 0.22 μJ and 0.18 μJ. As well, the PLC additive noise produced an energy amount

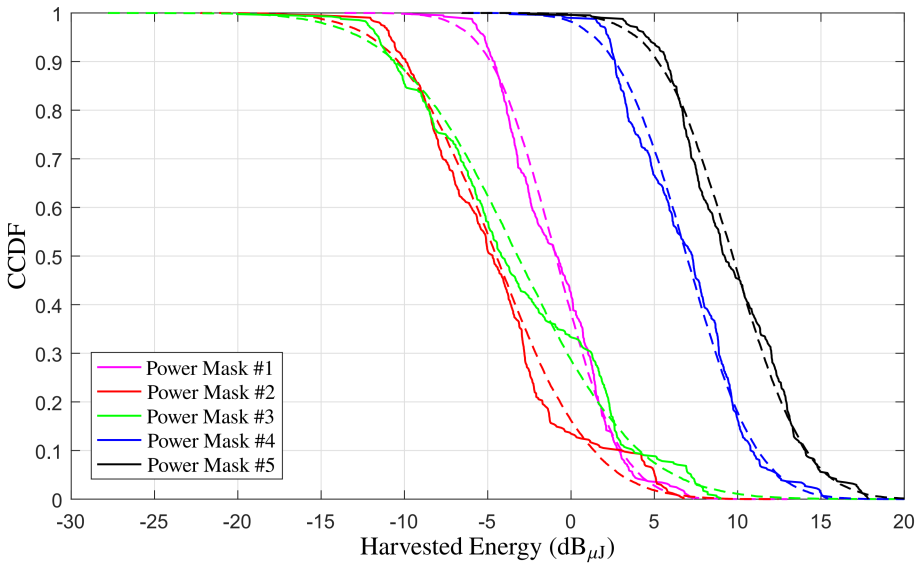
described by a log-normal distribution with mean and standard deviation equal to 7.09 μJ and 33.13 μJ, respectively, at the PLC device's energy storage element. As a result, the average harvested energy during T_{AC} is equal to 7.31 μJ. Here, the PLC additive noise has a considerable contribution to the total harvested energy.

3.5.4 Numerical Comparisons: Statistical Models and Measured Data Set

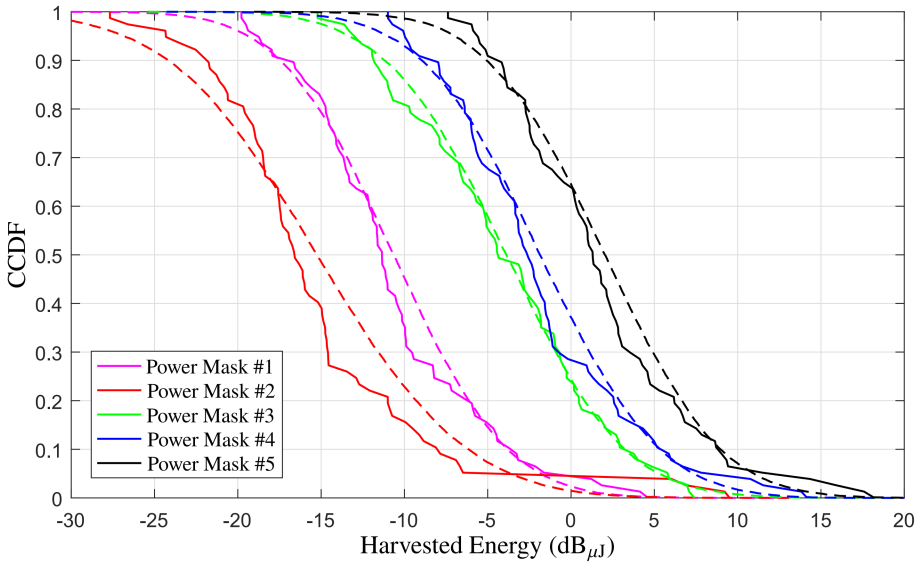
Aiming to validate the statistical modelings, this subsection deals with the comparison between the CCDFs of harvested energies generated by statistical models and the CCDFs of harvested energies obtained from the measured data set. In this regard, Figure 25(a) shows comparisons among CCDFs of harvested energies from the FoN received signal of a hybrid SP PLC-WLC channel (represented by continuous lines), which was calculated with the measured CFRs, and CCDFs of the log-normally distributed random variable obtained from the statistical modeling of the FoN received signal (dashed lines). These plots assume the use of the five power masks, $\mathcal{P}_x^q = 20$ dBm, and $\eta^q = 1$ to illustrate an ideal case of overall efficiency factor of the EH circuitry. Here, the harvested energies from the FoN received signal is modeled as a log-normally distributed random variable $\mathcal{E}_{\tilde{Y}}^q \sim \exp\left(\mathcal{N}(\mu_{\tilde{Y}^q}, \sigma_{\tilde{Y}^q}^2)\right)$, in which $\mu_{\tilde{Y}^q} = \mu_0 + \ln(100)$, whereas μ_0 and $\sigma_{\tilde{Y}^q}$ depend on the chosen power mask and the channel distance range, and are both obtained from the first column in Table 9. Under the same assumptions and for the hybrid LP PLC-WLC channel, Figure 25(b) shows similar comparisons, where μ_0 and $\sigma_{\tilde{Y}^q}$ are both obtained from the second column of Table 9. By comparing these two figures, it is possible to see that CCDFs of statistical models are closer to CCDFs from measured data set in hybrid SP PLC-WLC channels rather than in hybrid LP PLC-WLC channels due to the high variations of the magnitude of CFRs experienced by the latter. For instance, the highest discrepancy is noted in Figure 25(b) for Power Mask #2, in which -14.5 dB$_{\mu\text{J}}$ of harvested energy results in a difference of $(0.46 - 0.27) \times 100 = 19$ % between the CCDFs of statistical model and measured data set.

Similarly, Figure 26 shows a comparison between the CCDF of the harvested energies from WLC and PLC additive noises (continuous lines) and the CCDF of log-normally distributed random variables obtained from the statistical modeling of harvested energies from WLC and PLC additive noises (dashed lines) with $\eta^q = 1$. These random variables are modeled as $\mathcal{E}_V^q \sim \exp\left(\mathcal{N}(\mu_{v^q}, \sigma_{v^q}^2)\right)$, in which $\mu_{v^q} = \mu_0$ and σ_{v^q} are obtained from the first and second lines of Table 10 for the WLC and PLC additive noises, respectively. In this figure, a discrepancy is observe between CCDFs of harvested energies of statistical models and measured data set, which is in the worst case $0.47 - 0.26 \times 100 = 21$ % (at 0 dB$_{\mu\text{J}}$) and $0.46 - 0.26 \times 100 = 20$ % (at 13.5 dB$_{\mu\text{J}}$) for the WLC and PLC additive noises, respectively. It is important to emphasize that the impulsive components of the PLC additive noise may be responsible for increasing the inaccuracy between harvested energies from the statistical model and measured data set due to its high amplitude values in relation to the background component, which makes the statistical modeling of it by a single random variable not extremely precise; however, the

Figure 25 – CCDF of the harvested energy from the FoN received signal: The five power masks, $\mathcal{P}_x^q = 20$ dBm and $\eta^q = 1$.



(a) SP channel



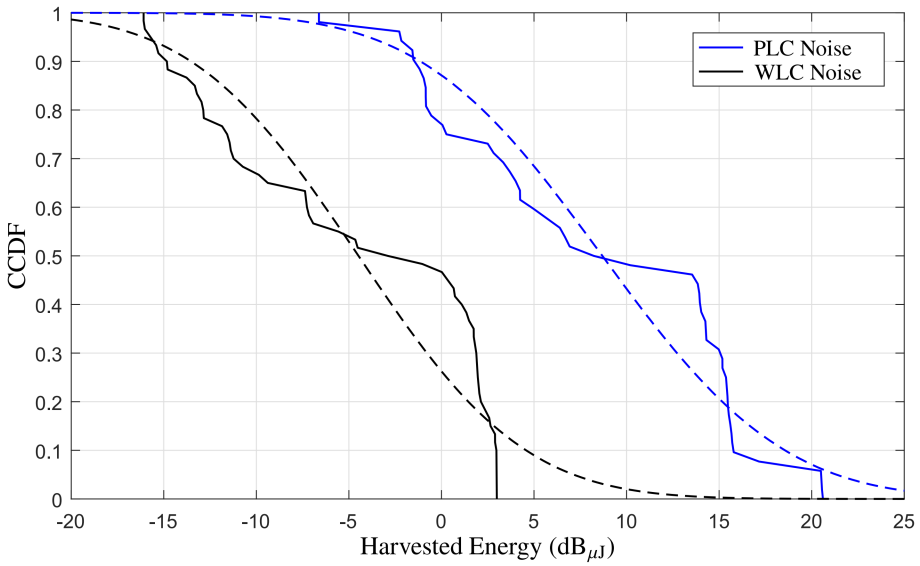
(b) LP channel

Source: Personal collection.

presented modeling is easily to mathematically handle and it has a limited inaccuracy between the harvested energy obtained from the statistical model and measured data set.

Figure 27(a) shows comparisons among CCDFs of total harvested energies, calculated from the measured data set, by a WLC device through a hybrid SP PLC-WLC channel (continuous lines) and CCDFs of random variables generated with the statistical modeling of these harvested energies (dashed lines). The random variables are the sum of two log-normally distributed random variables, one for the FoN received signal and one to the WLC additive noise. These plots are obtained with the five power masks, $\mathcal{P}_x^{\text{PLC}\rightarrow\text{WLC}} = 20$ dBm, and $\eta^{\text{PLC}\rightarrow\text{WLC}} = 1$

Figure 26 – CCDF of the harvested energy from the additive noises with $\eta^q = 1$.



Source: Personal collection.

because the chosen values represent a situation in which the PLC device operates with a typical value of transmission power and the WLC device's EH circuitry has an ideal overall efficiency factor. Under the same assumptions, Figure 27(b) shows similar comparisons, but assuming hybrid LP PLC-WLC channels. In both cases, the total harvested energy is modeled as a random variable $\mathcal{E}_Y^{\text{PLC}\to\text{WLC}} = \mathcal{E}_{\tilde{Y}}^{\text{PLC}\to\text{WLC}} + \mathcal{E}_V^{\text{PLC}\to\text{WLC}}$, where

$$\mathcal{E}_{\tilde{Y}}^{\text{PLC}\to\text{WLC}} \sim \exp\left(\mathcal{N}(\mu_{\tilde{Y}^{\text{PLC}\to\text{WLC}}}, \sigma^2_{\tilde{Y}^{\text{PLC}\to\text{WLC}}})\right)$$

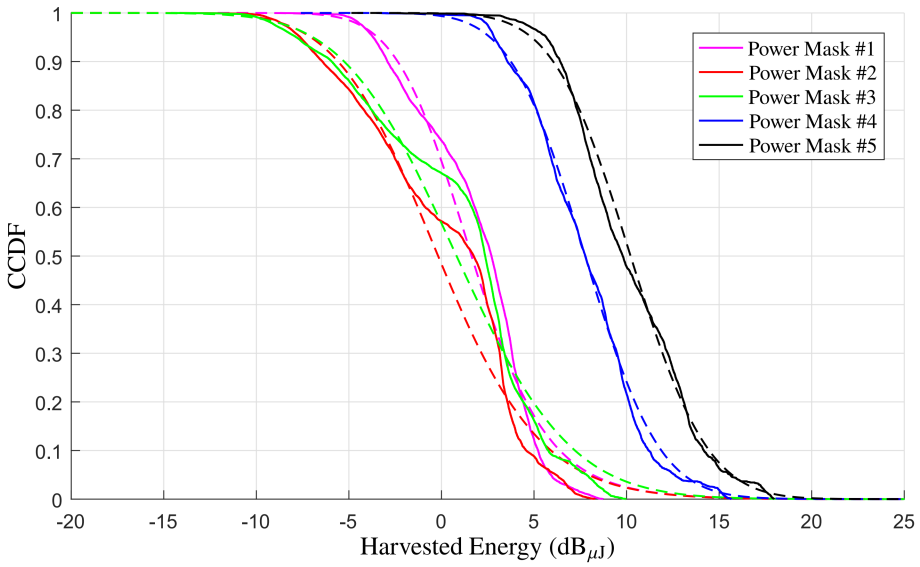
and

$$\mathcal{E}_V^{\text{PLC}\to\text{WLC}} \sim \exp\left(\mathcal{N}(\mu_{v^{\text{PLC}\to\text{WLC}}}, \sigma^2_{v^{\text{PLC}\to\text{WLC}}})\right),$$

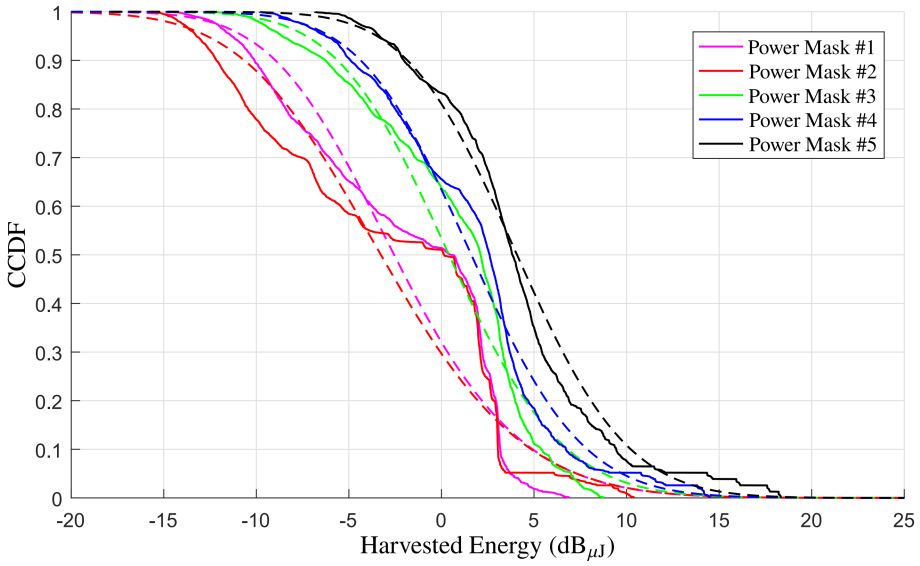
in which $\mu_{\tilde{Y}^{\text{PLC}\to\text{WLC}}} = \mu_0 + \ln(100)$, whereas μ_0 and $\sigma_{\tilde{Y}^{\text{PLC}\to\text{WLC}}}$ depend on the chosen power mask and the channel distance range, and both are obtained from the first and second columns of Table 9 for hybrid SP PLC-WLC and hybrid LP PLC-WLC channels, respectively, while $\mu_{v^{\text{PLC}\to\text{WLC}}} = -14.8483$ and $\sigma_{v^{\text{PLC}\to\text{WLC}}} = 1.6263$ are taken from the first line of Table 10.

From Figure 27(a), it is noticed that CCDFs of total harvested energies obtained from the measured data set and statistical model are, in general, close to each other, except in some specific range of values in which a slight disagreement can occur. As well, Figure 27(b) shows that total harvested energies of statistical model and measured data set present higher discrepancies in their CCDFs for Power Masks #1 and #2. For instance, Power Mask #2 has a good agreement at the harvested energies less than -4 dB$_{\mu J}$ and a disagreement is noticed from -4 dB$_{\mu J}$ to 3 dB$_{\mu J}$, in which the highest difference between the CCDFs is $0.51 - 0.30 \times 100 = 21$ % and occurs when the total harvested energy is equal to 0 dB$_{\mu J}$. As Power Masks #1 and #2 are the ones with the lowest energy harvesting performances among the considered power masks, it indicates that the lower is the contribution of the FoN received signal on the total harvested energy, the higher is the inaccuracy between total harvested energies of statistical model and measured data set.

Figure 27 – CCDF of the total harvested energy by the WLC device: The five power masks, $\mathcal{P}_x^{\text{PLC}\to\text{WLC}} = 20$ dBm and $\eta^{\text{PLC}\to\text{WLC}} = 1$.



(a) SP channel



(b) LP channel

Source: Personal collection.

Figure 28(a) shows comparisons among CCDFs of total harvested energies, obtained from measured data set, from a PLC device through the hybrid SP PLC-WLC channels (continuous lines) and the ones obtained from the statistical modeling (dashed lines). In these plots, the five distinct power masks, $\mathcal{P}_x^{\text{WLC}\to\text{PLC}} = 20$ dBm, and $\eta^{\text{WLC}\to\text{PLC}} = 1$ are applied because the given parameters illustrates a situation in which the WLC device operates with a typical transmission power and the EH circuitry of the PLC device has an ideal overall efficiency factor. Regarding hybrid LP PLC-WLC channels, Figure 28(b) shows similar comparisons. Here, the total harvested energy is modeled as a random variable equal to $\mathcal{E}_Y^{\text{WLC}\to\text{PLC}} = \mathcal{E}_{\tilde{Y}}^{\text{WLC}\to\text{PLC}} + \mathcal{E}_V^{\text{WLC}\to\text{PLC}}$,

where

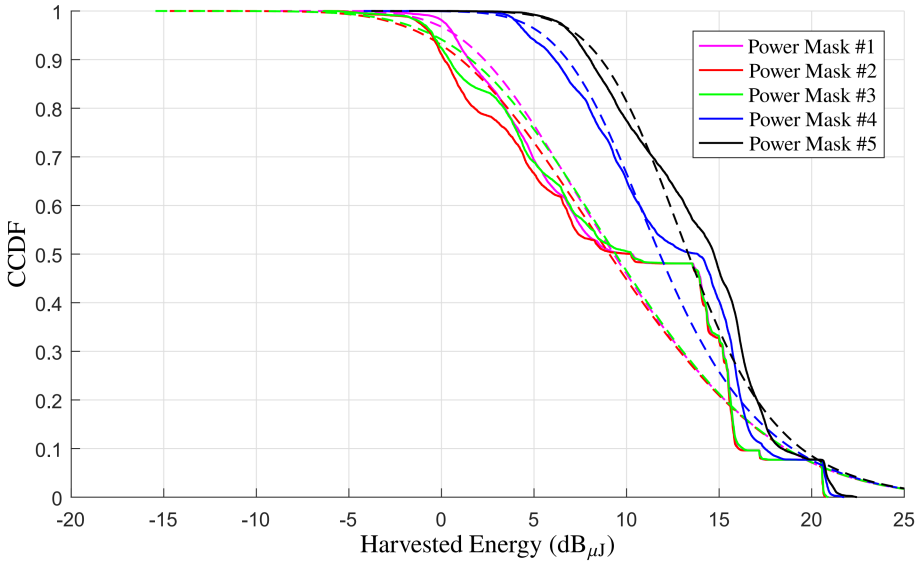
$$\mathcal{E}_{\tilde{Y}}^{\text{WLC}\to\text{PLC}} \sim \exp\left(\mathcal{N}(\mu_{\tilde{Y}^{\text{WLC}\to\text{PLC}}}, \sigma^2_{\tilde{Y}^{\text{WLC}\to\text{PLC}}})\right)$$

and

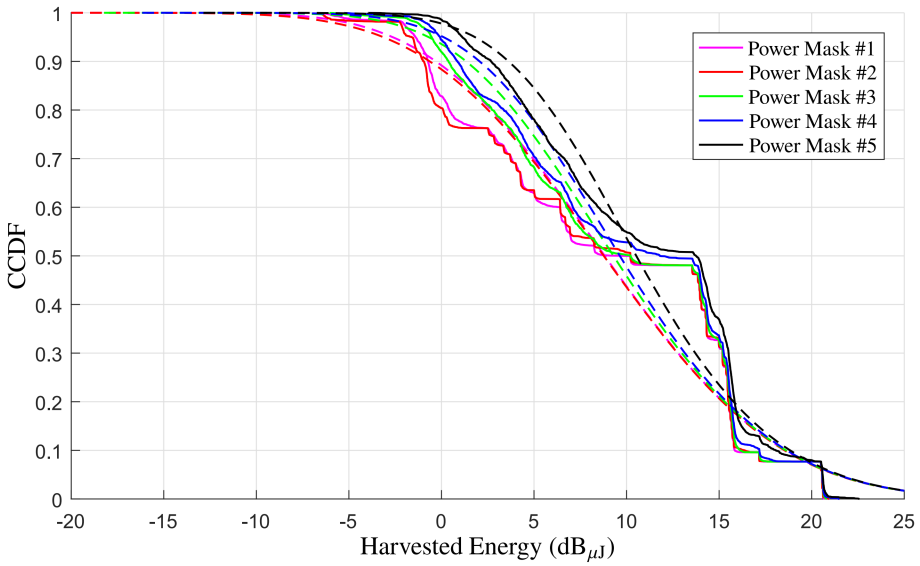
$$\mathcal{E}_{V}^{\text{WLC}\to\text{PLC}} \sim \exp\left(\mathcal{N}(\mu_{v^{\text{WLC}\to\text{PLC}}}, \sigma^2_{v^{\text{WLC}\to\text{PLC}}})\right),$$

in which $\mu_{\tilde{Y}^{\text{WLC}\to\text{PLC}}} = \mu_0 + \ln(100)$, whereas μ_0 and $\sigma_{\tilde{Y}^{\text{WLC}\to\text{PLC}}}$ are both obtained from the first and second columns of Table 9 for hybrid SP PLC-WLC and hybrid LP PLC-WLC channels, respectively, while $\mu_{v^{\text{WLC}\to\text{PLC}}} = -11.8117$ and $\sigma_{v^{\text{WLC}\to\text{PLC}}} = 1.7687$ are taken from the second line of Table 10.

Figure 28 – CCDF of the total harvested energy by the PLC device: The five power masks, $\mathcal{P}_x^{\text{WLC}\to\text{PLC}} = 20$ dBm and $\eta^{\text{WLC}\to\text{PLC}} = 1$.



(a) SP channel



(b) LP channel

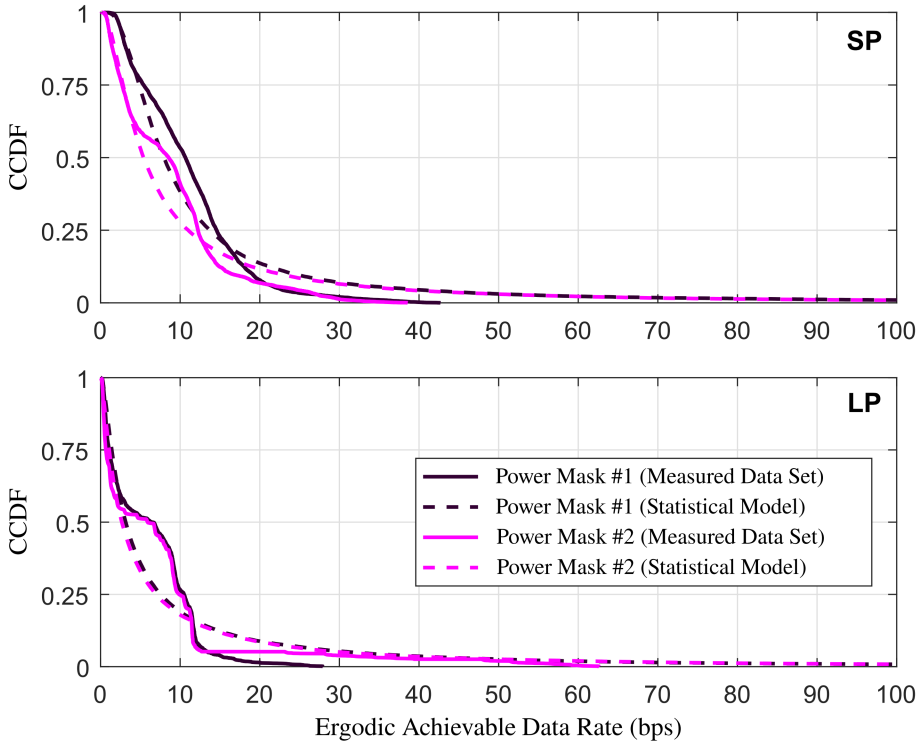
Source: Personal collection.

By means of Figure 28(a), it is clear that the lower is the contribution of the FoN received signal to the total harvested energy, the higher is the discrepancy between the CCDFs of total harvested energies of the statistical model and the measured data set. This can be observed in Power Masks #1 to #4 and almost not seen in Power Mask #5 because Power Mask #5 yields the highest contributions of the FoN received signal to the total harvested energy. In the worst case, the difference between the total harvested energy from the measured data set and statistical model occurs in Figure 28(b) and it is $0.48 - 0.27 \times 100 = 21$ %, at the point in which the total harvested energy is equal to 13.5 $\text{dB}_{\mu\text{J}}$ for Power Mask #2. Given this discussion, the characteristic that mostly affects the statistical modeling accuracy is related to the decreasing of the harvested energy from the FoN received signal in relation to the additive noise, which can be caused by: i) reducing $\mathcal{P}_x^q$, ii) the use of a power mask that worse takes advantage of $\mathcal{P}_x^q$, and iii) the use of higher distance ranges in hybrid PLC-WLC channels (i.e., LP channels instead of SP ones). Although the CCDFs of the statistical model have discrepancies with the ones from the measured data set when the highlighted characteristic occurs, the difference between them is expected since no statistical model has an excellent match to capture the complete behavior of the measured data set. Also, the difference between the CCDFs of statistical models and measured data set is not relevant and it is limited, in the worst case, by 21 % assuming typical values of $\mathcal{P}_x^q$, yielding a good agreement between them. Furthermore, if $\mathcal{P}_x^q \to 0$ W (i.e., ambient EH approach), then the highest discrepancy is the one of the additive noises, 21 % for the WLC and 20 % for the PLC, because there is no FoN received signal. On the other hand, if $\mathcal{P}_x^q \to \infty$, then the highest discrepancy is the one observed in the FoN received signal, which is 19 % for Power Mask #2 and hybrid LP PLC-WLC channels, because the additive noises yield irrelevant amounts of harvested energy in comparison to the FoN received signal under this condition.

Aiming to validate the statistical model, Figure 29 shows a numerical comparison between the CCDF of ergodic achievable data rates obtained in Scenario #A1 for Power Masks #1 and #2, with $\mathcal{P}_x^q = 20$ dBm and $\eta^q = 0.5$, when measured data set (continuous line) and the proposed statistical model (dashed line) are used to generate the total harvested energy values. These values are applied in (3.8) in order to obtain the ergodic achievable data rates. Also, the chosen scenario represents an interesting possibility of IoT application due to its high relation to LP-RF WLC device, which is commonly used in wireless sensors network for making each electronic device communicating to another. According to Subsection **3.4.6**, Scenario #A1 is described as follows: a WLC (EH) device harvests its energy from the hybrid PLC-WLC channel and, thus, realize a data communication with another LP-RF WLC device at one of the unlicensed ISM frequency band, which is centered at 5.8 GHz, with a frequency bandwidth of 500 kHz. It is assumed that the WLC device is consecutively communicating and harvesting energy, such that it uses half of the time for EH and the other half for data communication.

In Figure 29, it can be seen that the same inaccuracy observed between CCDFs of total harvested energies of statistical model and measured data set in Figures 27 and 28 are also noticed between CCDFs of ergodic achievable data rates when the total harvested energies, used

Figure 29 – Scenario #A1 - CCDF of the ergodic achievable data rate for hybrid SP PLC-WLC channel (top) and hybrid LP PLC-WLC channel (bottom): Power Masks #1 and #2, $\mathcal{P}_x^q = 20$ dBm and $\eta^q = 0.5$.



Source: Personal collection.

for data communication, are obtained from the statistical model and measured data set. In other words, the total harvested energy from the statistical model is in good agreement with the one obtained from the measured data set and it is also seen in the CCDF of ergodic achievable data rates. Therefore, the statistical models have made the harvested energies a generic and an easy-to-simulate feature for any value of η^q, $\mathcal{P}_x^q$, for five distinct power masks, and for two different regions that are associated with distinct distances of the WLC device from the power line (i.e., SP and LP channels), which can be used to perform data communications.

3.6 SUMMARY

In this chapter, the harvested energy from the concatenated hybrid PLC-WLC channels in a dedicated EH approach was formulated and modeled. Based on performance and statistical analyses, it was shown that hybrid PLC-WLC channels are valuable for EH because feasible values of energy can be harvested from these channels with high probability, especially from the BB-PLC additive noise. In this sense, the harvested energy from these channels for data communication purposes may offer a satisfactory low data rate for assisting SG, the IoT, and Industry 4.0 applications, while the statistical modeling of it can bring several benefits for carrying out studies for designing novel data network technologies.

4 A HYBRID PLC/WLC DUAL-HOP SYSTEM WITH ENERGY HARVESTING RELAY

The advance and widespread of smart devices, such as the ones in the IoT era, show how essential and fundamental are data communication systems to deploy high-density and ubiquitous data networks. As pointed out in Chapter 2, these data networks generate non-environmental signals, i.e., signals that carry information, which also can be seen as sources of energy for energy harvesting purposes. The presence of these signals is of utmost importance for EH devices because such devices can make use of energies from the received signals, which carry information and additive noises, to perform data communication. In the previous chapter, a discussion about the use of concatenated hybrid PLC-WLC channels for performing dedicated EH was carried out. However, there are still relevant research problems that need to be answered in respect to the parallel use of PLC and WLC systems, in which it is necessary to evaluate distinct approaches for performing energy harvesting together with data communication. Therefore, the investigation of hybrid PLC/WLC[1] systems for intermittently performing energy harvesting and data communication emerges as an interesting research direction. In this context, the focus of this chapter is on the association between the dedicated EH approach and cooperative communication for improving narrow-band hybrid PLC/WLC systems that are suitable for SG, the IoT, and Industry 4.0 applications. In this regard, the main contributions of this chapter can be summarized as follows:

- Formulation of ergodic achievable data rates of the hybrid power line/wireless dual-hop system (H2HS) model when the time switching (TS), power splitting (PS), or the proposed hybrid time switching (HTS) strategy together with the AF protocol and maximal ratio combining (MRC) technique are applied at the relay node.

- Introduction and discussion of four proposed approaches for performing energy harvesting and data communication in the H2HS: the H2HS harvests the energy at the relay node only from the wireless signal using HTS (Approach A); only from the power line signal using HTS (Approach B); from both power line and wireless signals using TS (Approach C); and from both power line and wireless signals using PS (Approach D).

- Evaluation and performance comparisons among H2HS, power line dual-hop system (P2HS) and wireless dual-hop system (W2HS) under four scenarios. These scenarios cover important simulation settings for evaluation purposes.

The rest of this chapter is organized as follows: Section 4.1 introduces the H2HS model and formulates the investigated problem; Section 4.2 briefly describes the TS and PS strategies and deals with ergodic achievable data rates of the four proposed approaches in the H2HS model; Section 4.3 discusses the numerical results and Section 4.4 states the concluding remarks.

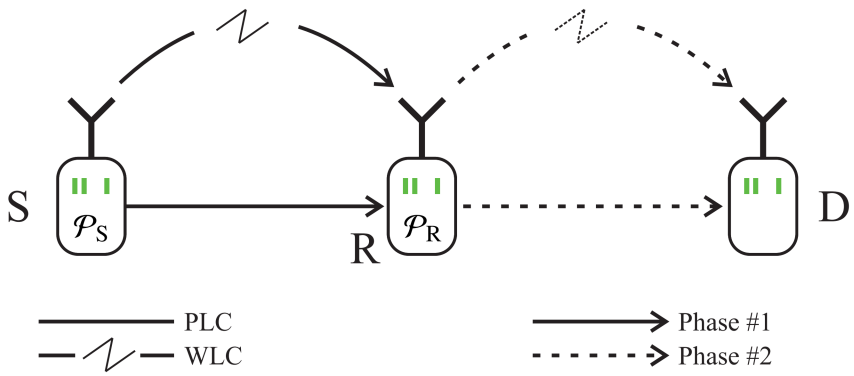
[1] The use of a slash between PLC and WLC means that these systems are in parallel.

4.1 PROBLEM FORMULATION

At the beginning of the XXI Century, a pivotal work investigated the viability of simultaneous performing WLC and EH [111], in which the author evaluated the trade-off between WLC channel capacity and EH, while [112] extended this analysis to address frequency-selective channels. As a matter of fact, [111] and [112] considered that the receiver could simultaneously decode the information and perform EH, which may not be a practical approach. Furthermore, [100] outlined two EH strategies, namely, time switching (TS) and power splitting (PS). In the former, the relay shares the time between EH and data communication tasks, while in the latter the relay simultaneously splits the power between EH and data communication ones. Also, [100] showed that TS outperforms PS in terms of throughput and data rates for low signal-to-noise conditions if AF relaying-based cooperative communication is adopted. Moreover, [113] provided a performance comparison between TS and PS strategies, by means of the rate-energy region, considering a MIMO broadcasting system. Furthermore, [114] investigated the power allocation techniques for a decode-and-forward (DF) EH-relaying system with multiple source-destination pairs and [115] extended this analysis when an interfering signal is present. Taken into account the simultaneous use of PLC and EH, a few works have addressed this topic in the literature [11–13], as highlighted in Chapter 1.

In order to take advantage of the two data communication media, the H2HS model is comprised of parallel power line and wireless dual-hop systems, as shown in Figure 30. In this model, each node makes use of power line and wireless media to transmit signals among source (S), relay (R), and destination (D) nodes. The R node operates in half-duplex mode and it uses the MRC technique to combine the signals received from the S node through the power line and wireless media. Also, it makes use of the AF protocol to forward the amplified version of the received signal to the D node. In this model, the power at the R node is exclusively obtained by the signals received by it, from which the energy is harvested.

Figure 30 – The hybrid power line/wireless dual-hop system model.



Source: Personal collection.

According to Figure 30, the S node transmits the source information to the R node through the PLC and WLC channels during the 1^{st} phase. During the 2^{nd} phase, the R node combines the

received information and forwards it to the D node. In this context, it is assumed that the direct (S $\rightarrow$ D) link is not feasible due to the high attenuation associated with the existing long-distance between S and D nodes. The transmission power spent at the S node is $\mathcal{P}_{\mathrm{S}} = \mathcal{P}_1^P + \mathcal{P}_1^W \geq 0$, in which $\mathcal{P}_1^P \geq 0$ and $\mathcal{P}_1^W \geq 0$ are the transmission power allocated to transmit data/energy through the PLC and WLC channels by the S node to the D node (S $\rightarrow$ R link), respectively. Similarly, $\mathcal{P}_{\mathrm{R}} = \mathcal{P}_2^P + \mathcal{P}_2^W \geq 0$ is the transmission power obtained from the energy harvested from the signals received by the R node, where $\mathcal{P}_2^P \geq 0$ and $\mathcal{P}_2^W \geq 0$ are the transmission power allocated to transmit data through the PLC and WLC channels by the R node to the D node (R $\rightarrow$ D link), respectively. Furthermore, it is assumed that $\mathcal{P} = \mathcal{P}_{\mathrm{S}} + \mathcal{P}_{\mathrm{R}}$ is the transmission power and $\mathcal{P}_t^q \geq 0$ is the transmission power allocated to the communication interface associated with the q^{th} data communication medium in the t^{th} phase, in which $q \in \{P, W\}$ refers to power line or wireless medium and $t \in \{1, 2\}$ denotes the 1^{st} and 2^{nd} phases, respectively. Moreover, the PLC and WLC channels are assumed to be linear and time varying among different phases, while both of them remain time invariant during one phase. In other words, one phase duration complies with the coherence time, which is the minimum time period within which PLC and WLC channels can be considered time-invariant. Thus, the discrete-time representations of CIRs, for a given N-block symbol duration (one phase duration), are denoted by $\{h_\ell^q[n]\}_{n=0}^{L_\ell^q-1}$, in which L_ℓ^q are their lengths, $\max_{\ell,q}\{L_\ell^q\} \leq L_{\max}, \forall q, \ell$, and $\ell \in \{SR, RD\}$ refers to the SR or RD link.

In [16, 17] it was shown that power line and wireless single-relay channels could be modeled as two parallel linear Gaussian relay channels (LGRCs). Similar to [16, 17], it is assumed that the H2HS is also modeled by two parallel LGRCs (one for power line and one for wireless), during one N-block symbol duration. In other words, the LGRC assumption is also applied to the power line and wireless dual-hop systems. Moreover, it is assumed that both PLC and WLC channels are statistically independent of each other and from the additive noise. Furthermore, direct data communication from the S node to the D node is not possible (i.e., there is no SD link).

Now, and most importantly, as [116] states, the direct computation of the achievable data rate of the LGRC is challenged by the presence of inter-block interference due to the fact that CIRs have memory and the additive noises are correlated random processes. As addressed in [117], the achievable data rate of the LGRC tends to be equal to that of the N-circular Gaussian relay channel (CGRC) as $N \rightarrow \infty$. In this setting, the N-block memoryless channel is defined as the channel where the outputs over any N-block transmission are independent of channel inputs and noise samples from previous or subsequent N-block transmissions because $N \gg L_{\max}$ [117]. Therefore, the inter-block interference caused by the memory of CIRs and the correlated noises is overcome by using the same idea proposed in [117]. In other words, LGRC tends to N-CGRC as $N \rightarrow \infty$, and it models the H2HS.

In this sense, let the discrete-time vectorial representation of the CIR associated with the q^{th} data communication medium and the ℓ^{th} link during one N-block symbol duration be $\mathbf{h}_\ell^q = [h_\ell^q[0], h_\ell^q[1], \ldots, h_\ell^q[L_\ell^q - 1]]^T$, then $\mathbf{H}_\ell^q = \left[H_\ell^q[0], H_\ell^q[1], \ldots, H_\ell^q[N-1]\right]^T$ is

the N-length discrete Fourier transform of the CIR of PLC or WLC channel such that $\mathbf{H}_{\ell}^{q} = \boldsymbol{\mathcal{F}}[\mathbf{h}_{\ell}^{q}, \mathbf{0}_{N-L_{\ell}^{q}}]^{T}$, in which $\boldsymbol{\mathcal{F}}$ is the $N \times N$ discrete Fourier transform matrix, $\mathbf{0}_{N-L_{\ell}^{q}}$ is an $(N-L_{\ell}^{q})$-length column vector of all zeros, and N is the number of subchannels. It is also defined the diagonal matrices $\boldsymbol{\mathcal{H}}_{\ell}^{q} \triangleq \mathbf{diag}\left\{H_{\ell}^{q}[0], H_{\ell}^{q}[1], \ldots, H_{\ell}^{q}[N-1]\right\}$, and similarly, $\boldsymbol{\Lambda}_{|\boldsymbol{\mathcal{H}}_{\ell}^{q}|^{2}} \triangleq \mathbf{diag}\left\{|H_{\ell}^{q}[0]|^{2}, |H_{\ell}^{q}[1]|^{2}, \ldots, |H_{\ell}^{q}[N-1]|^{2}\right\}$.

The vector representation of the N-block symbol transmitted through the q^{th} data communication medium, after digital modulation in the frequency domain, is given by $\mathbf{X}^{q} \in \mathbb{C}^{N\times 1}$, while $\mathbf{V}_{\ell}^{q} \in \mathbb{C}^{N\times 1}$ is the vectorial representation of the additive noise in the frequency domain for the q^{th} data communication medium associated with the ℓ^{th} link. Moreover, it is considered that $\mathbb{E}\{\mathbf{X}^{q}\} = 0$, $\mathbb{E}\{\mathbf{X}^{q}\mathbf{X}^{q\dagger}\} = \boldsymbol{\Lambda}_{\sigma_{X^{q}}^{2}} = \mathbf{I}_{N}$, in which $\mathbf{I}_{N}$ denotes the $N \times N$ identity matrix, $\mathbb{E}\{\cdot\}$ denotes expectation, and $\dagger$ denotes the conjugate transpose operator. Also, $\mathbb{E}\{\mathbf{V}_{\ell}^{q}\} = 0$ and $\mathbb{E}\{\mathbf{V}_{\ell}^{q}\mathbf{V}_{\ell}^{q\dagger}\} = \boldsymbol{\Lambda}_{\sigma_{\mathbf{V}_{\ell}^{q}}^{2}} = \mathbf{diag}\left\{\sigma_{\mathbf{V}_{\ell}^{q}}^{2}[0], \sigma_{\mathbf{V}_{\ell}^{q}}^{2}[1], \ldots, \sigma_{\mathbf{V}_{\ell}^{q}}^{2}[N-1]\right\}$. In addition, $\boldsymbol{\Lambda}_{\mathcal{P}_{t}^{q}} = \mathbf{diag}\left\{\mathcal{P}_{t,0}^{q}, \mathcal{P}_{t,1}^{q}, \ldots, \mathcal{P}_{t,N-1}^{q}\right\}$ as a matrix representation of power allocation, so that $\mathrm{Tr}(\boldsymbol{\Lambda}_{\mathcal{P}_{t}^{q}}) = \mathcal{P}_{t}^{q}$, where $\mathrm{Tr}(\cdot)$ denotes the trace operator. Therefore, $\boldsymbol{\Lambda}_{\sqrt{\mathcal{P}_{t}^{q}}} = \mathbf{diag}\left\{\sqrt{\mathcal{P}_{t,0}^{q}}, \sqrt{\mathcal{P}_{t,1}^{q}}, \ldots, \sqrt{\mathcal{P}_{t,N-1}^{q}}\right\}$ denotes the amplitude in the frequency domain of the transmitted symbol through the q^{th} data communication medium at the t^{th} phase.

Due to the intrinsic characteristics of both PLC and WLC channels and the need for guaranteeing fairness and exploiting the existing diversity between them, it is assumed that $\mathcal{P}_{v,\ell}^{W} = \mathcal{P}_{v,\ell}^{P}$, where $\mathcal{P}_{v,\ell}^{q}$ denotes the power of the additive noise associated with the q^{th} data communication medium and the ℓ^{th} link. Also,

$$\|\mathbf{h}_{\ell}^{P}\|^{2} = \|\mathbf{h}_{\ell}^{W}\|^{2} = K_{\mathrm{h}},$$

in which $\|.\|$ denotes the 2-norm and $K_{\mathrm{h}} \in \mathbb{R}_{+}$. Note that $\|\mathbf{h}_{\ell}^{q}\|^{2}$ is the energy of the CIR associated with the q^{th} data communication medium and the ℓ^{th} link.

Given the aforementioned formulation, the following research question arises: *Can an H2HS yield higher ergodic achievable data rates than the separate use of non-hybrid dual-hop systems (P2HS or W2HS) when a sum power constraint applies and EH is adopted at the R node*? The answer to this question gives guidance for the development of data networks that are sustainable and efficient in the energy consumption sense.

4.2 THE PROPOSED APPROACHES IN THE H2HS MODEL

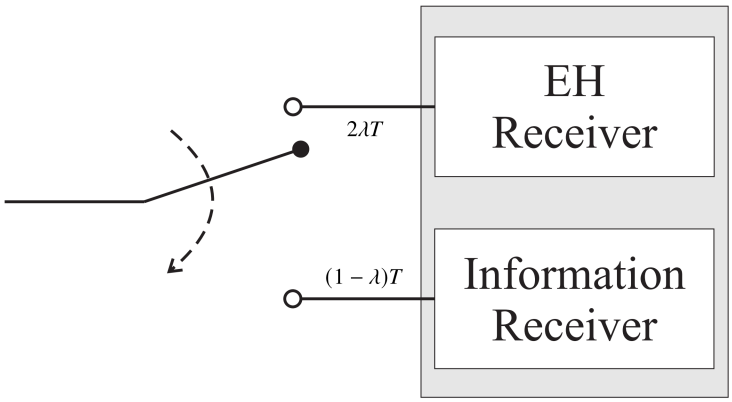
In order to evaluate distinct approaches for performing EH and data communication in the H2HS model, this section introduces and describes four proposed approaches. In general, they differ from each other in terms of the time interval usage before the 2^{nd} phase. In this context, the ergodic achievable data rate of the H2HS model without EH is formulated and then the same is done for the ergodic achievable data rate of these four approaches. This roadmap allows us to straightforwardly derive the four approaches from the H2HS model.

To do so, the TS and PS strategies are concisely reviewed from the EH perspective in Subsection **4.2.1**. In the sequel, Subsection **4.2.2** formulates the ergodic achievable data rate of the H2HS model without the use of EH. Finally, Subsection **4.2.3** details the Approaches A, B, C, and D, and how they are derived from the ergodic achievable data rate of the H2HS model.

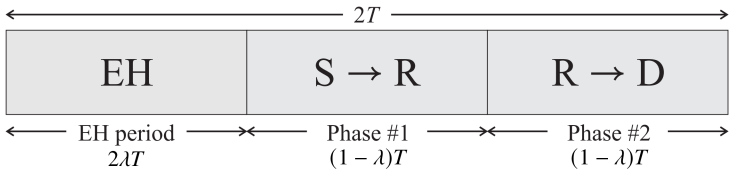
4.2.1 The TS and PS Strategies

Let assume that the harvested energy is equally split between both power line and wireless interfaces during the 2^{nd} phase, and the pessimistic assumption is considered because only the energy of the FoN received signal is utilized for EH [100, 113], which means that the energy associated with the additive noise is not taken into account.

Figure 31 – TS strategy block diagram.



(a) A block diagram of the TS strategy at the R node.



(b) An illustration of the key TS parameters.

Source: Personal collection.

Given these assumptions, Figure 31 illustrates the TS strategy, in which the R node uses the time period of $2\lambda T$ for EH, $(1-\lambda)T$ for the data communication in the SR link during the 1^{st} phase, and the remaining $(1-\lambda)T$ for the data communication in the RD link during the 2^{nd} phase, in which T is a time interval and $0 < \lambda < 1$ is the time switching factor. In this regard, the harvested energy from the FoN received signal associated with the q^{th} data communication medium at the R node is given by

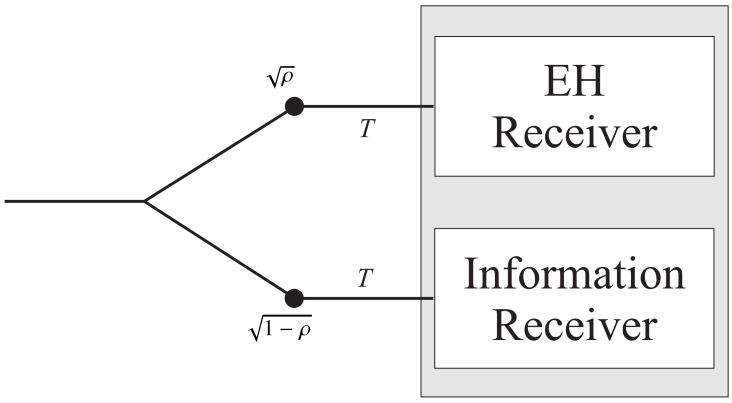
$$E_R^q = 2\eta\lambda\mathcal{P}_1^q \|\mathbf{h}_{SR}^q\|^2 T, \tag{4.1}$$

in which $0 < \eta \leq 1$ is the overall efficiency factor [80]. Also, using (4.1), the transmission power for data communication from the R node, through the q^{th} data communication medium,

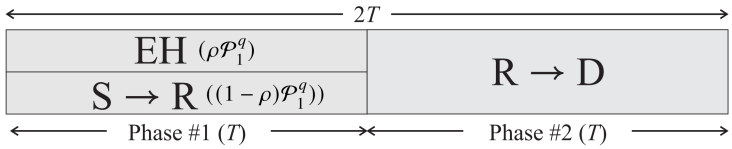
to the D node is expressed as

$$\begin{aligned}\mathcal{P}_2^q &= \frac{E_R^q}{(1-\lambda)T} \\ &= \frac{2\eta\lambda\mathcal{P}_1^q\|\mathbf{h}_{SR}^q\|^2}{(1-\lambda)}.\end{aligned} \tag{4.2}$$

Figure 32 – PS strategy block diagram.



(a) A block diagram of the PS strategy at the R node.



(b) An illustration of the key PS parameters.

Source: Personal collection.

On the other hand, in the PS strategy (see Figure 32), the received energy during the 1^{st} phase is split between data reception and EH with respect to the splitting factor, ρ. In other words, the R node harvests the energy from the $\sqrt{\rho}$ portion of the FoN received signal, while the remaining (proportional to $\sqrt{1-\rho}$) is used for recovering the transmitted signal at the R node. Therefore, the harvested energy from the FoN received signal associated with the q^{th} data communication medium at the R node is given by

$$E_R^q = \eta\rho\mathcal{P}_1^q\|\mathbf{h}_{SR}^q\|^2 T, \tag{4.3}$$

in which $0 < \rho < 1$. Furthermore, using (4.3), the available transmission power at the R node for data communication with the D node, through the q^{th} data communication medium, is expressed as

$$\begin{aligned}\mathcal{P}_2^q &= \frac{E_R^q}{T} \\ &= \eta\rho\mathcal{P}_1^q\|\mathbf{h}_{SR}^q\|^2.\end{aligned} \tag{4.4}$$

4.2.2 The Ergodic Achievable Data Rates

This subsection derives closed-form expressions for the ergodic achievable data rate of the H2HS model. To accomplish this aim, the AF cooperative protocol [12, 16, 100, 118, 119] and the MRC technique [119] are adopted.

To do so, let assume the frequency domain vectorial representation of a symbol at the output of the q^{th} data communication medium associated with the SR link, during the 1^{st} phase, is given by

$$\mathbf{Y}_{SR}^{q} = \mathbf{\Lambda}_{\sqrt{\mathcal{P}_1^q}} \boldsymbol{\mathcal{H}}_{SR}^{q} \mathbf{X}^{q} + \mathbf{V}_{SR}^{q}. \tag{4.5}$$

Note that the AF protocol allows the further transmission of the received symbol by the R node to the D node using an amplification factor, which is related to the power allocated to the R node during the 2^{nd} phase. Mathematically, the vectorial frequency domain representation of the symbol at the output of the q^{th} data communication medium associated with the RD link is given by [16]

$$\mathbf{Y}_{RD,AF}^{q} = \mathbf{\Lambda}_{\sqrt{\mathcal{P}_2^q}} \boldsymbol{\mathcal{H}}_{RD}^{q} \mathbf{X}_R + \mathbf{V}_{RD}^{q}, \tag{4.6}$$

in which $\mathbf{X}_R = \mathbf{\Lambda}_{\sigma_{\mathbf{Y}_{SR}}}^{-1} (\mathbf{D}^P \mathbf{Y}_{SR}^P + \mathbf{D}^W \mathbf{Y}_{SR}^W)$ and

$$\begin{aligned} \mathbf{\Lambda}_{\sigma^2_{\mathbf{Y}_{SR}}} = & |\mathbf{D}^P \mathbf{\Lambda}_{\sqrt{\mathcal{P}_1^P}} \boldsymbol{\mathcal{H}}_{SR}^{P} + \mathbf{D}^W \mathbf{\Lambda}_{\sqrt{\mathcal{P}_1^W}} \boldsymbol{\mathcal{H}}_{SR}^{W}|^2 + \\ & |\mathbf{D}^P|^2 \mathbf{\Lambda}_{\sigma^2_{\mathbf{V}_{SR}^P}} + |\mathbf{D}^W|^2 \mathbf{\Lambda}_{\sigma^2_{\mathbf{V}_{SR}^W}}, \end{aligned} \tag{4.7}$$

where $\mathbf{D}^q = \mathbf{\Lambda}_{\sqrt{\mathcal{P}_1^q}} \boldsymbol{\mathcal{H}}_{SR}^{q\ \dagger} \mathbf{\Lambda}^{-1}_{\sigma^2_{\mathbf{V}_{SR}^q}}$ [119]. From (4.5) and (4.6), the vectorial representation of the received symbol at the D node can be expressed by (4.8).

$$\begin{aligned} \mathbf{Y} &= \left[{\mathbf{Y}_{RD,AF}^{P}}^{T}, {\mathbf{Y}_{RD,AF}^{W}}^{T} \right]^T \\ &= \begin{bmatrix} \mathbf{\Lambda}_{\sqrt{\mathcal{P}_2^P}} \boldsymbol{\mathcal{H}}_{RD}^{P} \mathbf{\Lambda}^{-1}_{\sigma_{\mathbf{Y}_{SR}}} \mathbf{D}^P \mathbf{\Lambda}_{\sqrt{\mathcal{P}_1^P}} \boldsymbol{\mathcal{H}}_{SR}^{P} & \mathbf{\Lambda}_{\sqrt{\mathcal{P}_2^P}} \boldsymbol{\mathcal{H}}_{RD}^{P} \mathbf{\Lambda}^{-1}_{\sigma_{\mathbf{Y}_{SR}}} \mathbf{D}^W \mathbf{\Lambda}_{\sqrt{\mathcal{P}_1^W}} \boldsymbol{\mathcal{H}}_{SR}^{W} \\ \mathbf{\Lambda}_{\sqrt{\mathcal{P}_2^W}} \boldsymbol{\mathcal{H}}_{RD}^{W} \mathbf{\Lambda}^{-1}_{\sigma_{\mathbf{Y}_{SR}}} \mathbf{D}^P \mathbf{\Lambda}_{\sqrt{\mathcal{P}_1^P}} \boldsymbol{\mathcal{H}}_{SR}^{P} & \mathbf{\Lambda}_{\sqrt{\mathcal{P}_2^W}} \boldsymbol{\mathcal{H}}_{RD}^{W} \mathbf{\Lambda}^{-1}_{\sigma_{\mathbf{Y}_{SR}}} \mathbf{D}^W \mathbf{\Lambda}_{\sqrt{\mathcal{P}_1^W}} \boldsymbol{\mathcal{H}}_{SR}^{W} \end{bmatrix} \mathbf{X} \\ &+ \begin{bmatrix} \mathbf{\Lambda}_{\sqrt{\mathcal{P}_2^P}} \boldsymbol{\mathcal{H}}_{RD}^{P} \mathbf{\Lambda}^{-1}_{\sigma_{\mathbf{Y}_{SR}}} \mathbf{D}^P & \mathbf{I}_N & \mathbf{\Lambda}_{\sqrt{\mathcal{P}_2^P}} \boldsymbol{\mathcal{H}}_{RD}^{P} \mathbf{\Lambda}^{-1}_{\sigma_{\mathbf{Y}_{SR}}} \mathbf{D}^W & 0 \\ \mathbf{\Lambda}_{\sqrt{\mathcal{P}_2^W}} \boldsymbol{\mathcal{H}}_{RD}^{W} \mathbf{\Lambda}^{-1}_{\sigma_{\mathbf{Y}_{SR}}} \mathbf{D}^P & 0 & \mathbf{\Lambda}_{\sqrt{\mathcal{P}_2^W}} \boldsymbol{\mathcal{H}}_{RD}^{W} \mathbf{\Lambda}^{-1}_{\sigma_{\mathbf{Y}_{SR}}} \mathbf{D}^W & \mathbf{I}_N \end{bmatrix} \mathbf{V} \\ &= \mathbf{A}\mathbf{X} + \mathbf{B}\mathbf{V}, \end{aligned} \tag{4.8}$$

where $\mathbf{X} = \left[\mathbf{X}^{P^T}, \mathbf{X}^{W^T} \right]^T$ and $\mathbf{V} = \left[{\mathbf{V}_{SR}^{P}}^{T}, {\mathbf{V}_{RD}^{P}}^{T}, {\mathbf{V}_{SR}^{W}}^{T}, {\mathbf{V}_{RD}^{W}}^{T} \right]^T$.

Now, let $f(\mathbf{Z})$ denote the entropy of a random vector $\mathbf{Z}$, and $\mathbf{Y} \in \mathbb{C}^{2N \times 1}$ be the received symbol in the D node after the two phases, then the mutual information between the transmitted and received symbols is given by [16, 119]

$$I(\mathbf{X}, \mathbf{Y}) = f(\mathbf{Y}) - f(\mathbf{B}\mathbf{V}). \tag{4.9}$$

Based on the assumption that $\mathbf{X}$ is Gaussian distributed, it is had that

$$f(\mathbf{Y}) = \log_2[(\pi e)^{2N}\det(\mathbf{R}_{\mathbf{YY}})], \tag{4.10}$$

and, due to the Gaussianity of the additive noise, it can be written

$$f(\mathbf{BV}) = \log_2[(\pi e)^{2N}\det(\mathbf{B}\mathbf{R}_{\mathbf{VV}}\mathbf{B}^{\dagger})], \tag{4.11}$$

where $\mathbf{R}_{\mathbf{YY}} = \mathbb{E}\{\mathbf{Y}\mathbf{Y}^{\dagger}\} = \mathbf{A}\mathbf{R}_{\mathbf{XX}}\mathbf{A}^{\dagger} + \mathbf{B}\mathbf{R}_{\mathbf{VV}}\mathbf{B}^{\dagger}$, $\mathbf{R}_{\mathbf{XX}} = \mathbb{E}\{\mathbf{X}\mathbf{X}^{\dagger}\}$, and $\mathbf{R}_{\mathbf{VV}} = \mathbb{E}\{\mathbf{V}\mathbf{V}^{\dagger}\}$. On defining $\mathbf{C}_{AF} = \mathbf{A}\mathbf{R}_{\mathbf{XX}}\mathbf{A}^{\dagger}$ and $\mathbf{D}_{AF} = \mathbf{B}\mathbf{R}_{\mathbf{VV}}\mathbf{B}^{\dagger}$, in which $\mathbf{C}_{AF}$ and $\mathbf{D}_{AF}$ are given by (4.14) and (4.15), respectively, from (4.9), the mutual information is given by

$$I(\mathbf{X},\mathbf{Y}) = \log_2\left[\det(\mathbf{I}_{2N} + \mathbf{C}_{AF}\mathbf{D}_{AF}^{-1})\right]. \tag{4.12}$$

As a result, the ergodic achievable data rate of the H2HS model adopting AF and MRC at the R node is given by

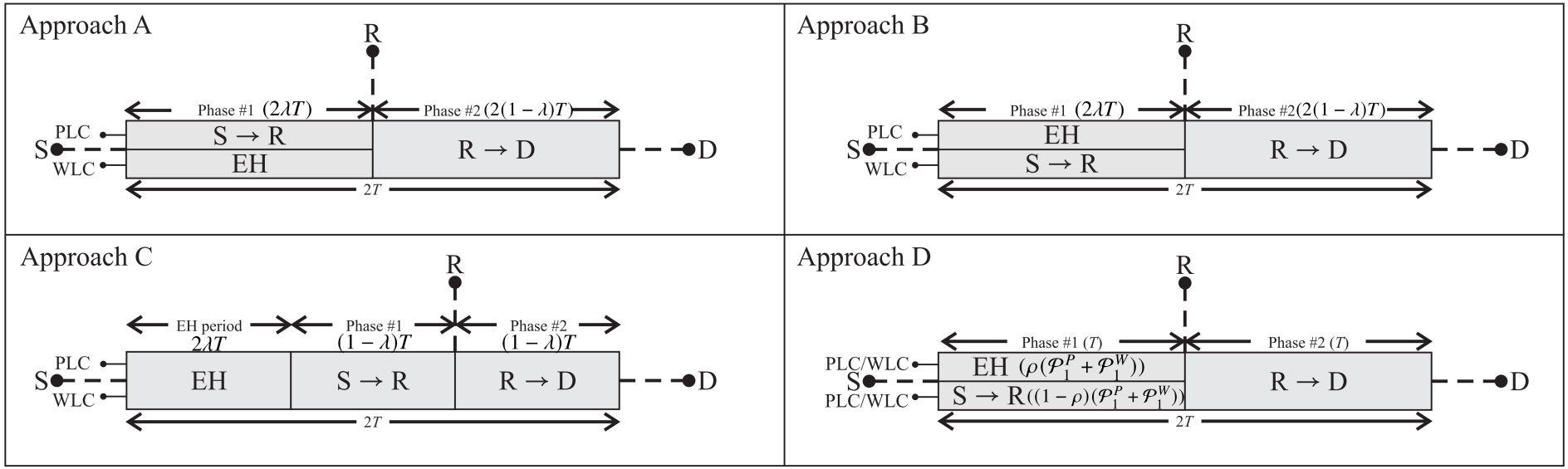
$$C^{\text{H2HS}} = \mathbb{E}_{\mathbf{H}_{\ell}^{P},\mathbf{H}_{\ell}^{W}}\left\{\max_{\mathbf{\Lambda}_{\mathcal{P}}}\frac{B_W}{N}\log_2\left[\det(\mathbf{I}_{2N} + \mathbf{C}_{AF}\mathbf{D}_{AF}^{-1})\right]\right\}, \tag{4.13}$$

subject to $\text{Tr}(\mathbf{\Lambda}_{\mathcal{P}}) \leq \mathcal{P}$, where $\mathbf{\Lambda}_{\mathcal{P}} = \mathbf{diag}\left\{\mathbf{\Lambda}_{\mathcal{P}_1^P}, \mathbf{\Lambda}_{\mathcal{P}_1^W}, \mathbf{\Lambda}_{\mathcal{P}_2^P}, \mathbf{\Lambda}_{\mathcal{P}_2^W}\right\}$; B_W and $\mathbb{E}_{\mathbf{H}_{\ell}^{P},\mathbf{H}_{\ell}^{W}}\{.\}$ are the frequency bandwidth and the expectation operation related to both PLC and WLC channels, respectively.

$$\begin{aligned}\mathbf{C}_{AF} = \mathbf{diag}\Big\{&\mathbf{\Lambda}_{\mathcal{P}_2^P}\mathbf{\Lambda}_{|\boldsymbol{\mathcal{H}}_{RD}^{P}|^2}\mathbf{\Lambda}^{-1}_{\sigma^2_{\mathbf{Y}_{SR}}}|\mathbf{D}^{P}\mathbf{\Lambda}_{\sqrt{\mathcal{P}_1^P}}\boldsymbol{\mathcal{H}}_{SR}^{P} + \mathbf{D}^{W}\mathbf{\Lambda}_{\sqrt{\mathcal{P}_1^W}}\boldsymbol{\mathcal{H}}_{SR}^{W}|^2,\\ &\mathbf{\Lambda}_{\mathcal{P}_2^W}\mathbf{\Lambda}_{|\boldsymbol{\mathcal{H}}_{RD}^{W}|^2}\mathbf{\Lambda}^{-1}_{\sigma^2_{\mathbf{Y}_{SR}}}|\mathbf{D}^{P}\mathbf{\Lambda}_{\sqrt{\mathcal{P}_1^P}}\boldsymbol{\mathcal{H}}_{SR}^{P} + \mathbf{D}^{W}\mathbf{\Lambda}_{\sqrt{\mathcal{P}_1^W}}\boldsymbol{\mathcal{H}}_{SR}^{W}|^2\Big\},\end{aligned} \tag{4.14}$$

$$\begin{aligned}\mathbf{D}_{AF} = \mathbf{diag}\Big\{&\mathbf{\Lambda}_{\mathcal{P}_2^P}\mathbf{\Lambda}_{|\boldsymbol{\mathcal{H}}_{RD}^{P}|^2}\mathbf{\Lambda}^{-1}_{\sigma^2_{\mathbf{Y}_{SR}}}(|\mathbf{D}^{P}|^2\mathbf{\Lambda}_{\sigma^2_{\mathbf{V}^P_{SR}}} + |\mathbf{D}^{W}|^2\mathbf{\Lambda}_{\sigma^2_{\mathbf{V}^W_{SR}}}) + \mathbf{\Lambda}_{\sigma^2_{\mathbf{V}^P_{RD}}},\\ &\mathbf{\Lambda}_{\mathcal{P}_2^W}\mathbf{\Lambda}_{|\boldsymbol{\mathcal{H}}_{RD}^{W}|^2}\mathbf{\Lambda}^{-1}_{\sigma^2_{\mathbf{Y}_{SR}}}(|\mathbf{D}^{P}|^2\mathbf{\Lambda}_{\sigma^2_{\mathbf{V}^P_{SR}}} + |\mathbf{D}^{W}|^2\mathbf{\Lambda}_{\sigma^2_{\mathbf{V}^W_{SR}}}) + \mathbf{\Lambda}_{\sigma^2_{\mathbf{V}^W_{RD}}}\Big\}.\end{aligned} \tag{4.15}$$

Figure 33 – Block diagrams of Approach A (HTS), Approach B (HTS), Approach C (TS), and Approach D (PS).



Source: Personal collection.

4.2.3 The Proposed Approaches

The four proposed approaches for the H2HS model are depicted in Figure 33. Basically, these approaches refer to distinct manners to harvesting energy and performing data communication in the H2HS model by exploiting the PS and TS strategies and the existing diversity in the hybrid data communication channel (i.e., parallel use of PLC and WLC channels). Based on (4.14) and (4.15), closed-form expressions for the ergodic achievable data rates of these approaches are concisely obtained as follows:

- **Approach A (HTS)**: During the 1^{st} phase, the energy at the R node is harvested only from the signal associated with the wireless SR link, while the power line SR link is used for performing the data communication. To evaluate the ergodic achievable data rate, the terms related to the wireless SR link (i.e., $\mathbf{D}^W$, $\mathbf{\Lambda}_{\sqrt{\mathcal{P}_1^W}}$ and $\mathcal{H}_{SR}^W$) are removed from (4.14) and (4.15). Also, 2λ multiplies $\mathbf{\Lambda}_{\mathcal{P}_1^P}$, while $2(1-\lambda)$ multiplies $\mathbf{\Lambda}_{\mathcal{P}_2^P}$ and $\mathbf{\Lambda}_{\mathcal{P}_2^W}$. Further, the harvested energy is the one obtained from the wireless signal, and, as a consequence, the total harvested energy is $E_R = E_R^W = 2\eta\lambda\mathcal{P}_1^W\|\mathbf{h}_{SR}^W\|^2 T$.

- **Approach B (HTS)**: This is the opposite of Approach A. In particular, energy is harvested from the power line signal associated with the SR link, while the wireless SR link is used for carrying out data communication, during the 1^{st} phase. To evaluate the ergodic achievable data rate, the terms related to the power line SR link (i.e., $\mathbf{D}^P$, $\mathbf{\Lambda}_{\sqrt{\mathcal{P}_1^P}}$ and $\mathcal{H}_{SR}^P$) are removed from (4.14) and (4.15). Moreover, 2λ multiplies $\mathbf{\Lambda}_{\mathcal{P}_1^W}$, while $2(1-\lambda)$ multiplies $\mathbf{\Lambda}_{\mathcal{P}_2^P}$ and $\mathbf{\Lambda}_{\mathcal{P}_2^W}$. As a result, the total harvested energy is $E_R = E_R^P = 2\eta\lambda\mathcal{P}_1^P\|\mathbf{h}_{SR}^P\|^2 T$. The strategy for harvesting energy in Approaches A and B is termed the HTS strategy.

- **Approach C (TS)**: In this approach, EH is carried out in the power line and wireless signals associated with SR links by using the TS strategy. Thus, the signals associated with both power line and wireless SR links are used for harvesting energy during the EH period and, after that, they are used for performing data communication based on the use of the time switching factor. To evaluate the ergodic achievable data rate, a change is made in (4.14) and (4.15) by multiplying the terms $\mathbf{\Lambda}_{\mathcal{P}_1^P}$, $\mathbf{\Lambda}_{\mathcal{P}_2^P}$, $\mathbf{\Lambda}_{\mathcal{P}_1^W}$, and $\mathbf{\Lambda}_{\mathcal{P}_2^W}$ by $(1-\lambda)$. Also, the total harvested energy is given by $E_R = E_R^P + E_R^W = 2\eta\lambda T(\mathcal{P}_1^P\|\mathbf{h}_{SR}^P\|^2 + \mathcal{P}_1^W\|\mathbf{h}_{SR}^W\|^2)$.

- **Approach D (PS)**: This approach is based on the simultaneous use of power line and wireless signals received by the R node. From these signals, EH and data communication in the SR link are accomplished by adopting the PS strategy. To evaluate the ergodic achievable data rate, (4.14) and (4.15) are changed by multiplying the terms $\mathbf{\Lambda}_{\mathcal{P}_1^P}$ and $\mathbf{\Lambda}_{\mathcal{P}_1^W}$ by $(1-\rho)$ and the harvested energy is expressed as $E_R = E_R^P + E_R^W = \eta\rho T(\mathcal{P}_1^P\|\mathbf{h}_{SR}^P\|^2 + \mathcal{P}_1^W\|\mathbf{h}_{SR}^W\|^2)$.

4.3 NUMERICAL RESULTS

In order to carry out numerical simulations regarding the H2HS model, it is assumed that the signal transmission occurs in one of the ISM frequency bands for WLC and in the narrow-regulated frequency band for PLC. The NB-PLC is standardized to operate in the frequency band from 3 up to 500 kHz [73]. For the sake of fairness, the LP-RF WLC data transmission occupies an approximate bandwidth equal to 500 kHz in the frequency band between 915 and 915.5 MHz. Brief descriptions of the adopted NB-PLC and LP-RF WLC channel models are as follows:

NB-PLC channel model: The well-known Zimmermann and Dostert [10] channel model is used with the parameters taken from the IEEE 1901.2 standard [73, Annex D]. The additive noise in this NB-PLC channel is modeled as a zero-mean colored Gaussian random process. Adopted from [105], its PSD is expressed as $S^P(f) = \varsigma/2\exp(-\nu|f|)$, where $\nu, \varsigma \in \mathbb{R}_+$ are constants equal to 1.2×10^{-5} and 1.0×10^{-15}, respectively, and f is the frequency in Hertz. Given the subchannel bandwidth, $\Delta f = B_W/N$, it is had that $\mathbf{\Lambda}_{\sigma^2_{\mathbf{v}^P_\ell}} = \Delta f \mathbf{diag}\left\{S^P(0), S^P(\Delta f), \ldots, S^P([N-1]\Delta f)\right\}, \forall \ell$.

LP-RF WLC channel model: It is obtained from a wideband wireless channel by adopting the procedure suggested in the 802.15.4a IEEE wireless channel model report [106]. Essentially, it is accomplished by filtering the wideband WLC channel model. The zero-mean circularly symmetric complex Gaussian assumption is made for the LP-RF WLC additive noise. From [21], the PSD of the additive noise in the LP-RF WLC channel is considered to be $S^W(f) = -173.8 + NF$ dBm/Hz, where the receiver noise figure NF is equal to 7 dB. Consequently, $\mathbf{\Lambda}_{\sigma^2_{\mathbf{v}^W_\ell}} = \Delta f \mathbf{diag}\left\{S^W(0), S^W(\Delta f), \ldots, S^W([N-1]\Delta f)\right\}, \forall \ell$.

Furthermore, a large value of N is used such that the subchannel gains and PSD of the additive noise are flat within each subchannel. This choice is useful to accomplish realizable numerical simulations. Note that $\mathcal{P}_\mathrm{S} \in \{1, 100\}$ mW is adopted in order to emphasize scenarios in which data communications have low and high quality, respectively, and $\eta = 1$ is chosen. Moreover, it is used $K_\mathrm{h} = 10^{-2}$ because $K_\mathrm{h} \gg 10^{-2}$ would make the EH more advantageous than it really is. On the other hand, $K_\mathrm{h} \ll 10^{-2}$ results in very low values of harvested energy. In other words, the chosen value of K_h is the most realistic since it is close to the real value of CIR's energies experienced by NB-PLC channels.

The comparative numerical analyses will rely on the achievable data rate ratio, which is defined by

$$\varphi^a_b \triangleq \frac{C^a}{C^\mathrm{H}}, \tag{4.16}$$

where C^a is the ergodic achievable data rate associated with the system a and $a \in \{\mathrm{H2HS}, \mathrm{P2HS}, \mathrm{W2HS}\}$ denotes the H2HS (any approach), P2HS, or W2HS model. Note that the source of energy at the R node comes from the use of one of the proposed approaches. It means that each one of them uses the TS, PS, or HTS strategy and, as a consequence, $b \in \{\mathrm{TS}, \mathrm{PS}, \mathrm{HTS}\}$. Also,

C^{H} refers to the ergodic achievable data rate attained by the H2HS model by assuming a source of energy at the R node and EH is not used.

Further, it is assumed the complete CSI is available at the transmitter side if the optimal power allocation (OA) is applied (i.e., the WF technique [107]) at the S and R nodes. The WF technique optimally allocates the transmission power among subcarriers based on knowledge of the normalized signal-to-noise ratio (nSNR) matrix, which is expressed as

$$\mathbf{\Lambda}_{\overline{\zeta_\ell^q}} = \mathbf{\Lambda}_{|\boldsymbol{\mathcal{H}}_\ell^q|^2} \mathbf{\Lambda}^{-1}_{\sigma^2_{\mathbf{v}_\ell^q}} = \mathbf{diag}\left\{\overline{\zeta_\ell^q}[0], \overline{\zeta_\ell^q}[1], \ldots, \overline{\zeta_\ell^q}[N-1]\right\}$$

for the q^{th} data communication medium associated with the ℓ^{th} link, in which, for a given q and ℓ, $\overline{\zeta_\ell^q}[k]$ is the k^{th} subchannel nSNR with $k \in \{0, 1, \ldots, N-1\}$ corresponding to the frequencies $f_k = k\Delta f$.

Past works have shown that the intrinsic characteristic of the PLC additive noise can increase the system performance when EH is applied [11–13]. Taking into account this issue, numerical analyses are performed by considering that the NB-PLC additive noise can be white or colored. In this sense, the following four scenarios are taken into account to support the quantitative analyses:

- Scenario #C1: OA is used at the S and R nodes and the NB-PLC channel output is corrupted by an additive colored Gaussian noise (ACGN).
- Scenario #C2: OA is used at the S and R nodes and the NB-PLC channel is disturbed by additive white Gaussian noise (AWGN).
- Scenario #C3: uniform power allocation (UA) is used at the S and R nodes and the NB-PLC channel is corrupted by the presence of the ACGN.
- Scenario #C4: UA is used at the S and R nodes, and the NB-PLC channel is disturbed by AWGN.

Also, the four approaches for performing EH and data communication in the H2HS model, see Subsection **4.2.3** for more details, may be described as follows:

- Approach A: H2HS harvests the energy in the R node only from the wireless signal by means of the HTS strategy.
- Approach B: H2HS harvests the energy in the R node only from the power line signal and using the HTS strategy.
- Approach C: H2HS harvests the energy in the R node from both power line and wireless signals with the TS strategy.
- Approach D: H2HS harvests the energy in the R node from both power line and wireless signals using the PS strategy.

Furthermore, the non-hybrid P2HS and W2HS models make use of the power line and wireless SR link, respectively, for both data communication and EH by means of TS or PS strategy and they are straightforwardly associated with their acronyms as follows:

- P2HS-TS: P2HS harvests the energy in the R node using the TS strategy.
- P2HS-PS: P2HS harvests the energy in the R node using the PS strategy.
- W2HS-TS: W2HS harvests the energy in the R node using the TS strategy.
- W2HS-PS: W2HS harvests the energy in the R node using the PS strategy.

In this regard, Subsection **4.3.1** discusses numerical results of the achievable data rate ratio in Scenario #C1, while Subsection **4.3.2** does the same discussion for the Scenario #C2. In the sequel, Subsection **4.3.3** brings analyses of the achievable data rate ratio in Scenario #C3, whereas Subsection **4.3.4** makes the same analyses for the Scenario #C4.

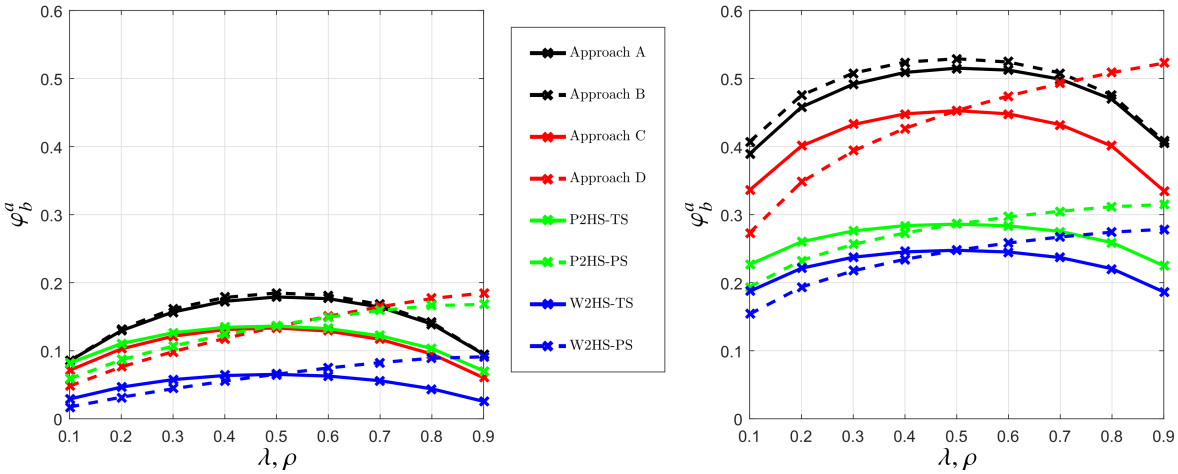
4.3.1 Scenario #C1: OA and NB-PLC Channel with ACGN

By considering Scenario #C1, Figure 34 shows achievable data rate ratios as functions of the time switching and power splitting factors for (a) $\mathcal{P}_{\mathrm{S}} = 1$ mW and (b) $\mathcal{P}_{\mathrm{S}} = 100$ mW. According to this plot, the use of $\mathcal{P}_{\mathrm{S}} = 100$ mW shows a clear performance gap among H2HS (Approaches A, B, C, and D) and the non-hybrid dual-hop systems (P2HS and W2HS). This gap is in favor of H2HS and is irrelevant when $\mathcal{P}_{\mathrm{S}} = 1$ mW. As a matter of fact, if the transmission power is low, then the PLC portion offers a greater contribution to the H2HS model than the WLC one and this behavior is less noticeable when the transmission power increases. Overall, this performance gap increase as $\mathcal{P}_{\mathrm{S}}$ grows. For instance, when $\mathcal{P}_{\mathrm{S}} = 1$ mW, the optimal time switching factor for the H2HS with Approach A and W2HS with TS is $\lambda_{OPT} = 0.5$, which results in $\varphi_{\mathrm{TS}}^{\mathrm{W2HS}} = 0.06$ and $\varphi_{\mathrm{HTS}}^{\mathrm{H2HS}} = 0.18$ (Approach A). Therefore, $\varphi_{\mathrm{HTS}}^{\mathrm{H2HS}} - \varphi_{\mathrm{TS}}^{\mathrm{W2HS}} = 0.12$. For $\mathcal{P}_{\mathrm{S}} = 100$ mW and $\lambda_{OPT} = 0.5$, it is had that $\varphi_{\mathrm{HTS}}^{\mathrm{H2HS}} - \varphi_{\mathrm{TS}}^{\mathrm{W2HS}} = 0.26$.

Regarding the use of the EH strategy in the H2HS model, it is noted that TS (Approach C) is better than PS (Approach D) for $\lambda, \rho < 1/2$ and the opposite occurs for $\lambda, \rho > 1/2$. Also, for any value of $\mathcal{P}_{\mathrm{S}}$ and optimal values of λ and ρ, PS attains better performance than TS. In fact, unlike TS, the PS strategy does not affect the time interval reserved for the 2^{nd} phase. In other words, independent of the value of the power splitting factor, the PS strategy has a T time interval for carrying out data communication in the RD link, resulting in a tendency to increase the use of $\mathcal{P}_{\mathrm{S}}$ to perform EH rather than to perform data communication in the SR link during the 1^{st} phase, which is confirmed by the high value of $\rho_{OPT} = 0.9$ in Approach D.

In the way it was formulated, the only channel characteristic that influences the amount of harvested energies is the energy of the CIR that is taken into account for performing EH. Therefore, for a given λ, the same energy is harvested in both Approaches A and B. That said, the only difference between Approaches A and B in the 1^{st} phase is the use of PLC and WLC

Figure 34 – Scenario #C1: φ_b^a versus λ, ρ for H2HS, P2HS, and W2HS.



(a) $\mathcal{P}_{\mathrm{S}} = 1$ mW. (b) $\mathcal{P}_{\mathrm{S}} = 100$ mW.

Source: Personal collection.

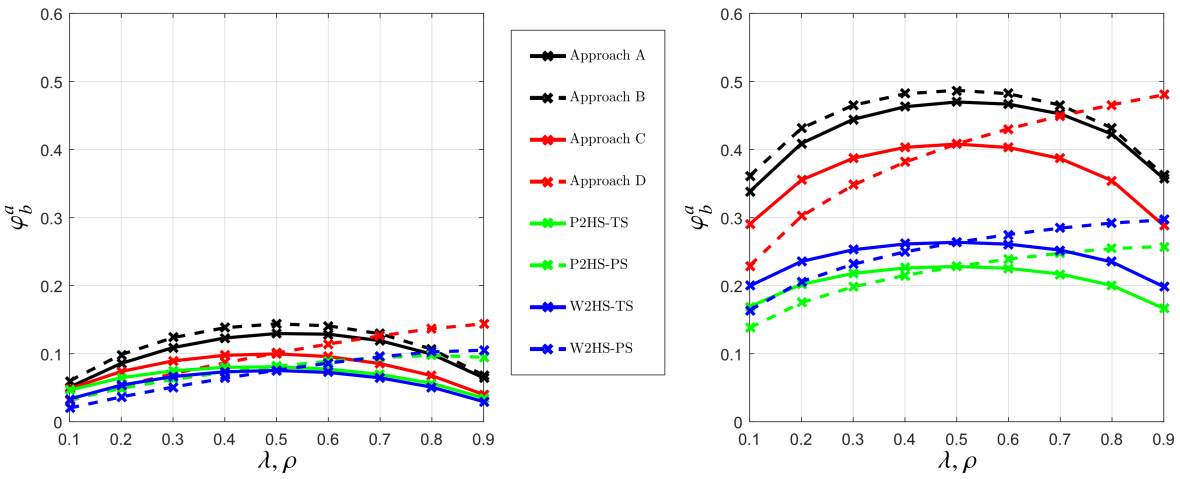
in the SR link, respectively, which offers an advantage in favor of PLC when OA is adopted. In fact, OA can efficiently exploit the existing diversity of nSNR, which is associated with the effect of the frequency-selective NB-PLC channel and non-flatness of the additive noise's PSD. In other words, the characteristics of the NB-PLC channel (i.e., frequency selectivity and non-flat PSD) cause OA to allocate the majority of $\mathcal{P}_1^P$ in a few subchannels (i.e., those showing the highest nSNR), something that does not happen in the LP-RF WLC ones because both the channel frequency response's magnitude associated with the ISM frequency band and the PSD of the LP-RF WLC additive noise are almost flat. Thus, Approach A offers better performance than Approach B in terms of SR link usage; however, these few subchannels may occupy distinct frequency bands when PLC and WLC are performed in the SR and RD links (Approach A), respectively, causing the whole system to lose performance. This is the reason behind the performance improvement of Approach B over Approach A in Scenario #C1.

Moreover, for a given EH strategy, P2HS is better than W2HS for any value of the time switching or power splitting factor. In P2HS, PLC is adopted in both SR and RD links, and, thus, the NB-PLC channels associated with these links share a large number of high nSNR subchannels, i.e., the high nSNR subchannels belonging to the SR and RD links are occupying the same frequency band due to the characteristics of the NB-PLC channel. Overall, it is better to have subchannels associated with the SR link with low nSNR variation and subchannels associated with the RD link with high nSNR variation when operating in the Scenario #C1 conditions. Finally, but not least, $\lambda = 0$ and $\rho = 0$ are not feasible values since no energy would be harvested for the data communication in the RD link. On the other hand, $\lambda = 1$ and $\rho = 1$ would make data communication impossible.

4.3.2 Scenario #C2: OA and NB-PLC Channel with AWGN

Figure 35 shows achievable data rate ratios as functions of λ and ρ for Scenario #C2, when (a) $\mathcal{P}_S = 1$ mW and (b) $\mathcal{P}_S = 100$ mW. Different from Scenario #C1, W2HS presents better performance than P2HS for any values of λ and ρ when $\mathcal{P}_S = 100$ mW. This occurs because, in this scenario, the NB-PLC additive noise has a flat PSD. In other words, one of the two advantages that P2HS offered in Scenario #C1 was removed (the other one is the high NB-PLC channel frequency selectivity). Consequently, the difference between the nSNR variation in the NB-PLC subchannels at both SR and RD links in comparison to the LP-RF WLC ones is not as great as in Scenario #C1. However, with $\mathcal{P}_S = 1$ mW, P2HS yields similar performance to W2HS because the lower is the transmission power, the higher is the gain achieved by the use of OA in frequency-selective channels or channels with a high variation on the nSNR in distinct subchannels [16].

Figure 35 – Scenario #C2: φ_b^a versus λ, ρ for H2HS, P2HS, and W2HS.



(a) $\mathcal{P}_S = 1$ mW. (b) $\mathcal{P}_S = 100$ mW.

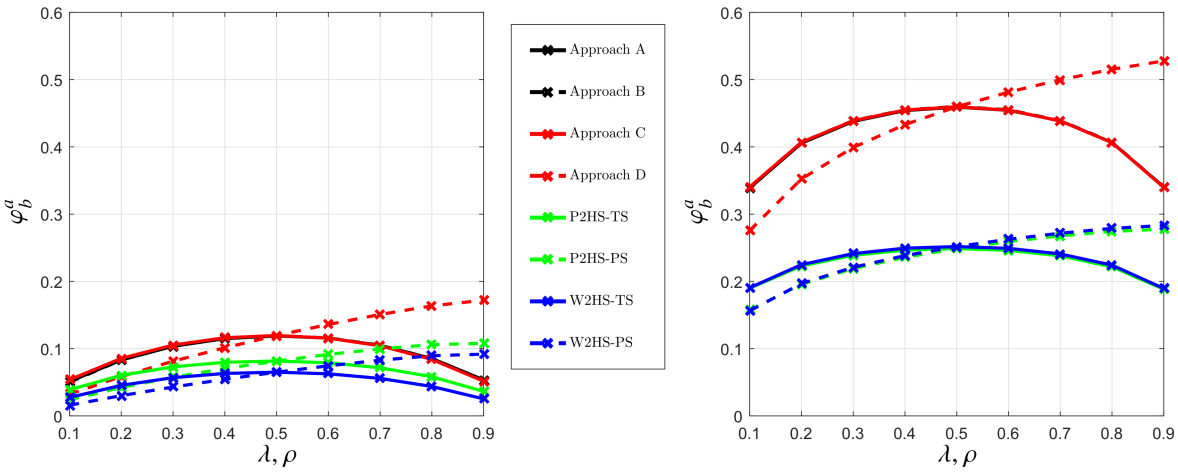
Source: Personal collection.

Also, the non-flatness characteristic of the PSD of the NB-PLC additive noise makes the absolute value of the ergodic achievable data rates higher than the flatness related to the PSD of the NB-PLC additive noise. For instance, assuming the TS strategy with λ_{OPT} and $\mathcal{P}_S = 100$ mW, the ratio between C^{P2HS} in Scenario #C1 and C^{P2HS} in Scenario #C2, results in more than 30% of improvement in favor of Scenario #C1. Overall, H2HS and P2HS offer improvements in Scenario #C1 in comparison to Scenario #C2. On the other hand, the W2HS has no gain of performance with the change of scenarios because it is not impacted by the flat PSD assumption of the NB-PLC additive noise.

4.3.3 Scenario #C3: UA and NB-PLC Channel with ACGN

For Scenario #C3, the achievable data rate ratios as functions of λ and ρ, for $\mathcal{P}_S = 1$ mW and $\mathcal{P}_S = 100$ mW are shown in Figure 36(a) and (b), respectively. A comparison between φ_{TS}^{P2HS} and φ_{TS}^{W2HS} in Scenarios #C3 (UA) and #C1 (OA) shows that the change of the power allocation from OA to UA has a great and negative impact on the performance of the power line systems compared to the wireless ones. This occurs due to the high variation of the nSNR among NB-PLC subchannels. Therefore, when OA is adopted, the variation of nSNRs of the NB-PLC channel is efficiently exploited, which does not happen when UA is applied. Due to that, in Scenario #C3, P2HS and W2HS attain similar performances as well the same occurs with the H2HS for Approaches A, B, and C.

Figure 36 – Scenario #C3: φ_b^a versus λ, ρ for H2HS, P2HS, and W2HS.



(a) $\mathcal{P}_S = 1$ mW. (b) $\mathcal{P}_S = 100$ mW.

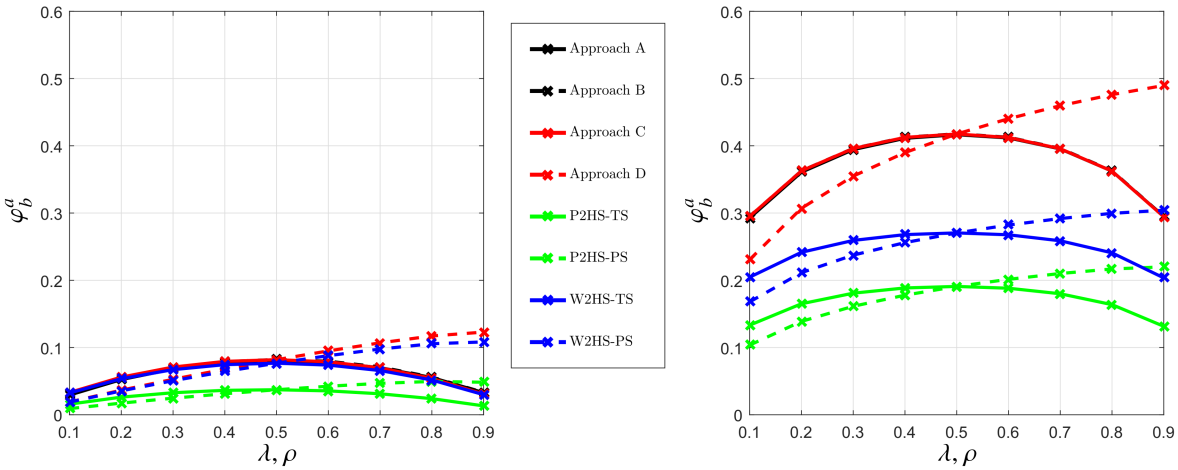
Source: Personal collection.

Different from what was noted in Scenarios #C1 and #C2, the performance of the H2HS model with power line or wireless EH (i.e., Approach A or B, respectively) is similar to that related to the H2HS with Approach C because both NB-PLC and LP-RF WLC channels offer similar contributions to the ergodic achievable data rates in Scenario #C3. Further, the increase of $\mathcal{P}_S$ from 1 to 100 mW made the P2HS and W2HS performances even closer to each other due to the similar performance among subchannels, which is caused by the use of UA together with the assumptions as follows: $\|\mathbf{h}_\ell^P\|^2 = \|\mathbf{h}_\ell^W\|^2$ and $\mathcal{P}_{v,\ell}^W = \mathcal{P}_{v,\ell}^P$.

4.3.4 Scenario #C4: UA and NB-PLC Channel with AWGN

Regarding Scenario #C4, Figure 37 shows achievable data rate ratios as functions of λ and ρ, for (a) $\mathcal{P}_S = 1$ mW and (b) $\mathcal{P}_S = 100$ mW. The lowest values of the ergodic achievable data rates for P2HS is noted in this scenario. As a consequence, it leads to the greatest performance difference between P2HS and W2HS for $\mathcal{P}_S = 100$ mW.

Figure 37 – Scenario #C4: φ_b^a versus λ, ρ for H2HS, P2HS, and W2HS.



(a) $\mathcal{P}_S$ = 1 mW. (b) $\mathcal{P}_S$ = 100 mW.

Source: Personal collection.

Concerning Scenario #C3, the change of behavior associated with P2HS is due to the noise assumption. In other words, if the PSD of the NB-PLC additive noise is flat, then the NB-PLC channel frequency selectivity is more noticed than when the PSD of the additive noise is non-flat. As a matter of fact, the subchannels with high nSNR occupying the same frequency band in the SR and RD links are less frequent in the flat PSD than in the non-flat one, due to the exponentially-decaying form with frequency increasing of the latter. Besides, the non-flat PSD of NB-PLC additive noise can result in more performance gain than the flatness of this PSD.

Furthermore, the change from OA (Scenario #C2) to UA (Scenario #C4) showed the flexibility of the W2HS and H2HS of simultaneously performing EH in both power line and wireless signals (Approaches C and D) to deal with the lack of optimal power allocation, which is not present in P2HS and H2HS with the energy harvested from the power line or wireless signal (Approaches A and B). In fact, the change in the power allocation is more perceived in the NB-PLC channels than in the LP-RF WLC ones when the NB-PLC additive noise has a flat PSD. Also, the H2HS with Approaches A and B outperforms the H2HS with Approach C when OA is adopted (Scenarios #C1 and #C2), and these three approaches have similar performances for the UA assumption (Scenarios #C3 and #C4). Moreover, the H2HS using Approach D with $\rho_{OPT} = 0.9$ showed the best results in terms of achievable data rate ratios. Also, Approach D is more resilient to a change of the PSD of the NB-PLC additive noise and the type of power allocation. In other words, the H2HS with Approach D appears to be more promising for implementation under the set of assumptions made.

4.4 SUMMARY

This chapter formulated ergodic achievable data rates of the H2HS model when dedicated EH is performed at the relay node by using the HTS strategy (Approaches A and B), the TS

strategy (Approach C), or the PS strategy (Approach D). Moreover, it discussed a performance comparison in terms of the achievable data rate ratio among the H2HS, P2HS, and W2HS models in four distinct scenarios. For any scenario, it showed that H2HS with Approaches A and B outperforms or, at least, has similar performance than the H2HS with Approach C, while H2HS using Approach D is the best option in terms of ergodic achievable data ratios. Furthermore, it stated the non-flat PSD feature of the NB-PLC additive noise contributes to increasing the performance of P2HS and H2HS.

5 ENERGY HARVESTING FROM THE UNB-PLC SPECTRUM: POTENTIAL IN THE ERA OF IOT

Chapter 3 highlighted the benefits and potential associated with the BB-PLC additive noise based on measured data set for EH purposes as well as Chapter 4 showed that the intrinsic non-flat PSD feature of the NB-PLC additive noise can be useful for performing EH in hybrid data communication systems. In other words, these chapters showed that the disturbances in electric signals in distinct frequency bands are interesting for intermittently performing energy harvesting and data communication. As discussed in Chapter 2, the interactions between non-linear loads and electric power systems produce disturbances in electric signals, which can be viewed as sources of energy for performing EH. Among these disturbances, the low-frequency harmonic components are the main ones that negatively impact the power quality, and consequently, the energy efficiency of electric power systems. These components are in the frequency band delimited by the UNB-PLC technology, the UNB-PLC spectrum[1]. In this context, it is of utmost importance to precisely evaluate the wasted energy associated with this part of WESs in order to verify its potential to benefit both power quality and energy efficiency of electric power systems while supplying energy for low-power data communication devices (i.e., IoT ones). In this regard, this chapter focuses on to what extent the harvested energy from WESs (i.e., WEH) in the lower part of the UNB-PLC spectrum can power the transceivers used by IoT devices. That said, this chapter comprehends the following contributions:

- Mathematical formulation for harvesting energy from the wasted power associated with WESs. Also, the extension of this formulation to the harvested power as well as the number of transceivers used by IoT devices that can be supplied by means of this power.
- Evaluation of the wasted energy dynamics of WESs on weekdays and weekends based on a measured in-building data set. This evaluation covers only the lower part of the UNB-PLC spectrum because its EH results in power quality improvements. By means of the harvested power, ergodic achievable data rate analyses of NB-PLC and LP-RF WLC channels are presented.
- Numerical analyses about the use of the harvested power to supply transceivers of IoT devices when five well-known and established data communication standards for IoT and distinct periods between two consecutive data transmissions are considered.

The rest of this chapter is organized as follows: Section 5.1 introduces the mathematical model of electric signals and the investigated problem; Section 5.2 formulates the wasted and harvested powers from WESs; Section 5.3 discusses numerical results, while Section 5.4 states concluding remarks.

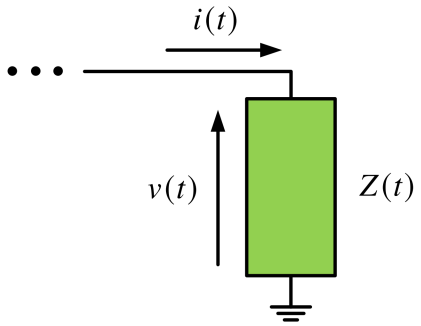
[1] The UNB-PLC spectrum is equivalent to the UNB-PLC additive noise when data communication occurs in the power line.

5.1 THE QUANTIFICATION OF WASTED ENERGY

Recently, [51] has addressed the use of the WEH to increase power quality and energy efficiency in the LV electric power systems. Based on a measurement campaign, the authors roughly estimated that Brazil can save millions of dollars annually if the wasted energy of WESs is harvested. Also, [51] showed that the wasted energy of WESs corresponds to a small percentage of the total energy consumption of buildings and it pointed out that the distributed nature of the production of this kind of wasted energy may benefit low-power IoT devices. Further, [50] analyzed the potential of WEH in urban and rural MV electric power systems. Based on a measured data set, the authors showed that achievable data rates of a few kbps can be obtained, by means of the wasted energy from the harvested power, if data communication and WEH intermittently take place in both urban and rural MV power lines.

In this sense, it is important to verify the wasted energy potential associated with low-frequency harmonic components of WESs because it can benefit both the energy efficiency of electric power systems and the widespread of low-power consumption and sustainable data networks. In other words, it is necessary to bring attention to the correct and precise quantification of the wasted energy associated with WESs in the frequency band that comprehends the components in electric signals that negatively impacts the power quality of electric power systems, which are located in the UNB-PLC spectrum. Usually, the evaluation of the average power recovered from both high- and low-frequency components of WESs, by the telecommunications community, is made by using $(1/T)\int_T \frac{v^2(t)}{R}dt$ with $R = 1\ \Omega$ denoting the value of the resistance component of a hypothetical load [11–13]. However, the impedance of loads in electric power systems is well-known to be both time- and frequency-varying [82] by nature, and it hardly is equal to 1 Ω. In this context, it is necessary to devise a mathematical tool to quantify the wasted energy of low-frequency components of WESs, and consequently to perform EH.

Figure 38 – A non-linear load model.



Source: Personal collection.

To do so, let assume the model for a non-linear and single-phase load of impedance $Z(t)$ that is connected to an electric power system as shown in Figure 38. For this model, the voltage

signal is given by [51]

$$\begin{aligned} v(t) = V_0 + \sum_{k=1}^{N_1} V_k(t)\cos(k\Omega_1 t + \theta_k(t)) + \\ \sum_{l=1}^{N_2} V_{I,l}(t)\cos(\Omega_{I,l} t + \theta_{I,l}(t)) + \\ \sum_{l=1}^{N_3} V_{S,l}(t)\cos(\Omega_{S,l} t + \theta_{S,l}(t)) + \\ \sum_{l=1}^{N_4} v_{\text{imp},l}(t) + \sum_{l=1}^{N_5} v_{\text{not},l}(t) + \sum_{l=1}^{N_6} v_{\text{osc},l}(t) + v_n(t), \end{aligned} \tag{5.1}$$

in which $-\infty < t < +\infty$; V_0 is the DC component; $\{V_1(t), \Omega_1, \theta_1(t)\}$, $\{V_k(t), \Omega_k, \theta_k(t)\}$, $\{V_{I,l}(t), \Omega_{I,l}, \theta_{I,l}(t)\}$, and $\{V_{S,l}(t), \Omega_{S,l}, \theta_{S,l}(t)\}$ are, respectively, the parameters of time-varying AC mains voltage signal, harmonic, interharmonic and supraharmonic components; $\Omega_1 = 2\pi f_1$ is the angular frequency, such that f_1 is the AC mains frequency. As well, $v_{\text{imp},l}(t)$, $v_{\text{not},l}(t)$, $v_{\text{osc},l}(t)$ denote, respectively, the l^{th} impulse, the l^{th} notch, and the l^{th} damped oscillatory transients that are supposed to be stationary random process, at least in the wide-sense. Moreover, N_1, N_2, and N_3 are the numbers of harmonics plus AC mains voltage signal, interharmonic, and supraharmonic components, respectively, while N_4, N_5, and N_6 refer to the numbers of these transients. The background noise, $v_n(t)$, is also a stationary random process. Similarly, the current signal flowing through such load is expressed as

$$\begin{aligned} i(t) = I_0 + \sum_{k=1}^{N_1} I_k(t)\cos(k\Omega_1 t + \theta_k(t)) + \\ \sum_{l=1}^{N_2} I_{I,l}(t)\cos(\Omega_{I,l} t + \theta_{I,l}(t)) + \\ \sum_{l=1}^{N_3} I_{S,l}(t)\cos(\Omega_{S,l} t + \theta_{S,l}(t)) + \\ \sum_{l=1}^{N_4} i_{\text{imp},l}(t) + \sum_{l=1}^{N_5} i_{\text{not},l}(t) + \sum_{l=1}^{N_6} i_{\text{osc},l}(t) + i_n(t), \end{aligned} \tag{5.2}$$

in which the definitions made to the voltage signal in (5.1) apply to (5.2) by changing the voltage word by the current one.

Assuming the parameters of AC mains signals, harmonics, interharmonics, and supraharmonics are constant, [51] demonstrated that the so-called extended complex power (ECP)

associated with these voltage and current signals is given by

$$\begin{aligned}\mathcal{S}_{EC} &= P_{EC} + jQ_{EC} \\ &\triangleq \frac{V_0 I_0}{2} + \sum_{k=1}^{N_1} \frac{V_k I_k}{2} e^{j\Delta\theta_k} + \sum_{l=1}^{N_2} \frac{V_{I,l} I_{I,l}}{2} e^{j\Delta\theta_{I,l}} + \\ &\sum_{l=1}^{N_3} \frac{V_{S,l} I_{S,l}}{2} e^{j\Delta\theta_{S,l}} + \frac{1}{8\pi^2}\Bigg(\sum_{l=1}^{N_4} \int_0^{+\infty} S_{\text{aimp},l}(j\Omega) d\Omega + \\ &\sum_{l=1}^{N_5} \int_0^{+\infty} S_{\text{anot},l}(j\Omega) d\Omega + \sum_{l=1}^{N_6} \int_0^{+\infty} S_{\text{aosc},l}(j\Omega) d\Omega + \\ &\int_0^{+\infty} S_{\text{an}}(j\Omega) d\Omega \Bigg),\end{aligned} \tag{5.3}$$

where P_{EC} and Q_{EC} are the extended active and reactive powers, respectively; $\Delta\theta_k = \theta_{v,k} - \theta_{i,k}$, $\Delta\theta_{I,l} = \theta_{v,I,l} - \theta_{i,I,l}$, $\Delta\theta_{S,l} = \theta_{v,S,l} - \theta_{i,S,l}$; $S_{\text{aimp},l}(j\Omega)$, $S_{\text{anot},l}(j\Omega)$, $S_{\text{aosc},l}(j\Omega)$, and $S_{\text{an}}(j\Omega)$ are the analytic cross-power spectral densities for the transient and background noise components, respectively. Note that any term different from the AC mains signals (i.e., $V_1 I_1 e^{j\Delta\theta_1}/2$) in P_{EC} constitutes the wasted power of WESs or the PLC additive noise, which corresponds to the ratio of the wasted energy per time interval, and, thus, it is the dynamic of the wasted energy.

As demonstrated in [51], (5.3) correctly quantify active and reactive powers associated with electric signals. Based on this mathematical model, the following research questions arise: *How is the dynamic of the wasted energy associated with WESs when the lower part of the UNB-PLC spectrum is considered? How advantageous is to harvest this wasted energy to supply the transceivers of low-power IoT devices?* Answers to these research questions are provided in the following sections.

5.2 HARVESTING ENERGY IN THE UNB-PLC SPECTRUM

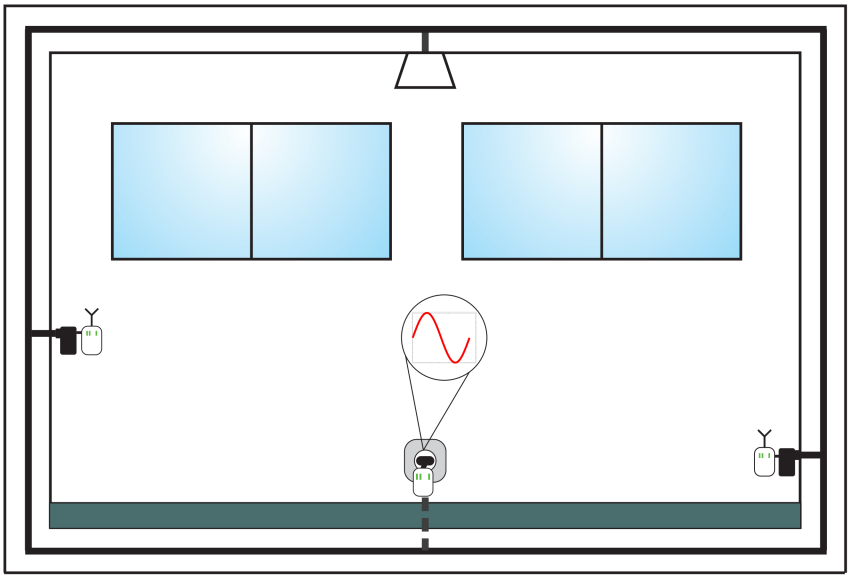
With the respect to the frequency band, PLC systems can be organized as follows [7,65,73]: i) UNB-PLC in the upper part of the super-low frequency (30-300 Hz) band or in the ultra-low frequency (0.3-3 kHz) band; ii) NB-PLC for the frequencies from 3 up to 500 kHz; and iii) BB-PLC in the frequency range from 1.7 up to 100 MHz. In the low frequencies, it is well-known that the PSD of the PLC additive noise decays inversely proportional to the growth of the frequency starting from the AC mains frequency [9]. Therefore, the frequency band used by UNB-PLC systems is promising for EH purposes.

In this context, [51] roughly estimated that the wasted energy of WESs (e.g., up to 11^{th} harmonic) in a building facility corresponds to at least $\sim 0.4\%$ of the total energy consumed by the building, which is powered by the AC mains signal. Despite being a small percentage, it represents a considerable amount of wasted energy spread over worldwide electric power systems. The recovery of the wasted energy associated with WESs is of paramount importance because it increases energy efficiency and reduces power quality degradation [51]. For instance,

harvesting the wasted energy of WESs reduces the total harmonic distortion and positively impacts power quality in electric power systems. The wasted energy associated with WESs is categorized as an artificial source for EH purposes that can be lost entirely as these signals propagate through power lines. Consequently, the harvesting of the wasted energy needs to be carried out near their sources, which are the non-linear loads connected to electric power systems.

Figure 39 illustrates the usefulness of harvesting the wasted energy associated with WESs to supply transceivers of IoT devices connected to outlets in an indoor facility. The device connected to the outlet receives AC mains signal and WESs, being WESs produced by the interactions between electric power systems and non-linear loads and RF signals induced into the electromagnetically unshielded power lines [26]. In this context, the idea is to harvest the wasted energy associated with these WESs, which constitute one of the primary sources of power quality degradation in electric power systems. In other words, EH applied to electric signals in electric power systems means reusing the active power associated with their components outside the AC mains frequency.

Figure 39 – Typical indoor environment. A device connected to the outlet is in contact with the AC mains signal and disturbances.



Source: Personal collection.

Assume that $v(t) \in \mathbb{R}$, $i(t) \in \mathbb{R}$, $\mathbb{E}\{.\}$ is the expectation operator, $\star$ and $*$ denote the convolution and conjugation operations, respectively,

$$\Pi(t/T) = \begin{cases} 1, & |t| < \frac{T}{2}, \\ \frac{1}{2}, & t = \frac{T}{2}, \\ 0 & |t| > \frac{T}{2} \end{cases} \tag{5.4}$$

is the rectangular function with a continuous-time Fourier transform (CTFT) given by

$\mathcal{F}\{\Pi(t/T)\} = T\text{sinc}(\Omega T/2)$, and

$$\text{sgn}(\Omega) = \begin{cases} -1, & \Omega < 0, \\ \frac{1}{2}, & \Omega = 0, \\ 1, & \Omega > 0 \end{cases} \tag{5.5}$$

is the sign function. Then the analytic cross-power spectral density is defined by

$$\begin{aligned} S_{\text{aVI}}(j\Omega) &\triangleq \int_{-\infty}^{+\infty} \mathbb{E}\{v_{\text{a}}(t) i_{\text{a}}^{*}(t-\tau)\} e^{-j\Omega\tau} d\tau \\ &= \lim_{T\to\infty} \mathbb{E}\left\{ \frac{V_{\text{a}T}(j\Omega) I_{\text{a}T}^{*}(j\Omega)}{T} \right\}, \end{aligned} \tag{5.6}$$

where $v_{\text{a}}(t) = v(t) + j\hat{v}(t)$ and $i_{\text{a}}(t) = i(t) + j\hat{i}(t)$ are the analytic signal representation for (5.1) and (5.2), respectively, while $\hat{v}(t)$ and $\hat{i}(t)$ are the Hilbert transforms of (5.1) and (5.2), respectively. Also, $V_{\text{a}T}(j\Omega) = \mathcal{F}\{v_{\text{a}T}(t)\}$ and $I_{\text{a}T}(j\Omega) = \mathcal{F}\{i_{\text{a}T}(t)\}$ are the corresponding frequency-domain representation of the sample function of the analytic signals given by $v_{\text{a}T}(t) = v_{\text{a}}(t)\Pi(t/T)$ and $i_{\text{a}T}(t) = i_{\text{a}}(t)\Pi(t/T)$, respectively.

To solve the right-hand side of the last line of (5.6), it is necessary to consider that

$$V_{\text{a}T}(j\Omega) = \frac{1}{2\pi} V_{\text{a}}(j\Omega) \star T\text{sinc}\left(\Omega\frac{T}{2}\right), \tag{5.7}$$

where

$$\begin{aligned} V_{\text{a}}(j\Omega) &= V(j\Omega) + \text{sgn}(\Omega) V(j\Omega) \\ &= \pi V_0 \delta(\Omega) + \sum_{k=1}^{N_1} 2\pi V_k e^{j\theta_{v,k}} \delta\big(\Omega - k\Omega_1\big) + \sum_{l=1}^{N_2} 2\pi V_{I,l} e^{j\theta_{v,I,l}} \delta\big(\Omega - \Omega_{I,l}\big) + \\ &\sum_{l=1}^{N_3} 2\pi V_{S,l} e^{j\theta_{v,S,l}} \delta\big(\Omega - \Omega_{S,l}\big) + \sum_{l=1}^{N_4} V_{\text{aimp},l}(j\Omega) + \\ &\sum_{l=1}^{N_5} V_{\text{anot},l}(j\Omega) + \sum_{l=1}^{N_6} V_{\text{aosc},l}(j\Omega) + V_{an}(j\Omega), \end{aligned} \tag{5.8}$$

in which $V_{\text{aimp},l}(j\Omega)$, $V_{\text{anot},l}(j\Omega)$, $V_{\text{aosc},l}(j\Omega)$, and $V_{an}(j\Omega)$ are the analytic representations for $V_{\text{imp},l}(j\Omega)$, $V_{\text{not},l}(j\Omega)$, $V_{\text{osc},l}(j\Omega)$, and $V_n(j\Omega)$, respectively.

Note that $V_{\text{a}}(j\Omega)$ is the analytic representation of $V(j\Omega)$, which is a frequency-domain representation of a sample function of the random process $v(t)$. The closed-form expression of

$V(j\Omega)$ is given by

$$\begin{aligned} V(j\Omega) = 2\pi V_0\delta(\Omega) + \sum_{k=1}^{N_1}\pi V_k\Big[e^{j\theta_{v,k}}\delta\big(\Omega - k\Omega_1\big) + e^{-j\theta_{v,k}}\delta\big(\Omega + k\Omega_1\big)\Big] + \\ \sum_{l=1}^{N_2}\pi V_{I,l}\Big[e^{j\theta_{v,I,l}}\delta\big(\Omega - \Omega_{I,l}\big) + e^{-j\theta_{v,I,l}}\delta\big(\Omega + \Omega_{I,l}\big)\Big] + \\ \sum_{l=1}^{N_3}\pi V_{S,l}\Big[e^{j\theta_{v,S,l}}\delta\big(\Omega - \Omega_{S,l}\big) + e^{-j\theta_{v,S,l}}\delta\big(\Omega + \Omega_{S,l}\big)\Big] + \\ \sum_{l=1}^{N_4} V_{\text{imp},l}(j\Omega) + \sum_{l=1}^{N_5} V_{\text{not},l}(j\Omega) + \sum_{l=1}^{N_6} V_{\text{osc},l}(j\Omega) + V_n(j\Omega), \end{aligned} \tag{5.9}$$

Note that $V_{\text{imp},l}(j\Omega)$, $V_{\text{not},l}(j\Omega)$, $V_{\text{osc},l}(j\Omega)$, and $V_n(j\Omega)$ are CTFTs of sample functions of $v_{\text{imp},l}(t)$, $v_{\text{not},l}(t)$, $v_{\text{osc},l}(t)$, and $v_n(t)$, respectively. As a consequence, $V_{\text{a}T}(j\Omega)$ is defined by

$$\begin{aligned} V_{\text{a}T}(j\Omega) &\triangleq \frac{1}{2\pi}V_{\text{a}}(j\Omega) \star T\text{sinc}\left(\Omega\frac{T}{2}\right) \\ &= \frac{V_0}{2}T\text{sinc}\left(\Omega\frac{T}{2}\right) + \sum_{k=1}^{N_1} V_k e^{j\theta_{v,k}} T\text{sinc}\left[(\Omega - k\Omega_1)\frac{T}{2}\right] + \sum_{l=1}^{N_2} V_{I,l}e^{j\theta_{v,I,l}}T\text{sinc}\left[(\Omega - \Omega_{I,l})\frac{T}{2}\right] + \\ &\sum_{l=1}^{N_3} V_{S,l}e^{j\theta_{v,S,l}}T\text{sinc}\left[(\Omega - \Omega_{S,l})\frac{T}{2}\right] + \frac{1}{2\pi}\left[\sum_{l=1}^{N_4} V_{\text{aimp},l}(j\Omega) \star T\text{sinc}\left(\Omega\frac{T}{2}\right) + \right. \\ &\left. \sum_{l=1}^{N_5} V_{\text{anot},l}(j\Omega) \star T\text{sinc}\left(\Omega\frac{T}{2}\right) + \sum_{l=1}^{N_6} V_{\text{aosc},l}(j\Omega) \star T\text{sinc}\left(\Omega\frac{T}{2}\right) + V_{\text{an}}(j\Omega) \star T\text{sinc}\left(\Omega\frac{T}{2}\right)\right]. \end{aligned} \tag{5.10}$$

Similarly, $I_{\text{a}T}(j\Omega)$ is defined by

$$\begin{aligned} I_{\text{a}T}(j\Omega) &\triangleq \frac{1}{2\pi}I_{\text{a}}(j\Omega) \star T\text{sinc}\left(\Omega\frac{T}{2}\right) \\ &= \frac{I_0}{2}T\text{sinc}\left(\Omega\frac{T}{2}\right) + \sum_{k=1}^{N_1} I_k e^{j\theta_{i,k}} T\text{sinc}\left[(\Omega - k\Omega_1)\frac{T}{2}\right] + \sum_{l=1}^{N_2} I_{I,l}e^{j\theta_{i,I,l}}T\text{sinc}\left[(\Omega - \Omega_{I,l})\frac{T}{2}\right] + \\ &\sum_{l=1}^{N_3} I_{S,l}e^{j\theta_{i,S,l}}T\text{sinc}\left[(\Omega - \Omega_{S,l})\frac{T}{2}\right] + \frac{1}{2\pi}\left[\sum_{l=1}^{N_4} I_{\text{aimp},l}(j\Omega) \star T\text{sinc}\left(\Omega\frac{T}{2}\right) + \right. \\ &\left. \sum_{l=1}^{N_5} I_{\text{anot},l}(j\Omega) \star T\text{sinc}\left(\Omega\frac{T}{2}\right) + \sum_{l=1}^{N_6} I_{\text{aosc},l}(j\Omega) \star T\text{sinc}\left(\Omega\frac{T}{2}\right) + I_{\text{an}}(j\Omega) \star T\text{sinc}\left(\Omega\frac{T}{2}\right)\right], \end{aligned} \tag{5.11}$$

Now, multiplying (5.10) and (5.11) then

$$
\begin{aligned}
V_{\mathrm{a}T}(j\Omega)I^{*}_{\mathrm{a}T}(j\Omega) \triangleq\ & \frac{V_0 I_0}{4}T^2\mathrm{sinc}^2\left(\Omega\frac{T}{2}\right) + \sum_{k=1}^{N_1} V_k I_k e^{j\Delta\theta_k} T^2\mathrm{sinc}^2\left[(\Omega - k\Omega_1)\frac{T}{2}\right] + \\
& \sum_{l=1}^{N_2} V_{I,l} I_{I,l} e^{j\Delta\theta_{I,l}} T^2\mathrm{sinc}^2\left[(\Omega - \Omega_{I,l})\frac{T}{2}\right] + \\
& \sum_{l=1}^{N_3} V_{S,l} I_{S,l} e^{j\Delta\theta_{S,l}} T^2\mathrm{sinc}^2\left[(\Omega - \Omega_{S,l})\frac{T}{2}\right] + \\
& \frac{1}{4\pi^2}\left[\sum_{l=1}^{N_4} V_{\mathrm{aimp},l}(j\Omega) \star T\mathrm{sinc}\left(\Omega\frac{T}{2}\right) I^{*}_{\mathrm{aimp},l} \star T\mathrm{sinc}\left(\Omega\frac{T}{2}\right) + \right. \\
& \sum_{l=1}^{N_5} V_{\mathrm{anot},l}(j\Omega) \star T\mathrm{sinc}\left(\Omega\frac{T}{2}\right) I^{*}_{\mathrm{anot},l}(j\Omega) \star T\mathrm{sinc}\left(\Omega\frac{T}{2}\right) + \\
& \sum_{l=1}^{N_6} V_{\mathrm{aosc},l}(j\Omega) \star T\mathrm{sinc}\left(\Omega\frac{T}{2}\right) I^{*}_{\mathrm{aosc},l}(j\Omega) \star T\mathrm{sinc}\left(\Omega\frac{T}{2}\right) + \\
& \left. V_{\mathrm{a}n}(j\Omega) \star T\mathrm{sinc}\left(\Omega\frac{T}{2}\right) I^{*}_{an}(j\Omega) \star T\mathrm{sinc}\left(\Omega\frac{T}{2}\right) + \Gamma(j\Omega)\right],
\end{aligned}
\tag{5.12}
$$

where $\Gamma(j\Omega)$ denotes the summation of all terms resulting from the multiplication of two distinct terms in the product $V_{\mathrm{a}T}(j\Omega)I^{*}_{\mathrm{a}T}(j\Omega)$. It is assumed that the cross-power spectral density associated with $\Gamma(j\Omega)$ tends to zero because AC mains signals, harmonic, interharmonic and supraharmonic components do not overlap in the frequency-domain, and the transient components are spread over the frequency domain and occupy different frequency band because of their distinct natures.

Substituting (5.12) in the last line of (5.6) and evaluating the limit in such line with the knowledge that

$$
\lim_{T\to\infty} \frac{1}{T}T^2\mathrm{sinc}^2\left(\Omega\frac{T}{2}\right) = \delta(\Omega) \tag{5.13}
$$

result in the analytic cross-power spectral density, which is so-called frequency-domain extended complex power (FD-ECP), given by

$$
\begin{aligned}
\mathcal{S}_{FEC}(j\Omega) &\triangleq P_{FEA}(j\Omega) + jQ_{FEA}(j\Omega) \\
&\triangleq S_{\mathrm{aVI}}(j\Omega) \\
&\triangleq \frac{V_0 I_0}{4}\delta(\Omega) + \sum_{k=1}^{N_1} V_k I_k e^{j\Delta\theta_k}\delta(\Omega - k\Omega_1) + \sum_{l=1}^{N_2} V_{I,l} I_{I,l} e^{j\Delta\theta_{I,l}}\delta(\Omega - \Omega_{I,l}) + \\
&\sum_{l=1}^{N_3} V_{S,l} I_{S,l} e^{j\Delta\theta_{S,l}}\delta(\Omega - \Omega_{S,l}) + \frac{1}{8\pi^2}\left(\sum_{l=1}^{N_4} S_{\mathrm{aimp},l}(j\Omega) + \sum_{l=1}^{N_5} S_{\mathrm{anot},l}(j\Omega) + \right. \\
&\left.\sum_{l=1}^{N_6} S_{\mathrm{aosc},l}(j\Omega) + S_{\mathrm{an}}(j\Omega)\right),
\end{aligned}
\tag{5.14}
$$

where $P_{FEA}(j\Omega)$ and $Q_{FEA}(j\Omega)$ are real and imaginary components of $\mathcal{S}_{FEC}(j\Omega)$, respectively. In other words, (5.14) informs the amount of real and imaginary parts of the analytic cross-power spectrum density between voltage and current signals, which are defined by (5.1) and (5.2), respectively. The proof of (5.13) is given as follows.

Proof. Equation (5.13) can be expressed as

$$\begin{aligned}\lim_{T\to\infty}\frac{1}{T}T^2\mathrm{sinc}^2\left(\Omega\frac{T}{2}\right) &= \lim_{T\to\infty}\frac{1}{T}T^2\frac{\sin^2(\Omega T/2)}{\Omega^2T^2/4}\\ &= \lim_{T\to\infty}\frac{1}{T}\frac{\sin^2(\Omega T/2)}{\Omega^2/4}\end{aligned} \tag{5.15}$$

Note that (5.15) is equal to 0 when $\Omega \neq 0$. However, when $\Omega \to 0$, it is necessary to analyze the behavior (5.15) with the following expression:

$$\begin{aligned}\lim_{T\to\infty}\lim_{\Omega\to 0}\frac{1}{T}\frac{\sin^2(\Omega T/2)}{\Omega^2/4} &= 4\lim_{T\to\infty}\frac{1}{T}\lim_{\Omega\to 0}\frac{\sin^2(\Omega T/2)}{\Omega^2}\\ &= 4\lim_{T\to\infty}\frac{1}{T}\lim_{\Omega\to 0}\frac{1}{2}\left(\frac{1-\cos(\Omega T)}{\Omega^2}\right).\end{aligned} \tag{5.16}$$

As (5.16) outputs an undefined limit as $\Omega \to 0$, the L'Hôpital's rule applies and the attained result is given by

$$\begin{aligned}4\lim_{T\to\infty}\frac{1}{2T}\lim_{\Omega\to 0}\left(\frac{T\sin(\Omega T)}{2\Omega}\right) &= \lim_{T\to\infty}T\lim_{\Omega\to 0}\left(\frac{\sin(\Omega T)}{\Omega T}\right)\\ &= \lim_{T\to\infty}T\\ &= \infty.\end{aligned} \tag{5.17}$$

Finally, the only solution that fulfills the results of (5.15) for $\Omega \neq 0$ and $\Omega \to 0$ is given by

$$\lim_{T\to\infty}\frac{1}{T}T^2\mathrm{sinc}^2\left(\Omega\frac{T}{2}\right) = \delta(\Omega). \tag{5.18}$$

□

The ECP (5.3) obtained from the voltage and current signals at the terminals of a non-linear load (i.e., (5.1) and (5.2)), is the extended version of the complex power in electric power systems, which is the result of the integration of a scaled-version of FD-ECP (5.14). Note that (5.14) is the analytic cross-power spectral density between the voltage and current signals, and, as a consequence, the corresponding ECP is obtained by evaluating the following expression:

$$\mathcal{S}_{EC} = \int_0^{+\infty} K(j\Omega)\mathcal{S}_{FEC}(j\Omega)d\Omega, \tag{5.19}$$

where

$$K(j\Omega) = \begin{cases}2, & \Omega = 0,\\ \frac{1}{2}, & \Omega > 0.\end{cases} \tag{5.20}$$

Note that $K(0) = 2$ is necessary to agree with the definition of the sign function while $K(j\Omega) = 1/2$ for $\Omega > 0$ ensures the agreement with the complex power, which is based on root mean square (RMS) values. It means that (5.20) guarantees $\mathcal{S}_{EC}$ is an extended version of the complex power, which is well-established in the electricity sector since $K(j\Omega)$ given by (5.20) means that the RMS values of voltage and current signals are considered and, as a consequence, P_{EC} of (5.3) can be interpreted as the sum of active powers associated with a resistive load. If only the AC mains signals, harmonic, interharmonic, and supraharmonic components are considered, then P_{EC} results in an amount of power delivered to a resistive load equivalent to the application of DC voltage and current signals in its terminals, such that their amplitudes are given by RMS values of each aforementioned component [120, Section 11.4]. Finally, it is clear that (5.19) and (5.20) provide the link between the analytic cross-power spectral density and the complex power, and all tools related to the cross-power spectral density can be applied to analyze complex powers in electric power systems.

In this context, let assume that the amount of harvested power depends upon the circuitry responsible for harvesting and storing the energy, which has an overall efficiency factor given by $\eta \in \mathbb{R}_+$, $1 \geq \eta > 0$ [80]. Note that $\eta = 1$ refers to the total amount of energy associated with the active power that is harvested and stored. In these circumstances, the following definitions deserve attention:

Definition 1. The so-called harvested extended active power (HEAP) is defined as

$$\begin{aligned} P_{HEA} &\triangleq \eta P_{EC} \\ &= \eta \,\mathrm{Re}\{\mathcal{S}_{EC}\} \\ &= \eta \,\mathrm{Re}\left\{ \frac{V_0 I_0}{2} + \sum_{k=2}^{N_1} \frac{V_k I_k}{2} e^{j\Delta\theta_k} + \sum_{l=1}^{N_2} \frac{V_{I,l} I_{I,l}}{2} e^{j\Delta\theta_{I,l}} + \right. \\ &\sum_{l=1}^{N_3} \frac{V_{S,l} I_{S,l}}{2} e^{j\Delta\theta_{S,l}} + \frac{1}{8\pi^2} \left(\sum_{l=1}^{N_4} \int_0^{+\infty} S_{\mathrm{aimp},l}(j\Omega) d\Omega + \right. \\ &\sum_{l=1}^{N_5} \int_0^{+\infty} S_{\mathrm{anot},l}(j\Omega) d\Omega + \sum_{l=1}^{N_6} \int_0^{+\infty} S_{\mathrm{aosc},l}(j\Omega) d\Omega + \\ &\left. \left. \int_0^{+\infty} S_{\mathrm{an}}(j\Omega) d\Omega \right) \right\}, \end{aligned} \tag{5.21}$$

in which Re{.} is the real-part operator. Also, (5.21) quantifies the amount of wasted power of WESs when $\eta = 1$.

Definition 2. The so-called harvested extended complex power (HECP) is expressed as

$$\begin{aligned} \mathcal{S}_{HEC} &\triangleq P_{HEA} + jQ_{EC} \\ &= \eta P_{EC} + jQ_{EC}, \end{aligned} \tag{5.22}$$

where P_{EC} and Q_{EC} are the real and imaginary components of $\mathcal{S}_{EC}$, see (5.3). Note that (5.22) informs the extended complex power after performing energy harvesting.

It is noteworthy that HECP differs from ECP due to the reduction of the extended active power after applying the energy harvesting procedure to recover the wasted energy of WESs.

The extended apparent power associated with ECP is given by

$$|\mathcal{S}_{EC}| = \sqrt{P_{EC}^2 + Q_{EC}^2}, \tag{5.23}$$

while its counterpart for HECP is given by

$$\begin{aligned} |\mathcal{S}_{HEC}| &= \sqrt{P_{HEA}^2 + Q_{EC}^2} \\ &= \sqrt{\eta^2 P_{EC}^2 + Q_{EC}^2}. \end{aligned} \tag{5.24}$$

If $\beta \in \mathbb{R}_+, 1 \geq \beta > 0$ is a constant value, then one can relate the extended apparent powers of ECP (5.23) and HECP (5.24) by solving

$$\begin{aligned} \beta^2 |\mathcal{S}_{EC}|^2 &= |\mathcal{S}_{HEC}|^2 \\ \beta^2 (P_{EC}^2 + Q_{EC}^2) &= P_{HEA}^2 + Q_{EC}^2, \end{aligned} \tag{5.25}$$

and consequently it is obtained

$$\beta = \sqrt{\frac{\eta^2 P_{EC}^2 + Q_{EC}^2}{P_{EC}^2 + Q_{EC}^2}}, \tag{5.26}$$

where $\eta = 1$ implies that $\beta = 1$ and HECP is equal to the ECP as well as HEAP turns back into the extended active power definition. However, if $\eta \neq 1$ then β could assume any value ranging in the interval $(0, 1)$.

It is important to emphasize that recovering the wasted energy only from harmonic components can result in the best trade-off between cost and performance because their spectral natures facilitate the design of EH circuits. Considering only the presence of harmonic components, which are the ones that most negatively impact the power quality of electric power systems and represent the largest amount of wasted energy with WESs [51], the following definition is introduced:

Definition 3. The harvested power refers to the active power associated with the wasted energy that is harvested from harmonic components. It is given by

$$P_{\mathrm{HP}} \triangleq \eta \operatorname{Re}\left(\frac{1}{2}\sum_{k=2}^{N_1} V_k I_k e^{j\Delta\theta_k}\right), \tag{5.27}$$

in which $\eta = 1$ means that the wasted power associated with harmonics is numerically equivalent to the harvested power, P_{HP}.

5.3 NUMERICAL RESULTS

The numerical analyses rely on a data set obtained from a two-week measurement campaign, which used a Fluke 435-II Power Quality and Energy Analyzer. The measurement

campaign was carried out in the Electrical Engineering Post-Graduation Building at the Federal University of Juiz de Fora, Brazil. This data set is constituted by voltage and current signals measured in the three phases (A, B, and C), and they refer to measures obtained in a time interval of 10 minutes. Consequently, the average values of consecutive measures apply when long time intervals are considered. Measures of the AC mains signal and harmonic components up to the 11^{th} order constitute the measured data set and cover the lower part of the UNB-PLC spectrum. For the Brazilian AC mains frequency, 60 Hz, it corresponds to the the harmonic frequencies $f_i = 60i$, $i = 2, ..., 11$ (i.e., $N_1 = 11$ in (5.27)).

As the harvesting of the wasted energy is a dynamic process, the average harvested power during a period of N_w weeks will be considered as

$$\overline{P_{\text{HP}}} = \frac{1}{N_w N_d N_h} \sum_{i=1}^{N_w N_d N_h} P_{\text{HP}}(i), \tag{5.28}$$

where $P_{\text{HP}}(i)$ is the amount of harvested power in the i^{th} time interval, N_d is the number of days-per-week, and $N_h = \lfloor 24/T_h \rfloor$ is the number of time intervals in one day and depends on the time resolution, T_h, whereas $\lfloor x \rfloor = \max\{m \in \mathbb{Z} | m \leq x\}$. The average values of 6 consecutive measurements is considered, such that the time interval resolution is $T_h = 1$ hour and, as a consequence, $N_h = 24$ as well as $N_w = 2$, while $N_d = 5$ for the weekdays and $N_d = 2$ for the weekends.

Moreover, to evaluate the number of IoT devices' transceivers that could take advantage of the harvested power, these devices make use of distinct energy consumption models; however, all of them can rely on the use of the average current consumption, which is given by

$$I_{\text{avg}} = \frac{1}{T_{\text{notif}}} \sum_{i=1}^{N-1} I_i T_i + \frac{1}{T_{\text{notif}}} I_{\text{sleep}} T_{\text{sleep}}, \tag{5.29}$$

in which $\sum_{i=1}^{N-1} T_i$ corresponds to the active time period; T_{sleep} and I_{sleep} represent the sleep time period and sleep current consumption, respectively; $T_{\text{notif}} = \sum_{i=1}^{N-1} T_i + T_{\text{sleep}}$ is the notification period which stands for the time between two consecutive periodic message transmissions; N is the number of different states (e.g., sleep mode and transmission mode); I_i and T_i are, respectively, the current consumption and the time period of the i^{th} state. Furthermore, the average consumed power by a single transceiver of an IoT device is

$$\overline{P_{\text{IoT}}} = V_{\text{DC}} I_{\text{avg}}, \tag{5.30}$$

where V_{DC} is the DC voltage supply of the device. Details about each transceiver's energy consumption model used by IoT device are given in Subsection **5.3.3**. Further, the number of supplied transceivers of IoT devices is evaluated as

$$N_{\text{IoT}} = \left\lfloor \frac{\overline{P_{\text{HP}}}}{\overline{P_{\text{IoT}}}} \right\rfloor. \tag{5.31}$$

Based on the given measured data set and mathematical formulations, Subsection **5.3.1** discusses the wasted energy dynamics, while Subsection **5.3.2** brings attention to the ergodic achievable data rates of NB-PLC and LP-RF WLC channels, by means of the harvested power. Then, Subsection **5.3.3** presents an estimate of the number of powered transceivers of IoT devices when they are only supplied by the harvested power and one extension of this estimate to the Brazilian electricity sector is considered in Subsection **5.3.4**.

5.3.1 Wasted Energy Dynamics: Building Facility

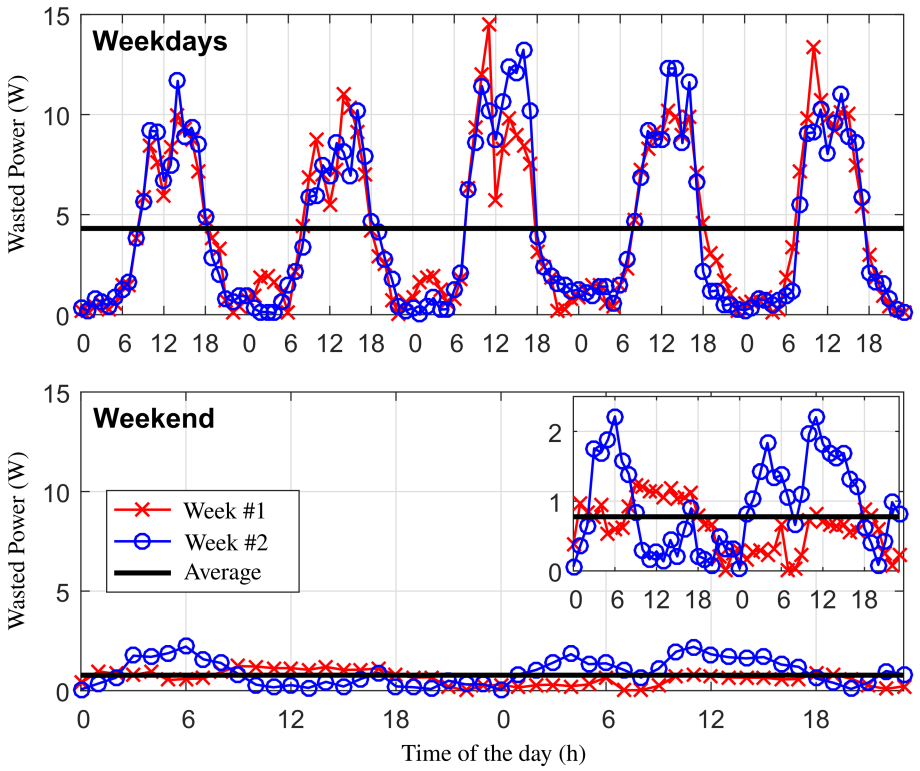
Figure 40 shows the wasted power (i.e., wasted energy dynamic) of harmonics as a function of the daytime, on weekdays (top) and weekends (bottom), for two different weeks, and also the average wasted power ($\eta = 1$). Each day is represented by time indexes of $\{0, 6, 12, 18\}$ hours, starting on Monday (weekdays) and Saturday (weekend). By comparing these two weeks, it can be seen that the wasted power on weekdays behaves as a cyclostationary random process with values ranging from ~ 0 to approximately 14.5 W. In this regard, the highest values occur around lunchtime, the lower ones at midnight, and the average is 4.3 W. On the other hand, on weekends, the wasted power ranges from ~ 0 to 2.2 W with stationary random behavior, which results in 0.8 W of average power. In other words, the wasted power is higher on weekdays than on the weekend. Moreover, the weekdays' wasted power presents a bell-shaped form with the higher values occurring near midday and the lower ones at midnight. Also, around the peaks of the wasted power (i.e., lunchtime) a variation is observed because students and staff leave the building and, as a consequence, the energy consumption associated with air conditioning, computers, and other types of electronic equipment decreases. It means that the wasted energy associated with WESs increases when the energy consumption is high, and consequently the possibility of harvesting more energy also increases.

For $\eta \in \{0.1, 0.2, \ldots, 1\}$, the impact of the choice of η on the amount of the harvested power is shown in Figure 41. These curves are obtained by first taking the average over the day for the two weeks and then obtaining the maximum, mean, and minimum values for each value of η. Note that η is directly proportional to the harvested power, see (5.27), and, consequently, the three power curves linearly vary with the overall efficiency factor. A practical value of the overall efficiency factor is $\eta = 0.5$ [80], which will be adopted in the following analyses and subsections. For this value, it can be seen that the weekdays' harvested power maximum and mean values are 6.2 and 2.2 W, respectively, while on the weekend these values are 0.8 and 0.4 W, respectively.

5.3.2 Ergodic Achievable Data Rates: Building Facility

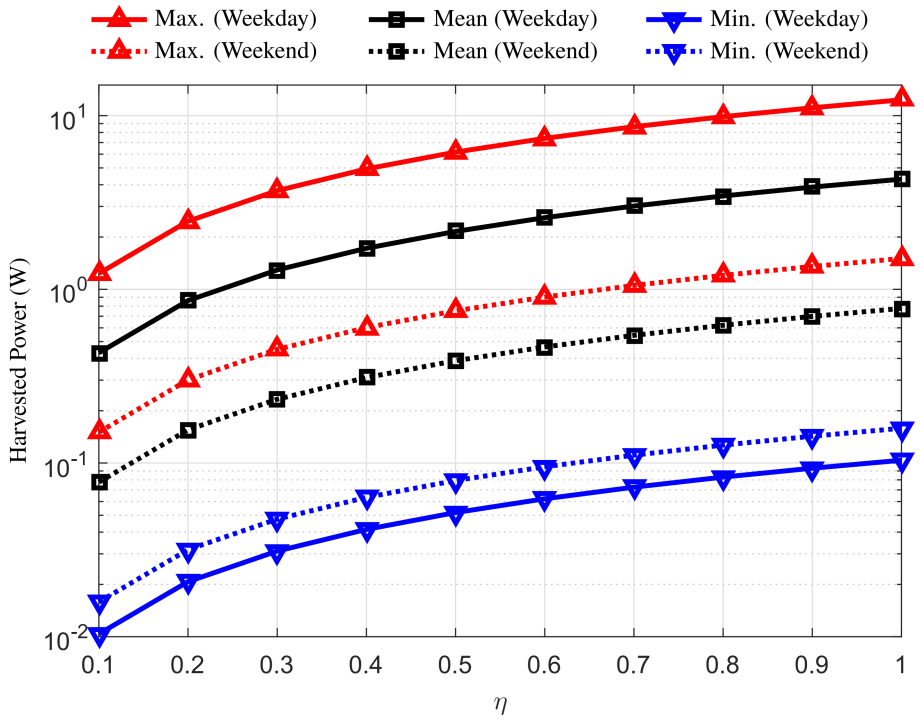
In this subsection, the calculation of the ergodic achievable data rates is performed. It is related to point-to-point data communication based on NB-PLC and LP-RF WLC systems when the transceivers have only the harvested power available. To do so, it is considered the narrow-regulated frequency band (3 – 500 kHz) for PLC [73] and in the ISM around (5.8 GHz)

Figure 40 – Wasted power for distinct days of the week ($\eta = 1$).



Source: Personal collection.

Figure 41 – Harvested power for distinct values of η.



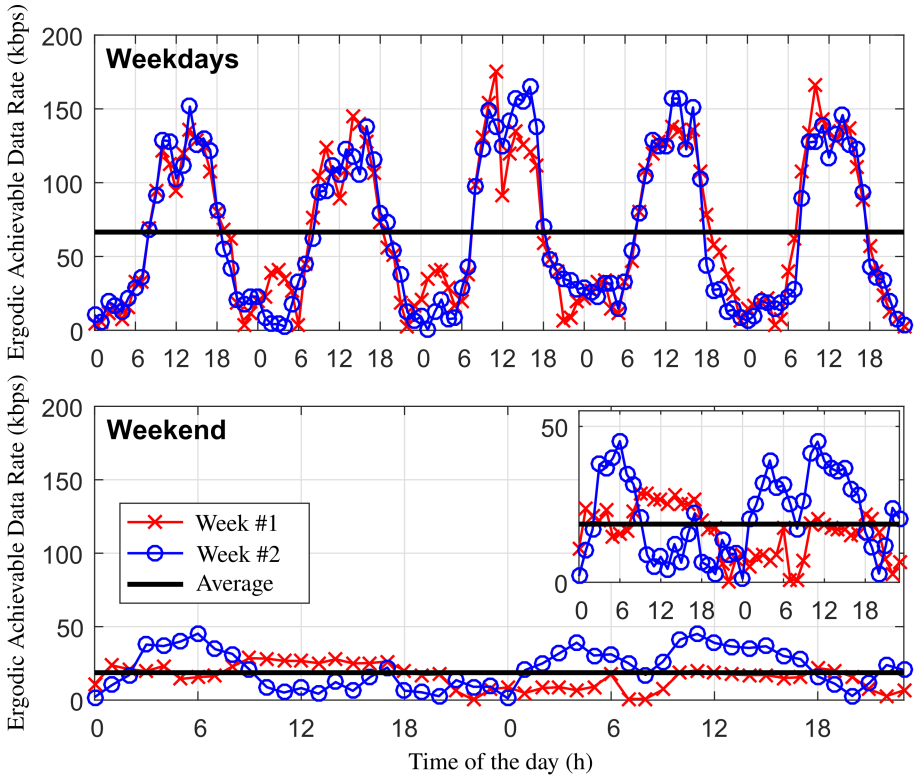
Source: Personal collection.

for WLC, in which the occupied frequency bandwidth is approximately 500 kHz in both media to ensure fairness.

Brief descriptions of the adopted NB-PLC and LP-RF WLC channel models, the ergodic achievable data rate formulation, and the assumptions were detailed in Subsection **3.4.6** of Chapter 3. In possession of the channel frequency responses, the additive noises' PSD, and assuming that the power allocation is yielded by the WF-power-optimizing technique, the ergodic achievable data rate of both channels is evaluated as mentioned above by using equation (3.8) subject to $\int_{-\infty}^{\infty} \upsilon_j^{\ell}(f)df \leq P_{\mathrm{HP}}(i)$.

Figure 42 shows the ergodic achievable data rates and its average over the NB-PLC channels on weekdays (top) and on the weekend (bottom). In this case, it is assumed the use of the harvested power with $\eta = 0.5$ to perform data communication. On weekdays, it can be seen ergodic achievable data rates as high as 175 kbps and the average around 66 kbps. On the weekend, 45 and 19 kbps for the maximum and average values, respectively, are attained. These results show that a NB-PLC device could communicate with a variable data rate, ranging from dozens to almost two hundreds of kbps during an entire week, using exclusively the harvested power as the power supply for a transceiver.

Figure 42 – Ergodic achievable data rate for the NB-PLC.

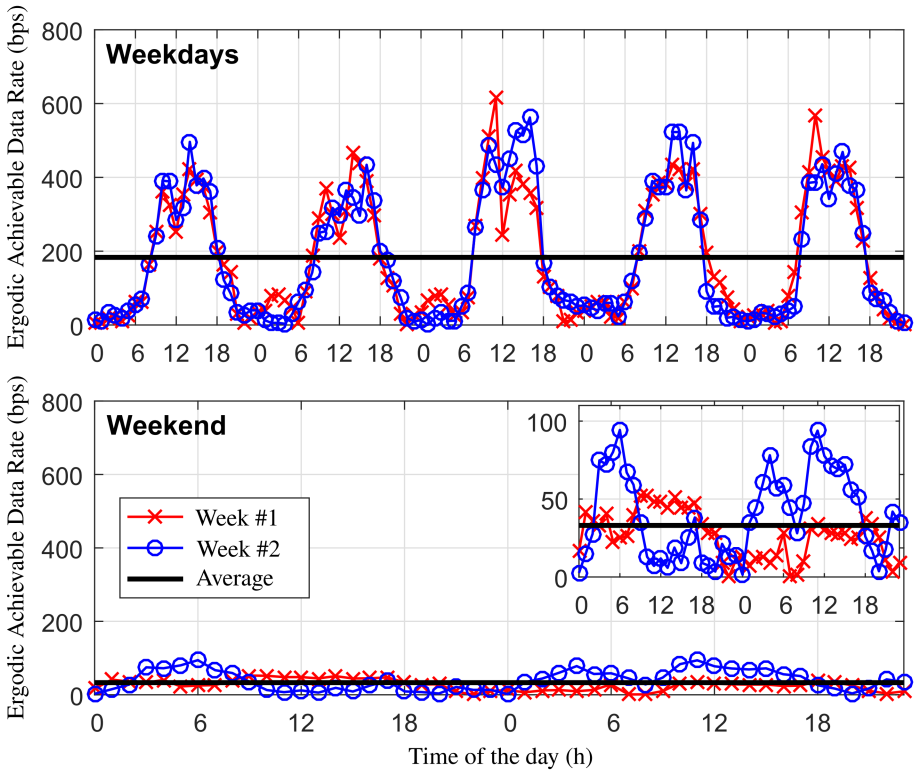


Source: Personal collection.

Similarly, Figure 43 shows ergodic achievable data rates when data communication is over the LP-RF WLC channels. It is noticed that the peak of the ergodic achievable data rate is 614 bps, while its average is approximately 183 bps on weekdays. Furthermore, the weekend has values of maximum and average ergodic achievable data rates of 94 and 33 bps, respectively.

Thus, a LP-RF WLC device may establish variable-data-rate communication, ranging from dozens to hundreds of bps during the entire week, using exclusively the amount of harvested power. Based on the characteristic of the LP-RF WLC channel model, the ergodic achievable data rates are much lower than the ones attained through NB-PLC channels.

Figure 43 – Ergodic achievable data rate for the LP-RF WLC.



Source: Personal collection.

5.3.3 Number of Transceivers of IoT Devices: Building Facility

In this subsection, it is assumed $\eta = 0.5$ to evaluate the number of transceivers of IoT devices by means of (5.31). In other words, one takes the ratio between the average harvested power during the two weeks ($N_w = 2$) and the average consumed power by a single device. To do so, it is taken into account two data communication standards related to wireless personal area networks (WPAN) (i.e., Zigbee and Bluetooth) and three related to wireless wide area network (WWAN) (i.e., Sigfox, LoRa, and NB-IoT). These data communication standards are associate with wireless technologies and they are detailed in the following subsections.

Moreover, numerical results when the notification period is lower bounded by each wireless technology's active period are obtained. In other words, an IoT device is unable to establish data communication when the notification period is lower than the active period. Approximate values for the active period are 0.2 s, 0.4 s, 3.1 s, 40.5 s, and 54.8 s for Zigbee, Bluetooth, LoRa, Sigfox, and NB-IoT, respectively.

5.3.3.1 *Zigbee*

Zigbee has based on IEEE 802.15.4 standard employed for various IoT solutions worldwide, being a short-range technology. Its transmission scheme relies on the CSMA/CA random access method, in which nodes are channel-sensitive and able to assess transmission channels in various ways. Also, it allows support in several operating frequencies, such as the 2.4 GHz (ISM frequency band), and achieves data rates up to 250 kbps [121], being these two assumed in this chapter. In addition, it has 16 channels that occupy a bandwidth of 2 MHz each. The Zigbee frame payload size of 102 bytes is used, which corresponds to the maximum IEEE 802.15.4 MAC frame payload size [122]. It is assumed the worst-case scenario without re-association, as given in [123]. The last-mentioned work provides a thorough description of a Zigbee experimental setup and energy consumption modeling as well as its operating states are detailed in Table 11. Furthermore, the Zigbee device is assumed to have $V_{\mathrm{DC}} = 3.6$ V.

Table 11 – Zigbee states and current consumption information.

Description (state)	**Duration (ms)**	**Current Consumption (mA)**
Activation/deactivation	13	13
Frame transmission	17.02	30.5
Channel listening	153.98	32.5
Sleep	Variable	0.00075

Source: [123].

5.3.3.2 *Bluetooth*

Bluetooth low energy (BLE) is a short-distance technology closely associated with IoT applications, especially due to its energy-saving feature. It operates from 2.40 GHz up to 2.483 GHz (ISM frequency band), counting with 40 channels, being 3 advertising channels and 37 data channels with a bandwidth of 2 MHz each [124]. In addition, it achieves data rates of 1 Mbps and has a maximum payload size of 20 bytes. One approach used for BLE communication is broadcasting, in which advertisements (i.e., messages sent over an advertising channel) are copied to all of the advertising channels and three transmissions are taken into account. Two important parameters are the time between two data-message transmissions (T_{data}) and the request-scan cycle interval ($T_{\mathrm{PollTimeout}}$). It is considered an energy consumption worst-case scenario, corresponding to $T_{\mathrm{data}} = T_{\mathrm{PollTimeout}}$ and a receive window of 255 ms based on what has been presented in [125]. The mentioned work also provides detailed information about BLE states and the energy consumption model. BLE operating states considered in this chapter are given in Table 12, in which the first nine states correspond to the advertisement transmitting ones and they are evaluated twice in (5.29). Finally, the BLE device has $V_{\mathrm{DC}} = 3.0$ V.

Table 12 – Bluetooth states and current consumption information.

Description (state)	Duration (ms)	Current Consumption (mA)
2 × Wake up	1.51	0.38
2 × 1st transmission	0.52	8.45
2 × 2nd transmission	0.53	8.85
2 × 3rd transmission	0.53	8.71
2 × 1st channel change	0.30	3.66
2 × 2nd channel change	0.33	3.91
2 × Radio off	0.29	5.48
2 × Post-processing	0.62	1.2
2 × Cool down	14.0	0.074
Wake up pre scan	1.57	0.34
Scan	255	13.9
Radio off & Processing	0.32	6.44
Post scanning cool down	26.3	0.07
Sleep	Variable	0.015

Source: [125].

5.3.3.3 LoRa

Long-range wide area network (LoRaWAN) is a low-power wide-area networks (LPWAN) technology envisioned for long-range and low-cost applications. LoRaWAN devices are split into three classes (A, B, and C). It is considered a class A device, which is the simplest LoRaWAN communication scheme: a device transmits a message at a random instant of time and the receiver responds after two predefined delays, corresponding to a bi-directional transaction [126]. Also, it has been considered the European 863−870 MHz uplink requirements, an unacknowledged transmission, and the data rate (DR)-5 specification, as follows: spreading factor (SF) equal to 7, maximum physical layer frame payload size (FRMPL) of 242 bytes and bandwidth of 125 kHz, as presented in [127]. DR-5 has been considered due to its high data rate (e.g., 5470 bps) and payload size. LoRaWAN energy consumption modeling is given by the last-mentioned work and further details about its states are then given in Table 13. For the LoRaWAN device, it is assumed $V_{\mathrm{DC}} = 5.0$ V.

5.3.3.4 Sigfox

Sigfox is a LPWAN technology that operates with an ultra-narrowband transmission in the unlicensed frequency spectrum, with values ranging from 862 MHz up to 928 MHz, which

Table 13 – LoRa states and current consumption information.

Description (state)	Duration (ms)	Current Consumption (mA)
Wake up	168.2	22.1
Radio preparation	83.8	13.3
Frame transmission	399.6	83.0
Wait 1st window	983.3	27.0
1st receive window	12.29	38.1
Wait 2nd receive window	987.71	27.1
2nd receive window	1.28	35.0
Radio off	147.4	13.2
Post processing	268.0	21.0
Turn off sequence	38.6	13.3
Sleep	Variable	0.045

Source: [127].

relies on each location across the globe [128]. Also, it counts with an uplink bandwidth of 100 Hz or 600 Hz, depending on the region, and a downlink one of 1.5 kHz. In addition, the former operates with a data rate of 100 bps (e.g., Europe), having a payload message up to 12 bytes, whilst the latter operates with data rates of 600 bps worldwide, counting with a payload message up to 8 bytes. An IoT device operating in Sigfox can perform unidirectional or bi-directional transactions between different devices. Moreover, Sigfox performs a data message scheme grounded on sending a frame over a randomly chosen frequency band, followed by two replicas of the same packet in randomly allocated frequency channels. After these transmissions are completed, the end-device opens up a receive window to enable downlink messages [129]. In this chapter, it has been considered a bi-directional transaction scenario without frame losses. Regarding the energy consumption model, the worst-case scenario related to power consumption is used [130] assuming the European Sigfox specifications. Its operational states are given in Table 14, in which the transmission and wait next transmission states are, respectively, evaluated thrice and twice in (5.29). Also, the Sigfox device uses $V_{\mathrm{DC}} = 3.0$ V.

5.3.3.5 NB-IoT

Narrowband-IoT (NB-IoT) is a narrowband LPWAN technology deployed through long term evolution (LTE) communication network, a well-established mobile communication standard [131]. It counts with three deployment modes: in-band, standalone, and guard-band, allowing data rates up to 50 kbps and 30 kbps in uplink and downlink, respectively, with a maximum frame payload size of 1600 bytes [132]. It operates in the LTE licensed spectrum,

Table 14 – Sigfox states and current consumption information.

Description (state)	Duration (ms)	Current Consumption (mA)
Wake up	305	10.7
3 × Transmission	2,080	27.6
2 × Wait next transmission	493	1.2
Wait next reception	16,493	1.3
Reception	12,690	18.5
Wait confirm. transm.	1,430	1.2
Confirmation transm.	1,850	27
Cool down	495	1.2
Sleep	Variable	0.016

Source: [130].

thus supporting several frequencies (e.g., 700, 800, and 900 MHz) with a bandwidth of 180 kHz or 200 kHz, depending on the operational mode [133]. Furthermore, NB-IoT has specific power-saving features: extended discontinuous reception mode (eDRX) and power saving mode (PSM). The former corresponds to a state in which devices do not listen to the radio channel for a defined period and become active periodically. The latter is the deep sleep mode, in which a device becomes unreachable by the network it belongs to, however it can wake up at any time to transmit data. It is also worth mentioning NB-IoT has greater power consumption compared to several other wireless technologies, such as Sigfox and LoRaWAN, due to its high-energy consumption associated with the network connection procedure. Moreover, the NB-IoT device's operational states are given in Table 15 and V_{DC} = 3.7 V is adopted. Its current consumption and time period for each operational state are found in [129].

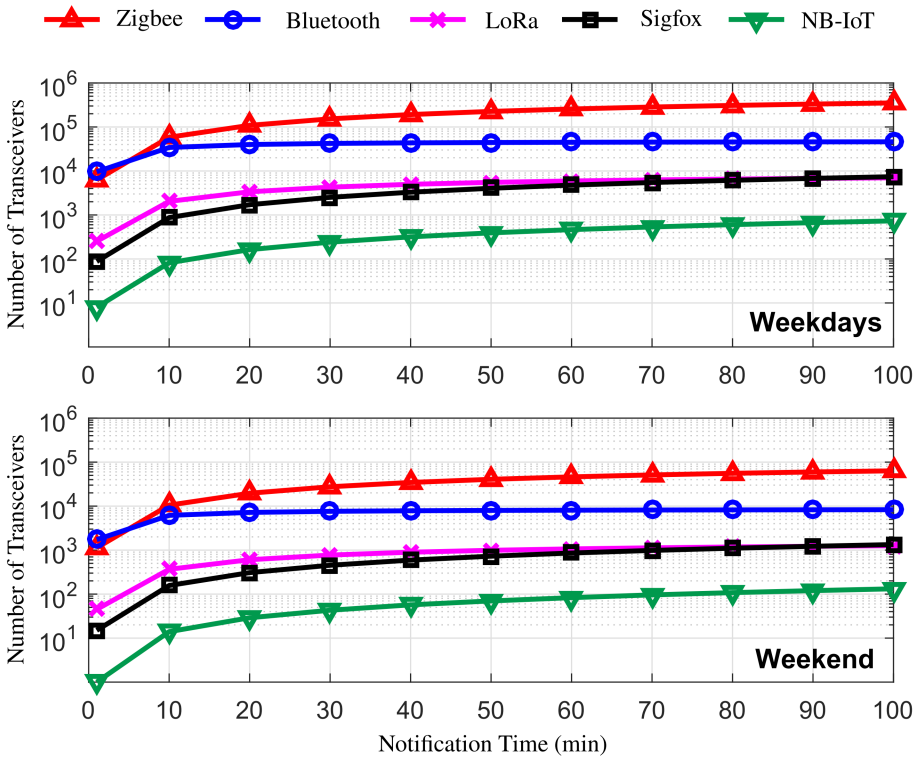
Table 15 – NB-IoT states and current consumption information.

Description (state)	Duration (ms)	Current Consumption (mA)
Initialization	5,390	8.46
Module activation with service provider	11,030	57.63
Connection	6,930	28.07
eDRX	31,000	9.58
Frame transmission	373	46.12
Deep sleep (PSM)	Variable	0.10

Source: [129].

Figure 44 shows estimates of the number of powered transceivers of IoT devices in terms of the notification period for the weekdays (top) and weekend (bottom). These devices are assumed to use one of the aforementioned data communication standards and they are only supplied by the harvested power. Note that the active period of a specific transceiver is constant as it depends on the previous set parameters. In other words, increasing the notification period only implies increasing the sleeping period. The notification period range in minutes is suitable for some applications such as lighting control, environmental control, and utility infrastructure [134]. It can be seen that the use of WPAN technologies results in a higher number of powered IoT devices' transceivers in comparison to WWAN. For instance, if $T_{\text{notif}} = 100$ min, then the numbers of Zigbee and Bluetooth transceivers that can be powered by the harvested power are in the order of 3×10^5 and 5×10^4 on weekdays while the others are much lower, being the number of IoT devices served by NB-IoT almost 7×10^2. Comparing LoRa and Sigfox technologies, the number of LoRa devices is larger than Sigfox ones for low values of T_{notif} and the opposite occurs for high values of T_{notif}. For instance, on weekdays and $T_{\text{notif}} = 100$ min, the number of devices is in the order of 7×10^3 for both Sigfox and LoRa.

Figure 44 – Number of powered IoT devices' transceivers versus notification period (in minutes).

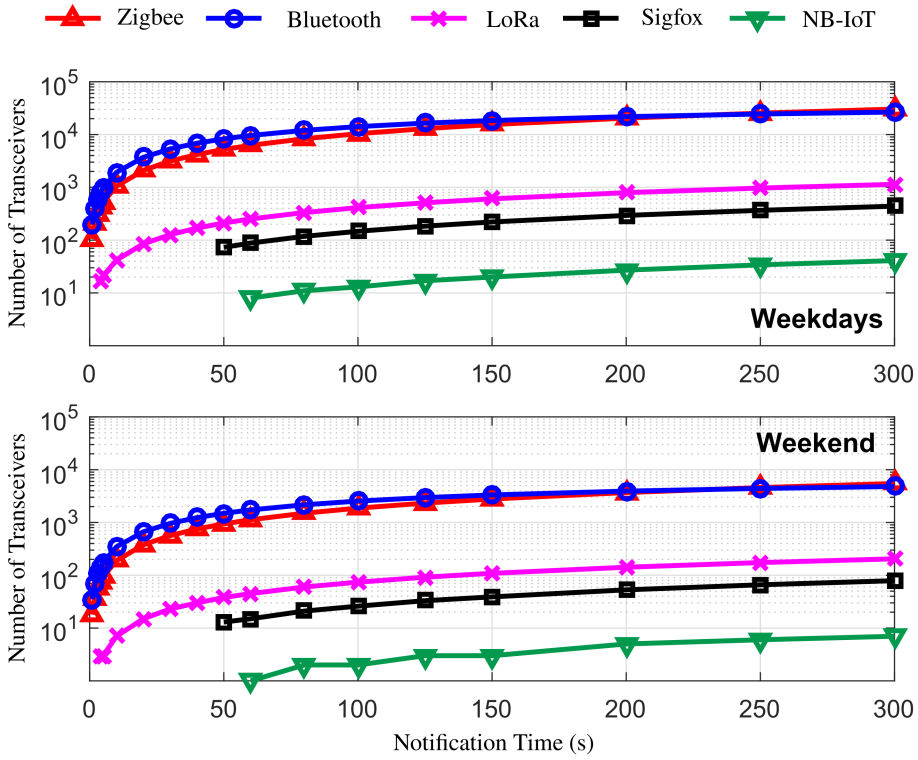


Source: Personal collection.

Considering the requirement to fast message exchanges, the analysis of a notification period in the range of seconds could be necessary, being this suitable for several applications such as parking availability, street traffic, and security [134]. In this regard, Figure 45 depicts the estimates of the number of powered transceivers of IoT devices in terms of the notification period for the weekdays (top) and weekend (bottom). In this plot, it can be seen that Bluetooth

outperforms Zigbee when $T_{\text{notif}} < 250$ s, and the opposite occurs after that. Overall and on weekdays, when the notification period is equal to 60 s, it is possible to power 9608 Bluetooth or 6258 Zigbee devices and 252, 88, or 8 devices for LoRa, Sigfox, and NB-IoT, respectively. Observe that if a fast change of messages is needed ($T_{\text{notif}} < 4$ s), then Sigfox and NB-IoT technologies should not be applicable.

Figure 45 – Number of powered IoT devices' transceivers versus notification period (in seconds).



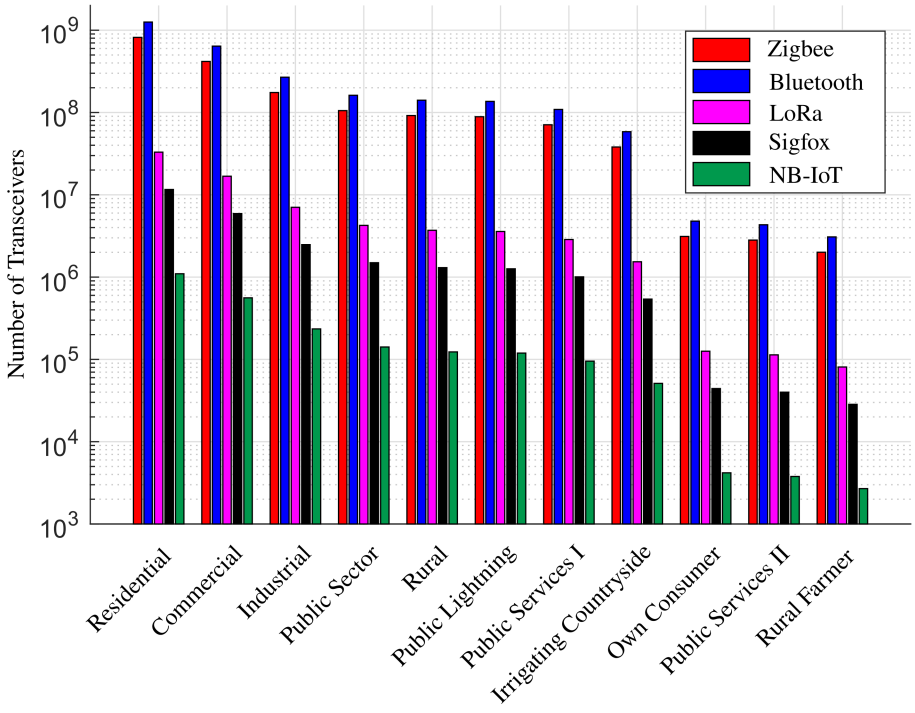
Source: Personal collection.

5.3.4 Number of Transceivers of IoT Devices in the Brazilian Electricity Sector

In this subsection, the aim is at paying attention to a national perspective of the usefulness of EH applied to the WES (i.e., WEH). In this context, Figure 46 shows rough estimates of the number of transceivers of IoT devices that could be powered by the wasted energy that is harvested in distinct Brazilian electricity sectors when $\eta = 0.5$ and $T_{\text{notif}} = 1$ min for the given data communication standards. To come out with this bar plot, it is evaluated the ratio between the harvested power and the active power of the AC mains signal, which resulted in approximately 0.2 % of average for both weekdays and weekends. This percentage was then applied to the power consumption of distinct sectors, based on Brazilian electricity regulatory agency (*Agência Nacional de Energia Elétrica* in Portuguese) (ANEEL) consumption profile [135]. Regarding Bluetooth, it is possible to notice that values as high as 1.3 billion of devices can be powered in the residential sector by performing EH in the UNB-PLC spectrum. The rural farmer sector results in the lowest values, which is approximately 3.1 million for Bluetooth.

When the overall Brazilian scenario (all electricity sectors) is considered, the values are detailed in Table 16. As can be seen, millions, or even billions, of transceivers of IoT devices can be powered up using the harvested power from WESs, which occupies the UNB-PLC spectrum, depending on the chosen data communication standard.

Figure 46 – A rough estimate of IoT devices' transceivers that could be powered within Brazilian electricity sectors in 2019 (T_{notif} = 1 min).



Source: Personal collection.

Table 16 – Estimate of IoT devices' transceivers that could be powered within all Brazilian electricity sectors (in millions).

Data Communication Standard	**Number of Transceivers**
Zigbee	1,813.85
Bluetooth	2,784.96
LoRa	73.12
Sigfox	25.72
NB-IoT	2.43

Source: Personal collection.

It is important to highlight that the harvested power is proportional to the consumed power that annually increases. Furthermore, the more non-linear loads are connected to the electric power system, the higher is the harvested power. Thus, the number of powered transceivers

of IoT devices with the harvested power from WESs is expected to increase with the spread and usage of electric power systems. Also, the improvements in terms of energy efficiency and power quality imposed by WEH reduce greenhouse effects.

Based on numerical analyses, it is pointed out that the wasted energy dynamics associated with the UNB-PLC spectrum are cyclostationary and stationary random processes on weekdays and weekends, respectively, which agrees with the energy consumption profile of consumers. Besides, it is shown that the amount of harvested energy from WESs that occupy the UNB-PLC spectrum constitutes an additional and interesting source of energy. It can also be used to power transceivers of a large number of IoT devices, which run well-known and established data communication standards.

5.4 SUMMARY

This chapter discussed the wasted and harvested powers of WESs that occupy the lower part of the UNB-PLC spectrum and their usefulness to power transceivers based on typical data communication standards applied to IoT devices. Also, it detailed numerical analyses based on a measurement campaign carried out in a building facility. Analyses of numerical results showed that cyclostationary and stationary random processes model the dynamic of the wasted energy on weekdays and weekends, respectively. Also, a large number of transceivers used by low-power IoT devices, which run Zigbee, Bluetooth, LoRa, Sigfox, or NB-IoT, can be powered with such harvested power in the Brazilian electric power systems.

6 CONCLUSIONS

This dissertation investigated energy harvesting applied to concatenated hybrid PLC-WLC channels, parallel hybrid PLC/WLC channels, and disturbances in electric signals by means of dedicated and ambient energy harvesting approaches in LV electric power systems. Based on a measured data set, numerical results assessed the potential of harvested energies by quantitatively evaluating ergodic achievable data rates of low-bit-rate devices and the number of transceivers of IoT devices that could take advantage of these energies.

Chapter 2 discussed general aspects of energy harvesting in electric power systems, bringing attention to two well-known artificial sources of energy (electric field and magnetic field) and the inclusion of the WES as another possible artificial source of energy. As discussed, WESs correspond to the summation of disturbances such as harmonics, interharmonics, supraharmonics, transients, and RF induced signals and the covered frequency band by them comprehends the PLC additive noise. Furthermore, this chapter presented advantages and drawbacks related to typical classifications for harvesting energy in the electric power systems in terms of the voltage levels of the AC mains voltage signal (i.e., HV, MV, and LV) and frequency bands of the spectrum occupied by the electric signals (i.e., AC mains frequency, UNB-PLC, NB-PLC, and BB-PLC) when *dedicated* and *ambient* energy harvesting approaches are adopted. Moreover, three harvesting methods (*harvest-use*, *harvest-store-use*, and *harvest-use-store*) have been covered and discussed in the context of IoT applications when scheduled and unscheduled data communications are considered. Also, the overall efficiency factor of an energy harvesting device's circuitry has been contextualized for harvesting energy from artificial sources of energy in electric power systems. Lastly, the energy harvesting perspective about hybrid data communication systems composed of PLC and WLC systems has been discussed, in which two configurations (parallel and concatenated) and the use of a relaying node have been detailed when *in-band* and *out-of-band* strategies are adopted.

Chapter 3 addressed both the use of in-home concatenated hybrid PLC-WLC channels for dedicated energy harvesting, by means of a measured data set, and the statistical modeling of harvested energies (from the FoN received signal, additive noises, and a combination of them - total received signal). The harvested energies have been evaluated for two typical distance regions, namely *short-path* and *long-path*, and five distinct power masks (Uniform, IEEE 1901, Uniform B_u, Optimal B_o, and Single Tone). First, the harvested energies from hybrid PLC-WLC channels have been analyzed for the FoN received signal, additive noises, and total received signal. Then, the ergodic achievable data rates have been evaluated for NB-PLC, LP-RF WLC, and hybrid PLC-WLC channels, when the only available energy for performing data communication through these channels is the one harvested from the total received signal (i.e., total harvested energy). Numerical analyses based on the CCDFs of the harvested energy have shown that the BB-PLC additive reaches a high probability of plentiful contributing to increasing the total harvested energy. Furthermore, the attained ergodic achievable data rates vary from dozens of bps or kbps to dozens of Mbps, depending on the used channel for data

communication. Based on the log-likelihood criterion, the statistical modeling has indicated that the log-normal distribution is the most suitable for representing both the harvested energy of the FoN received signal and additive noises in concatenated hybrid PLC-WLC channels, and, as a consequence, the summation of these two log-normal random variables has been proposed as a model to the total harvested energy. Also, a comparison between the CCDFs of the harvested energies obtained from the measured data set and the statistical model has shown a good accuracy of the proposed statistical model, in which a maximum discrepancy of 21% was noted in the worst case. Thus, the harvested energy from these channels has been turned in an easy-to-simulate feature for carrying out future investigations on its potentialities and has been demonstrated to be essential for providing energy-efficient data communications for assisting SG, the IoT, and Industry 4.0 applications.

Chapter 4 formulated the ergodic achievable data rate of the H2HS model, in which the relay node performed energy harvesting and data communication based on four approaches, named Approach A - HTS strategy with the energy harvested from the wireless signal; Approach B - HTS strategy with the energy harvested from the power line signal; Approach C - TS strategy with the energy harvested from both signals; Approach D - PS strategy with the energy harvested from both signals. Also, four scenarios have been considered, varying the power allocation technique (optimal or uniform) and the NB-PLC additive noise behavior (i.e., flat PSD, AWGN or non-flat PSD, ACGN), in order to compare the H2HS model with P2HS and W2HS ones. Among these models and independent of the adopted scenario, numerical results have shown the H2HS using Approach D is the best option in terms of ergodic achievable data ratios, while the H2HS with Approaches A and B outperforms or, at least, has similar performance than the H2HS with Approach C. For optimal values of TS and PS factors, better performance has been obtained with the PS strategy in the studied models. When the optimal power allocation is adopted and NB-PLC additive noise has a non-flat PSD (i.e., practical assumption), the numerical analyses have shown that the ergodic achievable data rate increases for any PLC-based system in comparison to the ones that do not use it. Therefore, similar to the BB-PLC additive noise, the NB-PLC additive noise can be considered useful when energy harvesting is applied for data communication purposes.

Chapter 5 investigated the energy harvesting from the wasted power of WESs in the lower part of the UNB-PLC frequency band based on in-building measured data set. This frequency band contemplates the main components of electric signals that are responsible for degrading power quality in electric power systems (e.g., from 2^{nd} up to the 11^{th} harmonic components), which are considered a kind of wasted energy in electric signals. In order to do so, a novel mathematical formulation of the wasted power based on a telecommunications perspective has been introduced and the extension of this formulation to the harvested power has been addressed. Furthermore, the usefulness of the harvested power has been analyzed for NB-PLC and LP-RF WLC channels as well as for powering transceivers of IoT devices that adopt five common data communication standards, in which two are related to WPAN (Zigbee and Bluetooth) and three

to WWAN (LoRa, Sigfox, and NB-IoT). The numerical analyses have shown that the wasted energy dynamic on weekdays and weekends can be, respectively, considered cyclostationary and stationary random processes. Also, estimates of millions, or even billions, of transceivers powered by means of the harvested power in the Brazilian electric power systems have been presented. As discussed, the improvements in terms of energy efficiency and power quality imposed by harvesting the energy from WESs reduce greenhouse effects. Therefore, the energy present in the UNB-PLC additive noise has tremendous potential for feeding up low-power data communication devices, while its harvesting can benefit both electric power systems and the environment.

In order to expand the reach of the investigations presented in this dissertation, the following research issues deserve attention:

- To come up with efficient circuits to harvest the energy from WESs associated with harmonics and other components of the electric signal. Due to the time-varying access impedance of the electric power systems, this issue may be the bottleneck for the practical implementation of energy harvesting from WESs. Therefore, a deep study on the components of the energy harvesting device's circuitry as well as the investigation of the best techniques for implementing high-efficiency matching, rectification, and so on, are interesting future research directions.

- To analyze the energy harvesting in the concatenated configuration of PLC and WLC systems when multiple energy harvesting devices are considered. As shown, the concatenated configuration of a single PLC device and a WLC device was investigated in this dissertation; however, the use of multiple PLC and WLC devices in indoor facilities may be interesting for energy harvesting purposes and remains unexplored.

- To make a global estimate of the number of energy-harvesting-powered transceivers, by means of a most comprehensive measurement campaign. The analyses carried out in this dissertation were mainly focused on the Brazilian electricity sector and, thus, high variations on the amount of harvested powers and the number of IoT devices' transceivers may be experienced in other countries and worldwide.

REFERENCES

[1] P. Kamalinejad *et al.*, "Wireless energy harvesting for the Internet of Things," *IEEE Commun. Mag.*, vol. 53, no. 6, pp. 102–108, Jun. 2015.

[2] D. Mishra *et al.*, "Smart RF energy harvesting communications: Challenges and opportunities," *IEEE Commun. Mag.*, vol. 53, no. 4, pp. 70–78, Apr. 2015.

[3] A. Biason and M. Zorzi, "Joint transmission and energy transfer policies for energy harvesting devices with finite batteries," *IEEE J. Sel. Areas in Commun.*, vol. 33, no. 12, pp. 2626–2640, Dec. 2015.

[4] Z. Zou, A. Gidmark, T. Charalambous, and M. Johansson, "Optimal radio frequency energy harvesting with limited energy arrival knowledge," *IEEE J. Sel. Areas in Commun.*, vol. 34, no. 12, pp. 3528–3539, Dec. 2016.

[5] Y. Mao, G. Yu, and C. Zhong, "Energy consumption analysis of energy harvesting systems with power grid," *IEEE Wireless Commun. Lett.*, vol. 2, no. 6, pp. 611–614, Dec. 2013.

[6] M. Ku, W. Li, Y. Chen, and K. J. Ray Liu, "Advances in energy harvesting communications: Past, present, and future challenges," *IEEE Commun. Surveys Tuts.*, vol. 18, no. 2, pp. 1384–1412, 2016.

[7] S. Galli, A. Scaglione, and Z. Wang, "For the grid and through the grid: The role of power line communications in the smart grid," *Proc. IEEE*, vol. 99, no. 6, pp. 998–1027, Jun. 2011.

[8] M. V. Ribeiro, "Técnicas de processamento de sinais aplicadas a transmissão de dados via rede elétrica e ao monitoramento da qualidade de energia," Ph.D. dissertation, State University of Campinas, 2005.

[9] M. Nassar *et al.*, "Local utility power line communications in the 3-500 kHz band: Channel impairments, noise, and standards," *IEEE Signal Process. Mag.*, vol. 29, no. 5, pp. 116–127, Sep. 2012.

[10] M. Zimmermann and K. Dostert, "A multipath model for the power line channel," *IEEE Trans. Commun.*, vol. 50, no. 4, pp. 553–559, Apr. 2002.

[11] K. M. Rabie, B. Adebisi, and A. Salem, "Improving energy efficiency in dual-hop cooperative PLC relaying systems," in *Proc. IEEE Int. Symp. Power Line Commun. Appl.*, Mar. 2016, pp. 196–200.

[12] K. M. Rabie and B. Adebisi, "Enhanced amplify-and-forward relaying in non-Gaussian PLC networks," *IEEE Access*, vol. 5, pp. 4087–4094, Mar. 2017.

[13] K. M. Rabie, B. Adebisi, A. M. Tonello, and G. Nauryzbayev, "For more energy-efficient dual-hop DF relaying power-line communication systems," *IEEE Syst. J.*, no. 99, pp. 1–12, Jan. 2017.

[14] M. Sayed, T. A. Tsiftsis, and N. Al-Dhahir, "On the diversity of hybrid narrowband-PLC/wireless communications for smart grids," *IEEE Trans. Wireless Commun.*, vol. 16, no. 7, pp. 4344–4360, Jul. 2017.

[15] G. Sebaali and B. L. Evans, "Design tradeoffs in joint powerline and wireless transmission for smart grid communications," in *Proc. IEEE Int. Symp. on Power Line Commun. Appl.*, Mar. 2015, pp. 83–88.

[16] V. Fernandes, W. A. Finamore, H. V. Poor, and M. V. Ribeiro, "The low-bit-rate hybrid power line/wireless single-relay channel," *IEEE Syst. J.*, vol. 13, no. 1, pp. 98–109, Mar. 2019.

[17] V. Fernandes, H. V. Poor, and M. V. Ribeiro, "Analyses of the incomplete low-bit-rate hybrid PLC-wireless single-relay channel," *IEEE Internet Things J.*, vol. 5, no. 2, pp. 917–929, Apr. 2018.

[18] S. W. Lai and G. G. Messier, "Using the wireless and PLC channels for diversity," *IEEE Trans. Commun.*, vol. 60, no. 12, pp. 3865–3875, Dec. 2012.

[19] M. Kuhn, S. Berger, I. Hammerström, and A. Wittneben, "Power line enhanced cooperative wireless communications," *IEEE J. Sel. Areas in Commun.*, vol. 24, no. 7, pp. 1401–1410, Jul. 2006.

[20] S. Güzelgöz, H. B. Celebi, and H. Arsian, "Analysis of a multi-channel receiver: Wireless and PLC reception," in *Proc. Signal Process. Conf.*, Aug. 2010, pp. 1106–1110.

[21] J. Lee and Y. Kim, "Diversity relaying for parallel use of power-line and wireless communication networks," *IEEE Trans. Power Del.*, vol. 29, no. 3, pp. 1301–1310, Jun. 2014.

[22] L. de M. B. A. Dib, V. Fernandes, M. de L. Filomeno, and M. V. Ribeiro, "Hybrid PLC/wireless communication for smart grids and Internet of Things applications," *IEEE Internet Things J.*, vol. 5, no. 2, pp. 655–667, Apr. 2018.

[23] M. de L. Filomeno, G. R. Colen, L. G. de Oliveira, and M. V. Ribeiro, "Two-stage single-relay channel model for in-home broadband PLC systems," *IEEE Syst. J.*, vol. 13, no. 1, pp. 204–214, Mar. 2019.

[24] M. Kashef *et al.*, "Energy efficient resource allocation for mixed RF/VLC heterogeneous wireless networks," *IEEE J. Sel. Areas Commun.*, vol. 34, no. 4, pp. 883–893, Apr. 2016.

[25] J. Song *et al.*, "An indoor broadband broadcasting system based on PLC and VLC," *IEEE Trans. Broadcast.*, vol. 61, no. 2, pp. 299–308, Jun. 2015.

[26] T. R. Oliveira *et al.*, "Characterization of hybrid communication channel in indoor scenario," *J. Commun. Inf. Syst.*, no. 1, pp. 224–235, Sep. 2016.

[27] ANEEL, *Tariff Reports - Electric Energy Losses in Distribution*, 2020, https://www.aneel.gov.br/luz-na-tarifa. Accessed on Mar. 22, 2021.

[28] "Chapter 6 - Energy harvesting for sustainable smart spaces," ser. Advances in Computers, A. Hurson and A. Memon, Eds. Elsevier, 2012, vol. 87, pp. 203 – 251.

[29] O. B. Akan, O. Cetinkaya, C. Koca, and M. Ozger, "Internet of hybrid energy harvesting things," *IEEE Internet Things J.*, vol. 5, no. 2, pp. 736–746, 2018.

[30] R. Moghe, Y. Yang, F. Lambert, and D. Divan, "A scoping study of electric and magnetic field energy harvesting for wireless sensor networks in power system applications," in *IEEE Energy Conversion Congress and Exposition*, 2009, pp. 3550–3557.

[31] M. Zhu, P. C. Baker, N. M. Roscoe, M. D. Judd, and J. Fitch, "Alternative power sources for autonomous sensors in high voltage plant," in *IEEE Electrical Insulation Conference*, 2009, pp. 36–40.

[32] S. Sudevalayam and P. Kulkarni, "Energy harvesting sensor nodes: Survey and implications," *IEEE Commun. Surveys Tuts.*, vol. 13, no. 3, pp. 443–461, Third Quarter 2011.

[33] M. J. Moser, T. Bretterklieber, H. Zangl, and G. Brasseur, "Strong and weak electric field interfering: Capacitive icing detection and capacitive energy harvesting on a 220-kV high-voltage overhead power line," *IEEE Trans. Ind. Electron.*, vol. 58, no. 7, pp. 2597–2604, 2011.

[34] F. Guo, H. Hayat, and J. Wang, "Energy harvesting devices for high voltage transmission line monitoring," in *IEEE Power and Energy Society General Meeting*, 2011, pp. 1–8.

[35] X. Zhao *et al.*, "Energy harvesting for a wireless-monitoring system of overhead high-voltage power lines," *IET Gen., Trans. and Distr.*, vol. 7, no. 2, pp. 101–107, May 2013.

[36] H. Zangl, T. Bretterklieber, and G. Brasseur, "A feasibility study on autonomous online condition monitoring of high-voltage overhead power lines," *IEEE Trans. Instrum. Meas.*, vol. 58, no. 5, pp. 1789–1796, 2009.

[37] J. C. Rodríguez, D. G. Holmes, B. P. McGrath, and R. H. Wilkinson, "Maximum energy harvesting from medium voltage electric-field energy using power line insulators," in *Australasian Universities Power Engineering Conference*, 2014, pp. 1–6.

[38] R. Moghe, A. R. Iyer, F. C. Lambert, and D. M. Divan, "A low-cost wireless voltage sensor for monitoring MV/HV utility assets," *IEEE Trans. Smart Grid*, vol. 5, no. 4, pp. 2002–2009, 2014.

[39] R. Moghe, A. Iyer, F. C. Lambert, and D. Divan, "A low-cost electric field energy harvester for an MV/HV asset-monitoring smart sensor," *IEEE Trans. Ind Appl.*, vol. 51, no. 2, pp. 1828–1836, 2015.

[40] O. Cetinkaya and O. B. Akan, "Electric-field energy harvesting in wireless networks," *IEEE Trans. Wireless Commun.*, vol. 24, no. 2, pp. 34–41, Apr. 2017.

[41] K.-S. Chang *et al.*, "Electric field energy harvesting powered wireless sensors for smart grid," *J. Electrical Engineering and Tech.*, vol. 7, no. 1, pp. 75–80, 2012.

[42] H. Kim *et al.*, "Stray electric field energy harvesting technology using MEMS switch from insulated AC power line," *Electronics Lett.*, vol. 50, no. 17, pp. 1236–1238, Aug. 2014.

[43] J. Qu, L. He, N. Tang, and C. K. Lee, "Wireless power transfer using domino-resonator for 110-kV power grid online monitoring equipment," *IEEE Trans. Power Electron.*, vol. 35, no. 11, pp. 11 380–11 390, 2020.

[44] S. Yuan, Y. Huang, J. Zhou, Q. Xu, C. Song, and P. Thompson, "Magnetic field energy harvesting under overhead power lines," *IEEE Trans. Power Electron.*, vol. 30, no. 11, pp. 6191–6202, 2015.

[45] Z. Wang, J. Hu, J. Han, G. Zhao, J. He, and S. X. Wang, "A novel high-performance energy harvester based on nonlinear resonance for scavenging power-frequency magnetic energy," *IEEE Trans. Ind. Electron.*, vol. 64, no. 8, pp. 6556–6564, 2017.

[46] N. M. Roscoe and M. D. Judd, "Harvesting energy from magnetic fields to power condition monitoring sensors," *IEEE Sensors Journal*, vol. 13, no. 6, pp. 2263–2270, 2013.

[47] F. Yang *et al.*, "Hybrid energy harvesting for condition monitoring sensors in power grids," *Energy*, vol. 118, pp. 435 – 445, 2017.

[48] T. Hosseinimehr and A. Tabesh, "Magnetic field energy harvesting from AC lines for powering wireless sensor nodes in smart grids," *IEEE Trans. Ind. Electron.*, vol. 63, no. 8, pp. 4947–4954, 2016.

[49] M. J. Vos, "A magnetic core permeance model for inductive power harvesting," *IEEE Trans. Power Electron.*, vol. 35, no. 4, pp. 3627–3635, 2020.

[50] V. Fernandes, T. R. Oliveira, T. F. A. Nogueira, and M. V. Ribeiro, "Ambient energy harvesting: The potential of additive noise in urban and rural medium-voltage electric power networks," in *Brazilian Telecommunications Symposium*, Sep. 2019.

[51] M. V. Ribeiro *et al.*, "Energy recovery from undesirable components in electric signals: Benefits to the electricity sector," *International Journal of Electrical Power and Energy Systems*, 2021, under review.

[52] V. Fernandes, T. R. Oliveira, and M. V. Ribeiro, "The usefulness of the energy harvested from additive noises in power line and wireless media," *J. Commun. and Inf. Syst.*, vol. 35, no. 1, pp. 61–65, Mar. 2020.

[53] V. Fernandes *et al.*, "Bernoulli-Gaussian distribution with memory as a model for power line communication noise," in *Proc. Brazilian Telecommunications and Signal Processing Symposium*, Sep. 2017, pp. 328–332.

[54] L. G. S. Costa *et al.*, "Coupling for power line communications: A survey," *J. Commun. Inf. Syst.*, vol. 32, no. 1, pp. 8–22, Jan. 2017.

[55] M. V. Ribeiro, *Power line communications: A promising communication systems paradigm for last miles and last meters applications*, in Telecommunications: Advances and Trends in Transmission, Networking and Applications, C. C. Cavalcante, R. F. Colares, and P. C. Barbosa, Eds. Fortaleza, CE: Fundação Edson Queiroz, 2006, ch. 6, pp. 133-152.

[56] COPEL, *Copel Transmissão vai aumentar a capacidade de linhas de transmissão na RMC*, accessed in December 2020. [Online]. Available: https://www.copel.com/hpcweb/copel-transmissao-vai-aumentar-a-capacidade-de-linhas-de-transmissao-na-rmc

[57] COPEL, *Copel segue com obras de rede trifásica para beneficiar consumidores rurais*, accessed in December 2020. [Online]. Available: https://www.copel.com/hpcweb/copel-segue-com-obras-de-rede-trifasica-para-beneficiar-consumidores-rurais/

[58] F. V. A. Pittolo, M. D. Piante, and A. Tonello, "In vehicle PLC: In-car and in-ship channel characterization," *IEEE Veh. Technol. Mag.*, Aug. 2015.

[59] S. Barmada, L. Bellanti, M. Raugi, and M. Tucci, "Analysis of power-line communication channels in ships," *IEEE Trans. Veh. Technol.*, vol. 59, no. 7, pp. 3161–3170, 2010.

[60] “Broadband over power lines could accelerate the transmission smart grid,” US Dept. of Energy, DOE/NETL-2010/1418, 2010.

[61] Â. Camponogara, “Physical layer security analyses for low-bit-rate hybrid PLC/WLC and broadband PLC systems,” Ph.D. dissertation, Federal University of Juiz de Fora, 2020.

[62] CENELEC, *Comité Européen de Normalisation Électrotechnique*, accessed in May 2019. [Online]. Available: https://www.cenelec.eu/

[63] ITU-T, *Unified high-speed wireline-based home networking transceivers-System architecture and physical layer specification*, Geneva, Switzerland, ITU-T Recommendation G.9960, pp. 1-126, 2015. [Online]. Available: https://www.itu.int/rec/T-RECG.9960-201507-I/en

[64] *HomePlug AV2 Technology*, HomePlug Std. AV2, 2012. [Online]. Available: https://cdn.shopify.com/s/files/1/0101/1335/1737/files/HomePlug_AV2_Whitepaper.pdf?5071969984116574505

[65] *IEEE Standard for Broadband over Power Line Networks: Medium Access Control and Physical Layer Specifications*, IEEE Std. 1901, 2010.

[66] HomePlug Power Alliance, *HomePlug 1.0 White Paper, document HPAVWP-050818*, San Ramon, CA, USA, 2005. [Online]. Available: http://www.solwise.co.uk/downloads/files/hp_1.0_technicalwhitepaper_final.pdf

[67] HomePlug Power Alliance, *HomePlug AV White Paper, document HPAVWP-050818*, San Ramon, CA, USA, pp. 1-11, 2005. [Online]. Available: http://www.homeplug.org/media/filer_public/b8/68/b86828d9-7e8a-486f-aa82-179e6e95cab5/hpav-whitepaper_050818.pdf

[68] *HomePlug Green PHY*, HomePlug Std. GP, 2012. [Online]. Available: https://www.codico.com/fxdata/codico/prod/media/Datenblaetter/AKT/HomePlug_Green_PHY_whitepaper_100614%5B1%5D.pdf

[69] *IEEE 1901 HD-PLC (High Definition Power Line Communication)*, HomePlug Std. HD-PLC, Feb. 2018. [Online]. Available: https://www.hd-plc.org

[70] *Unified High-Speed Wireline-Based Home Networking Transceivers: Multiple Input/Multiple Output Specification)*, ITU-T Std. G.9963, Nov. 2018. [Online]. Available: https://www.itu.int/rec/T-REC-G.9963/en

[71] R. M. de Oliveira, A. B. Vieira, H. A. Latchman, and M. V. Ribeiro, “Medium access control protocols for power line communication: A survey,” *IEEE Commun. Surveys Tuts.*, vol. 21, no. 1, pp. 920–939, 2019.

[72] FCC, *Federal Communications Commission*, accessed in May 2019. [Online]. Available: https://www.fcc.gov/

[73] *IEEE Standard for Low Frequency (less than 500 kHz) Narrow Band Power Line Communications for Smart Grid Application*, IEEE Std. 1901.2, 2013.

[74] *Narrowband Orthogonal Frequency Division Multiplexing Power Line Communication Transceivers for G3-PLC Networks*, ITU-T Std. G.9903, Aug. 2017. [Online]. Available: https://www.itu.int/rec/T-REC-G.9903-201708-I/en

[75] *Narrowband Orthogonal Frequency Division Multiplexing Power Line Communication Transceivers for ITU-T G.hnem Networks*, ITU-T Std. G.9902, Oct. 2012. [Online]. Available: https://www.itu.int/rec/T-REC-G.9903-201708-I/en

[76] *Technology Whitepaper: PHY, MAC and Convergence layers*, PRIME Std., Jul. 2008. [Online]. Available: https://www.prime-alliance.org/wp-content/uploads/2013/03/MAC_Spec_white_paper_1_0_080721.pdf

[77] L. Lampe, A. M. Tonello, and T. G. Swart, *Power Line Communications: Principles, Standards and Applications from Multimedia to Smart Grid*. Wiley Telecom, 2014.

[78] M. Zimmermann and K. Dostert, "Analysis and modeling of impulsive noise in broadband powerline communications," *IEEE Trans. Electromagn. Compat.*, vol. 44, no. 1, pp. 249–258, Feb. 2002.

[79] J. A. Cortés *et al.*, "Analysis of the indoor broadband power-line noise scenario," *IEEE Trans. Electromagn. Compat.*, vol. 52, no. 4, pp. 849–858, Nov. 2010.

[80] X. Lu *et al.*, "Wireless networks with RF energy harvesting: A contemporary survey," *IEEE Commun. Surveys Tuts.*, vol. 17, no. 2, pp. 757–789, 2015.

[81] M. Cansiz, D. Altinel, and G. K. Kurt, "Efficiency in RF energy harvesting systems: A comprehensive review," *Energy*, vol. 174, pp. 292 – 309, 2019.

[82] L. G. da S. Costa *et al.*, "Access impedance in brazilian in-home, broadband and low-voltage electric power grids," *Electr. Pow. Syst. Res.*, vol. 171, pp. 141–149, Jun. 2019.

[83] A. Mathur, M. R. Bhatnagar, Y. Ai, and M. Cheffena, "Performance analysis of a dual-hop wireless-power line mixed cooperative system," *IEEE Access*, pp. 34 380–34 392, 2018.

[84] J. N. Laneman, D. N. C. Tse, and G. W. Wornell, "Cooperative diversity in wireless networks: Efficient protocols and outage behavior," *IEEE Trans. Inf. Theory*, vol. 50, no. 12, pp. 3062–3080, Dec. 2004.

[85] B. Nikfar and A. J. H. Vinck, "Relay selection in cooperative power line communication: A multi-armed bandit approach," *J. Commun. Netw.*, vol. 19, no. 1, pp. 1–9, Feb. 2017.

[86] A. Dubey and R. K. Mallik, "PLC system performance with AF relaying," *IEEE Trans. Commun.*, vol. 63, no. 6, pp. 2337–2345, Jun. 2015.

[87] R. M. Oliveira, M. S. P. Facina, M. V. Ribeiro, and A. B. Vieira, "Performance evaluation of in-home broadband PLC systems using a cooperative MAC protocol," *Comput. Netw.*, vol. 95, pp. 62–76, Dec. 2015.

[88] R. M. Oliveira, L. G. de Oliveira, A. B. Vieira, and M. V. Ribeiro, "An enhanced cooperative MAC protocol for hybrid PLC/wireless systems," *Computer Networks*, vol. 163, p. 106878, 2019.

[89] Â. Camponogara, H. V. Poor, and M. V. Ribeiro, "The complete and incomplete low-bit-rate hybrid PLC/wireless channel models: Physical layer security analyses," *IEEE Internet Things J.*, no. 2, pp. 2760–2769, Apr. 2019.

[90] V. L. R. da Costa, V. Fernandes, and M. V. Ribeiro, "Narrowband hybrid PLC/wireless: Transceiver prototype, hardware resource usage and energy consumption," *Ad Hoc Networks*, vol. 94, p. 101945, 2019.

[91] M. de L. Filomeno, M. L. R. de Campos, H. V. Poor, and M. V. Ribeiro, "Hybrid power line/wireless systems: An optimal power allocation perspective," *IEEE Trans. Wireless Commun.*, no. 10, pp. 6289–6300, Oct. 2020.

[92] T. R. Oliveira *et al.*, "The characterization of hybrid PLC-wireless channels: A preliminary analysis," in *Proc. IEEE Int. Symp. on Power Line Commun. Appl.*, Mar. 2013, pp. 98–102.

[93] T. R. Oliveira *et al.*, "On the statistical characterization of hybrid PLC-wireless channels," *Electr. Pow. Syst. Res.*, pp. 329–337, Oct. 2018.

[94] T. F. A. Nogueira, G. R. Colen, V. Fernandes, and M. V. Ribeiro, "Statistical modeling of magnitudes of brazilian in-home PLC and hybrid PLC-wireless channels," *Phys. Commun.*, vol. 39, Apr. 2020.

[95] M. Schwartz, "Carrier-wave telephony over power lines: Early history," *IEEE Commun. Mag.*, vol. 47, no. 1, pp. 14–18, Jan. 2009.

[96] M. Gebhardt, F. Weinmann, and K. Dostert, "Physical and regulatory constraints for communication over the power supply grid," *IEEE Commun. Mag.*, no. 5, pp. 84–90, May 2003.

[97] IEC 610003-8, *Electromagnet compatibility (EMC) - part 3: Limits - section 8: Signaling on low-voltage electrical installations - emission levels, frequency bands and electromagnet disturbances levels*, Geneva, Switzeland, 2002.

[98] FCC, *Code of federal regulations - title 47: Telecommunication - chapter I: FCC part 15 - radio frequency devices*, Washington, DC, 2002.

[99] N. Shlezinger and R. Dabora, "On the capacity of narrowband PLC channels," *IEEE Trans. Commun.*, vol. 63, no. 4, pp. 1191–1201, Apr. 2015.

[100] A. A. Nasir, X. Zhou, S. Durrani, and R. A. Kennedy, "Relaying protocols for wireless energy harvesting and information processing," *IEEE Trans. Wireless Commun.*, vol. 12, no. 7, pp. 3622–3636, Jul. 2013.

[101] *Measured Brazilian places*, accessed in April 2018. [Online]. Available: https://sites.google.com/a/ifsudestemg.edu.br/oliveira/plc

[102] T. R. Oliveira, W. A. Finamore, and M. V. Ribeiro, "A sounding method based on OFDM modulation for PLC channel measurement," in *Proc. IEEE Int. Symp. on Power Line Commun. Appl.*, 2013, pp. 185–190.

[103] G. R. Colen *et al.*, "Measurement setup for characterizing low-voltage and outdoor electric distribution grids for PLC systems," in *Proc. PES Conf. Innov. Smart Grid Technol. Latin Amer.*, Apr. 2013, pp. 1–5.

[104] M. V. Ribeiro *et al.*, "Clustered-orthogonal frequency division multiplexing for power line communication: When is it beneficial?" *IET Commun.*, vol. 8, no. 13, pp. 2236–2347, Sep. 2014.

[105] M. Katayama, T. Yamazato, and H. Okada, "A mathematical model of noise in narrowband power line communication systems," *IEEE J. Sel. Areas Commun.*, vol. 24, no. 7, pp. 1267–1276, Jul. 2006.

[106] A. F. Molisch *et al.*, "IEEE 802.15.4a channel model - final report," IEEE 802.15 WPAN Low Rate Alternative PHY Task Group, Tech. Rep., Nov. 2004.

[107] J. M. Cioffi, *Chap. 4: Multi-channel Modulation*, accessed in May 2018. [Online]. Available: http://web.stanford.edu/group/cioffi/book/chap4.pdf

[108] C. R. B. Cabral, V. H. Lachos, and C. B. Zeller, "Multivariate measurement error models using finite mixtures of skew-Student t distributions," *J. Multivariate Analysis*, vol. 124, pp. 179 – 198, Feb. 2014.

[109] Â. Camponogara, "Measurement and characterization of aircraft PLC channels," Master's thesis, Federal University of Juiz de Fora, Aug. 2016.

[110] C. Walck, *Hand-book on statistical distributions for experimentalists*, 1996. [Online]. Available: http://www.stat.rice.edu/~dobelman/textfiles/DistributionsHandbook.pdf

[111] L. R. Varshney, "Transporting information and energy simultaneously," in *Proc. IEEE Int. Symp. on Inf. Theory*, 2008, pp. 1612–1616.

[112] P. Grover and A. Sahai, "Shannon meets Tesla: Wireless information and power transfer," in *Proc. IEEE Int. Symp. on Inf. Theory*, 2010, pp. 2363–2367.

[113] R. Zhang and C. K. Ho, "MIMO broadcasting for simultaneous wireless information and power transfer," *IEEE Trans. Wireless Commun.*, vol. 12, no. 5, pp. 1989–2001, May 2013.

[114] Z. Ding, S. M. Perlaza, I. Esnaola, and H. V. Poor, "Power allocation strategies in energy harvesting wireless cooperative networks," *IEEE Trans. Wireless Commun.*, vol. 13, no. 2, pp. 846–860, Feb. 2014.

[115] L. Elmorshedy and C. Leung, "Power allocation in an RF energy harvesting DF relay network in the presence of an interferer," *IEEE Access*, vol. 5, pp. 7606–7618, 2017.

[116] C. Choudhuri and U. Mitra, "Capacity bounds for relay channels with intersymbol interference and colored Gaussian noise," *IEEE Trans. Inf. Theory*, vol. 60, no. 9, pp. 5639–5652, Sep. 2014.

[117] A. J. Goldsmith and M. Effros, "The capacity region of broadcast channels with intersymbol interference and colored Gaussian noise," *IEEE Trans. Inf. Theory*, vol. 47, no. 1, pp. 219–240, Jan. 2001.

[118] W. Jiang, T. Kaiser, and A. J. H. Vinck, "A robust opportunistic relaying strategy for co-operative wireless communications," *IEEE Trans. Wireless Commun.*, vol. 15, no. 4, pp. 2642–2655, Apr. 2016.

[119] M. S. P. Facina, H. A. Latchman, H. V. Poor, and M. V. Ribeiro, "Cooperative in-home power line communication: Analyses based on a measurement campaign," *IEEE Trans. Commun.*, vol. 64, no. 2, pp. 778–789, Feb. 2016.

[120] C. K. Alexander and M. N. O. Sadiku, *Fundamentals of Electric Circuits*, 5th ed. McGraw-Hill Higher Education, 2013.

[121] S. Farahani, "Chapter 1 - ZigBee basics," in *ZigBee wireless networks and transceivers*. Burlington: Newnes, 2008, pp. 1–24.

[122] *IEEE Standard for Information technology– Local and metropolitan area networks– Specific requirements– Part 15.4: Wireless Medium Access Control (MAC) and Physical Layer (PHY) Specifications for Low Rate Wireless Personal Area Networks (WPANs)*, IEEE Std. 802.15.4, 2006.

[123] E. Casilari, J. Cano-García, and G. Campos-Garrido, "Modeling of current consumption in 802.15.4/ZigBee sensor motes," *Sensors*, vol. 10, pp. 5443–5468, Jun. 2010.

[124] C. Gomez, J. Oller, and J. Paradells, "Overview and evaluation of Bluetooth Low Energy: An emerging low-power wireless technology," *Sensors*, vol. 12, no. 9, pp. 11 734–11 753, Aug. 2012.

[125] S. Darroudi, R. Caldera-Sánchez, and C. Gomez, "Bluetooth mesh energy consumption: A model," *Sensors*, vol. 19, no. 1238, Mar. 2019.

[126] R. Eriksen, "Energy consumption of low power wide area network node devices in the industrial, scientific and medical band," Master's thesis, KTH Royal Institute of Technology - Electrical Engineering and Computer Science, 2019.

[127] L. Casals, B. Mir, R. Vidal, and C. Gomez, "Modeling the energy performance of LoRaWAN," *Sensors*, vol. 17, no. 2364, Oct. 2017.

[128] Sigfox, *Radio configurations*, accessed on Sept. 30, 2020. [Online]. Available: https://build.sigfox.com/sigfox-radio-configurations-rc

[129] R. Singh, P. Puluckul, R. Berkvens, and M. Weyn, "Energy consumption analysis of LPWAN technologies and lifetime estimation for IoT application," *Sensors*, vol. 20, no. 4794, Aug. 2020.

[130] C. Gomez *et al.*, "A Sigfox energy consumption model," *Sensors*, vol. 19, no. 681, Feb. 2019.

[131] E. T. S. Institute, *4th Generation (LTE)*, accessed on Oct. 07, 2020. [Online]. Available: https://www.etsi.org/technologies/mobile/4g

[132] A. Rico-Alvarino *et al.*, "An overview of 3GPP enhancements on machine to machine communications," *IEEE Commun. Mag.*, vol. 54, no. 6, pp. 14–21, 2016.

[133] E. M. Migabo, K. D. Djouani, and A. M. Kurien, "The narrowband internet of things (NB-IoT) resources management performance state of art, challenges, and opportunities," *IEEE Access*, vol. 8, pp. 97 658–97 675, 2020.

[134] C. Gomez and J. Paradells, "Urban automation networks: Current and emerging solutions for sensed data collection and actuation in Smart Cities," *Sensors*, vol. 15, pp. 22 874–22 898, Sep. 2015.

[135] ANEEL, *Electric Energy Consumption and Revenue Reports*, 2019, www.aneel.gov.br/relatorios-de-consumo-e-receita. Accessed on Jun. 27, 2020.

APPENDIX A – Publications

The published and submitted papers during the doctoral period are listed as follows. These papers are separate between dissertation-related and non-dissertation-related.

- Dissertation related papers:

- **V. Fernandes**, H. V. Poor, and M. V. Ribeiro, "Dedicated Energy Harvesting in Hybrid PLC-Wireless Systems," *IEEE Transactions on Wireless Communications*, vol. 19, no. 6, pp. 3839-3853, Jun. 2020.
- **V. Fernandes**, T. R. Oliveira, and M. V. Ribeiro, "The Usefulness of the Energy Harvested from Additive Noises in Power Line and Wireless Media," *Journal of Communication and Information Systems*, vol. 35, no. 1, pp. 61-65, Mar. 2020.
- **V. Fernandes**, T. R. Oliveira, T. F. A. Nogueira, and M. V. Ribeiro, "Ambient Energy Harvesting: The Potential of Additive Noise in Urban and Rural Medium-Voltage Electric Power Networks," in *Proc. Brazilian Communications and Signal Processing Symposium*, Oct. 2019.
- **V. Fernandes**, H. V. Poor, and M. V. Ribeiro, "A Hybrid Power Line/Wireless Dual-Hop System with Energy Harvesting Relay," *IEEE Internet of Things Journal*, vol. 5, no. 5, pp. 4201-4211, Oct. 2018.

- Not related papers:

- M. V. Ribeiro, **V. Fernandes**, H. L. M. Monteiro, N. Cravo, E. J. de Oliveira, H. V. Poor, and P. F. Ribeiro, "Benefits of Energy Recovery from the Undesirable Components in Electric Signals in Electric Power Systems," *International Journal of Electrical Power and Energy Systems*, accepted for publication.
- M. V. Ribeiro, **V. Fernandes**, N. Cravo, H. L. M. Monteiro, "Benefits of Energy Recovery from Undesirable Components in Electric Signals," in *Proc. Brazilian Communications and Signal Processing Symposium*, accepted for publication.
- A. F. S. Toledo, L. G. de O. Souza, R. N. de S. Assis, **V. Fernandes**, "Robô controlado remotamente via Arduino," *ANALECTA*, vol. 6, no. 3, pp. 1-20, Nov. 2020.
- T. F. do A. Nogueira, G. R. Colen, **V. Fernandes**, and M. V. Ribeiro, "Statistical Modeling of Magnitudes of Brazilian In-Home PLC and Hybrid PLC-Wireless Channels," *Physical Communcation*, vol. 39, pp. 101014, Apr. 2020.
- V. L. R. da Costa, **V. Fernandes**, and M. V. Ribeiro, "Narrowband Hybrid PLC / Wireless: Transceiver Prototype, Hardware Resource Usage and Energy Consumption," *Ad Hoc Networks*, vol. 94, pp. 101945, Nov. 2019.

- D. T. Silva, J. V. N. Cardoso, A. P. Guimarães, P. A. R. Mendes, **V. Fernandes**, "Captura de Energia Ambiente: O Potencial dos Sinais de Radiofrequência," *ANALECTA*, vol. 5, pp. 1-16, Nov. 2019.

- **V. Fernandes**, W. A. Finamore, H. V. Poor, and M. V. Ribeiro, "The Low-Bit-Rate Hybrid Power Line/Wireless Single-Relay Channel," *IEEE Systems Journal*, vol. 13, no. 1, pp. 98-109, Mar. 2019.

- D. Fernandes, G. R. Colen, **V. Fernandes**, G. F. C. Lemos, W. A. Finamore, and M. V. Ribeiro, "Low-cost Implementation of M-QAM Signal Constellations," *Digital Signal Processing*, vol. 79, pp. 91-101, Aug. 2018.

- **V. Fernandes**, H. V. Poor, and M. V. Ribeiro, "Analyses of the Incomplete Low-Bit-Rate Hybrid PLC-Wireless Single-Relay Channel," *IEEE Internet of Things Journal*, vol. 5, no. 2, pp. 917-929, Apr. 2018.

- L. de M. B. A. Dib, **V. Fernandes**, M. de L. Filomeno, and M. V. Ribeiro, "Hybrid PLC/Wireless Communication for Smart Grids and Internet of Things Applications," *IEEE Internet of Things Journal*, vol. 5, no. 2, pp. 655-667, Apr. 2018.

- **V. Fernandes**, W. A. Finamore, M. V. Ribeiro, N. Marina, and J. Karamachoski, "Bernoulli-Gaussian Distribution with Memory as a Model for Power Line Communication Noise," in *Proc. Brazilian Communications and Signal Processing Symposium*, pp. 328-332, Sep. 2017.